1991

Analysis of ionized cluster beam thin film deposition

Dave Turner
Iowa State University

INFORMATION TO USERS

This manuscript has been reproduced from the microfilm master. UMI films the text directly from the original or copy submitted. Thus, some thesis and dissertation copies are in typewriter face, while others may be from any type of computer printer.

The quality of this reproduction is dependent upon the quality of the copy submitted. Broken or indistinct print, colored or poor quality illustrations and photographs, print bleedthrough, substandard margins, and improper alignment can adversely affect reproduction.

In the unlikely event that the author did not send UMI a complete manuscript and there are missing pages, these will be noted. Also, if unauthorized copyright material had to be removed, a note will indicate the deletion.

Oversize materials (e.g., maps, drawings, charts) are reproduced by sectioning the original, beginning at the upper left-hand corner and continuing from left to right in equal sections with small overlaps. Each original is also photographed in one exposure and is included in reduced form at the back of the book.

Photographs included in the original manuscript have been reproduced xerographically in this copy. Higher quality 6" x 9" black and white photographic prints are available for any photographs or illustrations appearing in this copy for an additional charge. Contact UMI directly to order.

U·M·I

University Microfilms International
A Bell & Howell Information Company
300 North Zeeb Road, Ann Arbor, MI 48106-1346 USA
313/761-4700 800/521-0600

Order Number 9126261

Analysis of ionized cluster beam thin film deposition

Turner, Dave Eric, Ph.D.

Iowa State University, 1991

U·M·I
300 N. Zeeb Rd.
Ann Arbor, MI 48106

Analysis of
ionized cluster beam thin film deposition

by

Dave Turner

A Dissertation Submitted to the
Graduate Faculty in Partial Fulfillment of the
Requirements for the Degree of

DOCTOR OF PHILOSOPHY

Department: Physics and Astronomy
Major: Solid State Physics

Approved:

Signature was redacted for privacy.

Signature was redacted for privacy.

In Charge of Major Work

Signature was redacted for privacy.

For the Major Department

Signature was redacted for privacy.

For the Graduate College

Iowa State University
Ames, Iowa
1991

TABLE OF CONTENTS

INTRODUCTION

Ionized cluster beam (ICB) deposition has received considerable attention since its introduction in 1972 by Takagi *et al.* at Kyoto University because of its potential for low temperature film growth.[1-5] In ICB deposition it is proposed that large clusters of 100-2000 loosely bound atoms are singly ionized and accelerated providing extra energy for increased mobility of atoms on the surface allowing films to be grown at lower substrate temperatures.[6-9] Since there is only one charge for every 100-2000 atoms, this method should not suffer adverse affects from a charge buildup on the substrate. ICB deposition is a low energy technique, adding only a few electron volts per atom, so films avoid the point defects that higher energy processes can induce.

A Takagi-type source for producing large clusters begins with a crucible, typically made of graphite, that has a cap with a small nozzle approximately 1 mm in diameter and length. The theory is that heating the source material in the crucible causes its vapor to be ejected in a supersonic flow that undergoes a pure vapor expansion in which nucleation and condensation of large clusters occurs. While classical nucleation theory predicts this for gases under high pressure,[10-11] it is less clear that large metallic clusters can be formed at the low crucible pressures of 1-5 Torr used in ICB deposition.[12-13] An alternate heterogeneous theory was proposed by Knaur *et al.*[14-15] where clusters nucleate and grow on the walls of the crucible and eventually break free and get swept away by the vapor flux.

While the theoretical justifications are still debatable,[15-17] the experimental evidence for large cluster production is equally controversial. The Kyoto University group has conducted three major experiments that indicated the presence of large clusters in varying concentrations.[1,13,18-21] These three experiments form the basis for all subsequent ICB research and are supplemented by a body of indirect evidence of film formation effects that have been attributed to the presence of large clusters.[22-27] Many other groups have tried to corroborate these cluster size experiments[28-33] with only a few suggesting the presence of large clusters.[15,33-35]

The cluster beam is, according to these experiments, composed mostly of single atoms with only a small number of large clusters. Even a small number of large clusters can be a significant contribution to the mass flux since each one may contain thousands of atoms. Some small clusters must also be present due to the increased chance of collision and nucleation in the nozzle area. In this dissertation, a small cluster is defined as having less than

ten atoms and includes single atoms while the general term cluster refers to all sizes from single atoms to large clusters.

Typically 1% of the cluster beam gets positively ionized by electron impact in the ionization region. This low rate of ionization means that few clusters will get doubly ionized. Electron beam currents of 1-300 mA are typical with the electrons having energies of 100-500 eV. This broad range in electron currents is due to the differing efficiencies of the two major types of ionizers in delivering the electrons through the cluster beam at the desired energy level (see Appendix A). The ion beam current that reaches the substrate is typically in the 2-20 μA range. The ionized clusters are then accelerated toward the substrate by a 1-6 kV potential while the neutral clusters drift there at thermal velocities. While the acceleration would provide 1-6 eV/atom of added energy to a cluster of 1000 atoms, it also supplies the small ionized clusters with up to several keV/atom of energy. The affect of this flux of highly energetic small ionized clusters has largely been ignored in the past and no current source design actively attempts to block the small ionized clusters from reaching the substrate even though they are expected to cause great damage upon impact.[36] Some indications are that sources similar in design to the Mitsubishi source may cause small ionized clusters to miss the substrate at high acceleration voltages due to the interference of the acceleration voltage with the ionization region (see Appendix A).

ICB films are reported to have some of the same general characteristics as in higher energy ion assisted deposition in that the films tend to be denser and better adhering.[1,37-50] They also tend to be smoother, especially when grown under higher acceleration voltages, and suffer less from defects that can be induced by high energy ion impacts. The added energy of incident clusters is said to lead to a sputtering of contaminant atoms allowing high purity films to be grown in dirtier environments. Large clusters are expected to break up and spread on impact but may also promote nucleation sites. Another trend is that ICB films are not well characterized, leading to a limited amount of quantitative evidence to support the generalizations above.

While further investigation of many aspects of ICB deposition is warranted, it is first necessary to determine with some certainty whether large clusters are being produced. It is toward this goal that the author has aimed the research reported here. A complete analysis of the Eaton ICB source involving computer calculation of the potential fields and computer simulation of the electrons and ions as they react to and influence these fields provides an in depth understanding of the dynamics that influence the final beam characteristics. A high resolution time-of-flight mass spectrometer was developed to investigate the most important

parameter, the cluster size distribution. Great effort was put toward developing a system that could detect even the smallest concentrations of large clusters and computer simulation of all aspects was done to assure the accuracy of the spectrometer. These results motivated a review of the primary evidence for large clusters; the three main cluster size experiments conducted by the Kyoto University group. A computer analysis of these critical experiments probes the basis of ICB and provides a more complete view of the broad range of cluster experiments.

THE EATON ICB SOURCE

There are two major kinds of Takagi-type ICB sources in use today. Sources like those produced by Mitsubishi have an open architecture that uses electron bombardment to heat the crucible and electrons accelerated through a screen to ionize the clusters. This is the more common type of source whether acquired from Mitsubishi or built in the laboratory. The author has an ICB source developed by the Eaton corporation that is functionally equivalent to the Mitsubishi source but accomplishes this functionality through a different design. It was designed to meet all the criteria that were found to be important from both experimental and theoretical considerations and was originally tested with a retarding field energy analyzer[1,13] in one of three major cluster size experiments done by the Kyoto University group.

Figure 1 shows a schematic diagram of the ISU Eaton source which sits vertically in a large UHV chamber capable of maintaining pressures as low as 10^{-10} Torr. The graphite crucible is heated radiatively by a graphite picket heater with a graphite cone separating the crucible compartment from the cluster beam to prevent any chance of interference. The vapor flux passes through a skimmer that narrows the beam before it enters the ionization region.

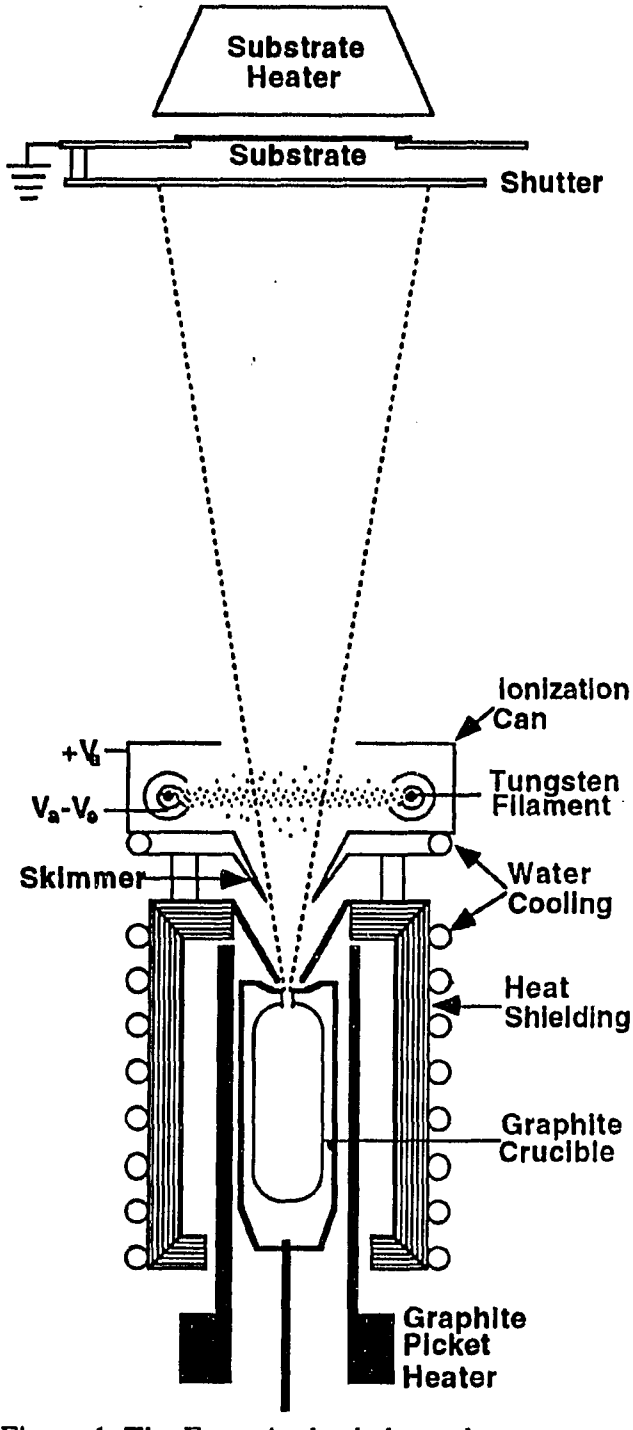

Figure 1 The Eaton ionized cluster beam source

The electrons that ionize the cluster beam are emitted from two thoriated tungsten filaments, one on each side of the ionization can. Each filament is inside a slotted tube that is electrically connected to the negative side of the filament. The filament and tube are themselves inside a larger slotted tube that is at the same potential as the ionization can. The electrons emitted from the filament are accelerated through both slots by an ionization potential V_e applied between the inner and outer tubes. These energetic electrons impact and positively ionize some of the clusters by knocking an additional electron off. A Mitsubishi source has a more open ionizer where electrons emitted from one of three filament wires on each side of the ionization can are accelerated toward and pass through a cylindrical wire screen to reach the cluster beam. While both ionizers are designed to accomplish the same task and operate in the same regimes, the fundamental difference in their construction affects the potential fields in the ionization region differently and can result in very different electron and ion dynamics.

The positively ionized clusters are accelerated toward the grounded substrate 20 cm away by applying a positive acceleration voltage V_a to the ionization can. The whole crucible compartment is also held at this potential to insure that the potential in the ionizer is not distorted by what's below the skimmer. The Mitsubishi source has a grounded ring directly above the ionization can to accelerate clusters toward the substrate. The nearness of this acceleration deforms the potential in the ionization region as does the crucible compartment underneath the ionizer which is held well below the acceleration potential to accomplish the electron bombardment heating of the crucible (see Appendix A for more information).

The beam characteristics in both types of sources are therefore controlled by setting several main parameters. The crucible temperature controls the vapor flux of the beam with deposition rates typically around 1 Å/s and it may also help determine the cluster size distribution. The electron beam current I_e is the number of electrons available for ionization (1-40 mA) while the ionization potential V_e sets the energy of each electron at 100-500 eV. The electron current is significantly lower than the 100-300 mA range typically used in the Mitsubishi source which is less efficient in delivering the electrons through the cluster beam at the energy level specified by the ionization potential. All three of these parameters affect the ion current I_{ion}=2-20 μA that eventually reaches the substrate or is measured by a 2.5 inch diameter Faraday cup mounted on a shield that can be swung in front of the substrate. Finally, the acceleration potential V_a fixes the energy that these clusters possess when they reach the substrate.

The Computer Model

The potential fields inside the Eaton source govern its efficiency and effectiveness in delivering the ionized clusters to the substrate in the desired manner. Understanding these potential fields and the dynamics of the ions and electrons that they affect is therefore crucial to understanding the source. The first and easiest step toward this goal is to calculate the non-space-charge potential throughout the source. This potential is a function of the geometry of the source and the acceleration and ionization voltages V_a and V_e. The electron and ion dynamics are then added into the computer model in the second stage to investigate the space-charge affects on the potential fields.

The cylindrical symmetry of the Eaton source allows the computer model to be reduced to a two dimensional slice through the source. The ionizer filaments are the only exceptions to the cylindrical symmetry but can be treated as such with little loss of accuracy. The source is mapped onto a two dimensional mesh on which Laplace's equation is solved using mesh relaxation (see Appendix B for details on mesh relaxation). The whole vacuum chamber with the Eaton source mounted vertically is modeled on a 1/16th inch mesh (15 inches by 9 inches). The potential within the ionization can is much more critical so a 1/64th inch mesh is used for more accuracy. The electrons that are added to this simulation later require even finer meshes near the filaments to properly simulate the electron trajectories so the filament area is modeled on a 1/256th inch mesh and the filament itself is on a 1/1024th inch mesh. With careful knitting together of these meshes, the potential can be solved on all four meshes simultaneously.

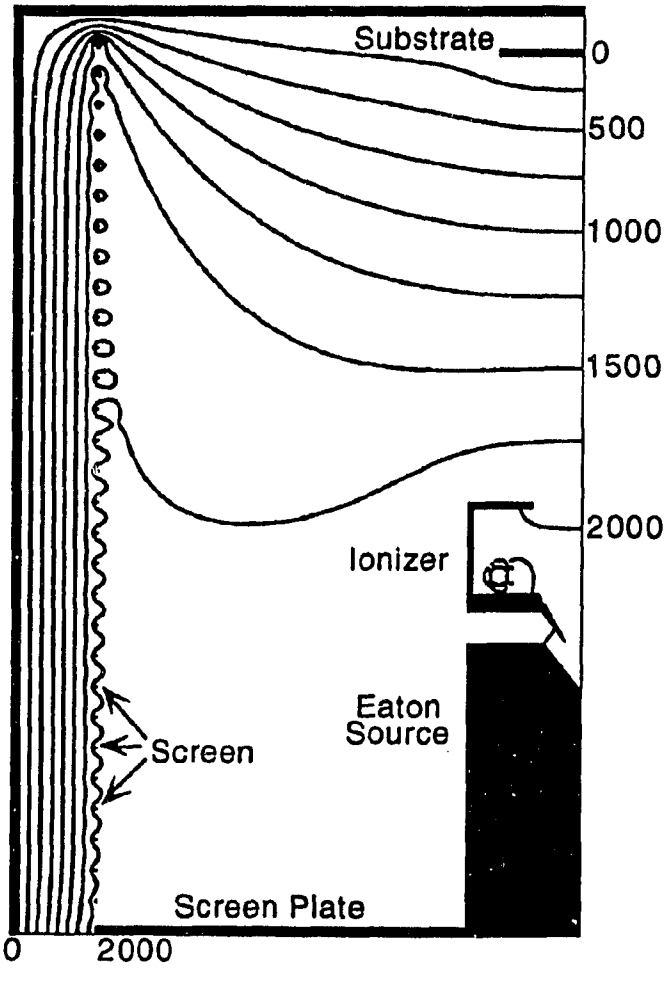

Figure 2 Laplace potential in the vacuum chamber

Figure 2 shows the potential outside the source for an acceleration potential of 2000 volts. The grounded vacuum chamber walls provide the outer and upper boundaries for the simulation. The lower boundary is a metal plate that is held at the acceleration potential along with the source and a vertical screen near the outer wall. The screen was added to help shape the fields between the source and the substrate to prevent divergence of the ion beam. These fields produce a very uniform acceleration of the ions over the whole distance between the source and substrate. The potential outside the source is not affected by the ionization potential inside the ionizer so these contours are scalable to any acceleration voltage.

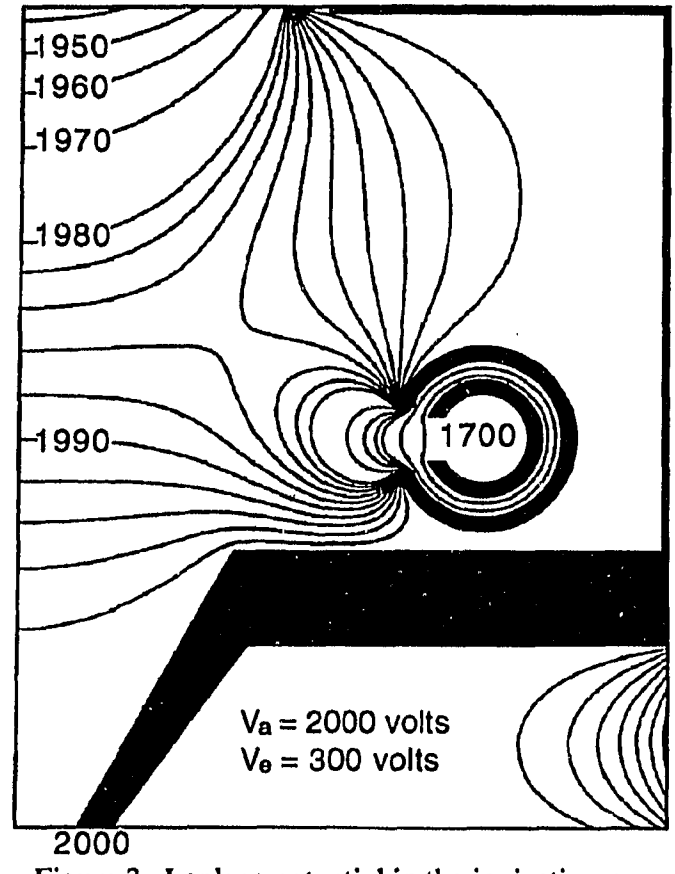

Figure 3 Laplace potential in the ionization can

The corresponding Laplace potential inside the ionization can is shown in Figure 3 for an ionization potential of 300 volts. While the ionization can and the outer tube around the filament are held at the acceleration voltage, the potential in the ionization region is lower due to leakage from the acceleration fields through the top of the ionization can and from the ionization potential through the slot in the filament assembly. In the center of the ionization can where the ionization occurs, the potential slopes gradually toward the mouth of the ionization can due to the acceleration fields. This provides a small extraction force of around 30 volts/inch for every 1000 volts of acceleration. The ionization potential also leaks out and pulls the potential down but only near the filament. At the voltages shown here it doesn't affect the ionization area greatly but, if the ionization potential is increased or the acceleration potential decreased, ions can be pulled toward or into the filament.

While the Laplace fields offer a basic understanding of the interplay between the acceleration and ionization potentials within the geometry of the ionization can, they are only valid when the electron and ion currents are too small to affect the potential fields. As will be demonstrated here, this is not true in the normal operating regime of the Eaton source.

Inclusion of the space-charge affects of the electrons and ions greatly increases the complexity of the simulation as well as the computational power required. The charge density cannot be determined experimentally so the simulation has to start by emitting electrons from the filament and observing where they go. The normal method for doing this involves introducing the electrons at the filament and moving them iteratively according to the potential fields that are calculated anew after each time step using Poisson's equation. Solving Poisson's equation on this complex set of meshes at each of several thousand time steps and moving the large number of electrons and ions involved is much too computationally intensive for even the fastest computers available to handle. It was therefore necessary to develop a more efficient, albeit less general, approach that takes advantage of the special traits of the problem without sacrificing the accuracy of the results.

What emerged was a self-consistent method that greatly reduces the number of times Poisson's equation needs to be solved as well as cutting the number of charged particles involved. After the Laplace fields are calculated, test electrons are introduced into the computer model at the filament and are moved iteratively in response to the Laplace potential. Electrons that are not immediately reflected back into the filament get accelerated out of the filament area, pass through the cluster beam, and hit the far side of the ionization can. The steady state electron charge density at each mesh point is proportional to the number of test electrons that pass by it and the amount of time they spend near it. Therefore, by recording where each test electron travels, the relative charge density for electrons in response to the Laplace fields is obtained. This is then scaled to match the number of electrons leaving the filament area with a known value for the electron beam current I_e from experiment.

The chance that ionization will occur at any point in the ionization region is proportional to both the number of neutral clusters and electrons present (each electron has approximately the same kinetic energy). By assuming that the crucible emits a uniformly expanding cone of neutral clusters, test ions are created using a predetermined size distribution (addressed later) and given an initial thermal velocity. The ions are moved iteratively according to the Laplace fields until they run into the ionization can, substrate, or vacuum chamber walls. Just as with the electrons, the relative ion density is obtained from the movement of the test ions and adjusted to match the experimental value for the number of ions that reach the substrate, the ion current I_{ion}.

It is only now, with both electron and ion charge densities for the Laplace fields known, that Poisson's equation is solved to produce a new potential. Some of this new potential is mixed into the starting Laplace potential and the process is repeated with the electrons and ions

reacting to the new potential instead of just the Laplace potential. This cycle is repeated until self-consistency is reached where the charge density reproduces the potential fields that were used to create it. This self-consistent method requires fewer test electrons and ions, just enough to produce a smoothly varying charge density (typically 10,000 of each), than standard methods and Poisson's equation only needs to be solved around 20 times, once for each cycle. A complete calculation typically takes 5 hours of cpu time at 44 Mflops.

This approach is analogous to starting with no electrons or ions present and slowly turning up the electron current. What this method lacks is the ability to include the very local particle-particle effects that can be important in some simulations. These local effects are not significant at the electron and ion densities that are typical for the Eaton source. It is only when very high electron currents (40 mA and above) are being simulated that these local effects become important near the filament where the electron density is greatest. Typical electron currents for the Eaton source are around 10 mA and if necessary there are ways to approximate high electron currents while still keeping most of the physics in the simulation.

One other point that needs to be addressed here is the interaction between the electron and cluster. Approximately one ionization occurs for every 1000 electrons that pass through the cluster beam. The electrons that are involved in ionization due so by knocking an additional electron off of a cluster. The change in velocity of the ionizing electron and the presence of the cluster electron are ignored in these simulations. This is justified by citing the small current involved (in the microamp range) and the fact that both electrons will have, with high probability, over a hundred electron volts of energy. They will therefore be moving rapidly through the ionization can and will not be affected much by the fields there nor will they affect the fields much. The affects of these factors become significant under certain circumstances and will be addressed as the need arises. It is the ability to handle the ions and electrons separately and the insignificance of the local particle-particle effects at most operating levels that makes this self-consistent method possible. An explanation of some of the details and testing methods used in these programs is available in Appendix B.

Space-Charge Results

An acceleration potential of 2000 volts and an ionization potential of 300 volts were chosen as standards for the simulations with an electron beam current of 10 mA and an ion current of 5 μA. These values are approximately in the middle of their respective ranges and

represent typical values used in experiments. Simulations were run where each of the independent variables was set to the high or low of its range and the results compared to the standard simulation to determine what effect each parameter has on the system. The electron current varies with the ionization potential but can be set absolutely by adjusting the filament's heat. The ion current depends on the ionization potential and electron current but can be adjusted directly by varying the vapor flux through changing the crucible temperature. Silver is used as a source metal since it has been used as a test case in most cluster size experiments. Time-of-flight measurements (presented in a later section) suggest that approximately 80% of the small clusters are monomers while 10% are dimers and 10% trimers. This cluster size distribution is chosen as the standard and the presence of large clusters and their effects are investigated as a special case.

Figures 4 and 5 show the electron charge densities in relative units in the filament area and the ionization can for the standard simulation. Electrons are emitted from the filament area with 300 eV of energy and spreads to 2.5 cm at the center axis with most being in a 3 mm band at the center of the electron beam. Another characteristic to note is the two secondary bands of high electron concentration at the top and bottom of the electron beam. Due to the high velocity of the electrons as they pass through the ionization area, they are not affected much by the fields there and likewise do not contribute to changing these fields. The electron

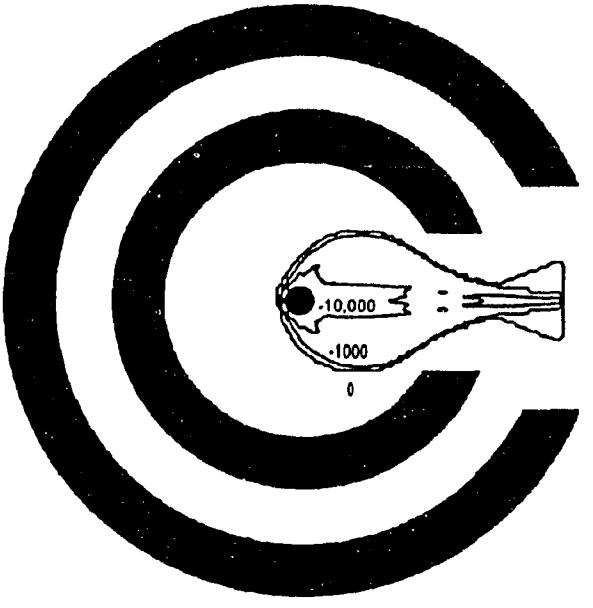

Figure 4 The electron density in the filament area (relative units)

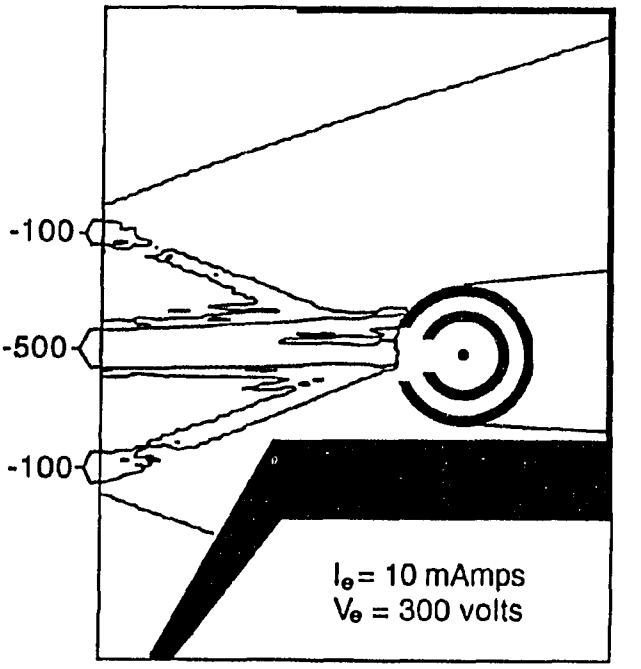

Figure 5 The electron density in the ionization can

density does define the ionization region which affects the dynamics of the ionized clusters inside the ionization can. Increasing the electron current or raising the ionization voltage results in more or higher energy electrons being available for ionizing clusters, especially in the center of the electron beam. Lowering either of these leads to an electron beam that is more uniform. Thus, the electron current and ionization potential can be used to adjust the size of the ionization region in addition to helping to set the level of ionization.

The potential fields and ion charge density inside the ionization can are shown in Figures 6 and 7 for the standard parameters. The narrow region of high ionization produces a large, slow moving concentration of ionized clusters that results in a large rise in the potential in the center of the ionization can. The magnitude of this rise is a function of the amount of ionization and, to a lesser extent, the shape of the ionization region. This "potential hill", 47 volts high for the standard simulation, dominates the ion dynamics inside the ionizer. Most clusters are ionized on or near the top and are accelerated down the sides in all directions with only those going down the front face making it to the substrate. Typically less than 20% of all the small ionized clusters will exit the ionization can due to the dominance of this space-charge buildup. About 30% get sucked into the filament as evidenced by the ion trail in Figure 7. The Laplace fields, in sharp contrast to these space-charge results, projected that nearly all of the

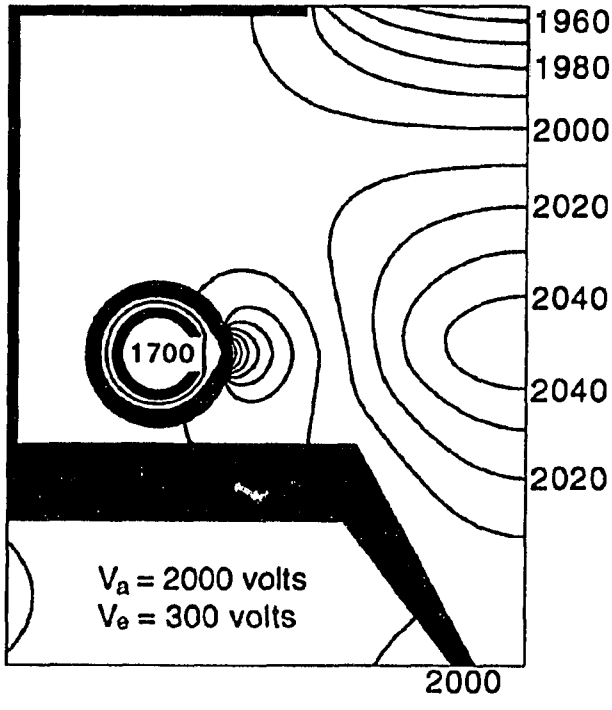

Figure 6 The space-charge potential in the ionization can

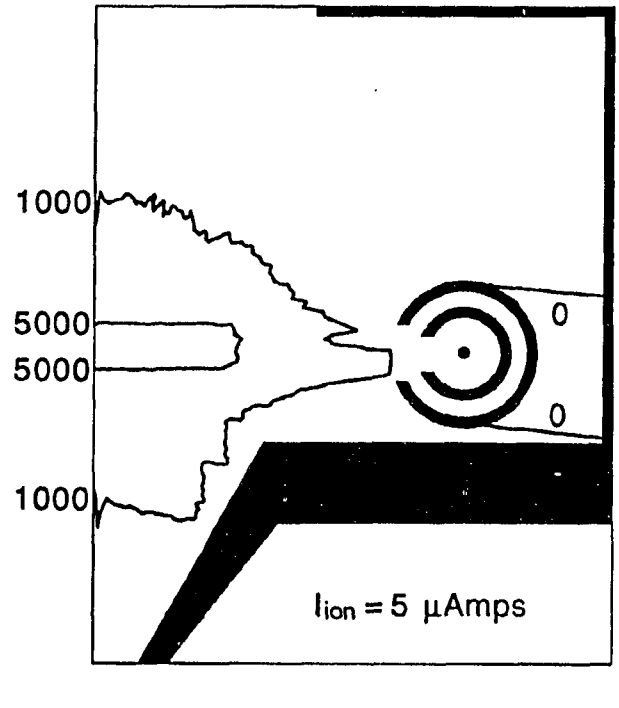

Figure 7 The ion charge density in the ionization can

ionized clusters would be swept by a gently sloping potential out of the ionizer and toward the substrate.

Higher ion currents, produced by raising the ionization potential, the electron current, or the flux of clusters, increase the potential hill to nearly 100 volts. Raising several of these parameters at once produces even higher potentials. Conversely, lowering any of these parameters results in a lowering of the potential hill and reducing several of these parameters produces fields closer to the Laplace calculation. In any case, the shape of the fields are similar in that they are dominated by the potential hill in the center of the ionization region; it is only the magnitude that changes. Running the simulation with germanium monomers, at 72.59 amu compared to silver at 107.868 amu, does not alter the results significantly. Running the standard simulation with a large ionized cluster distribution of 100-2000 atoms per cluster modeled as closely as possible to the distribution suggested by the Kyoto University group for silver from an Eaton source (see Figure 25) does not alter the potential or charge distribution either. Large ionized clusters move slower but there are not enough to affect the potential significantly.

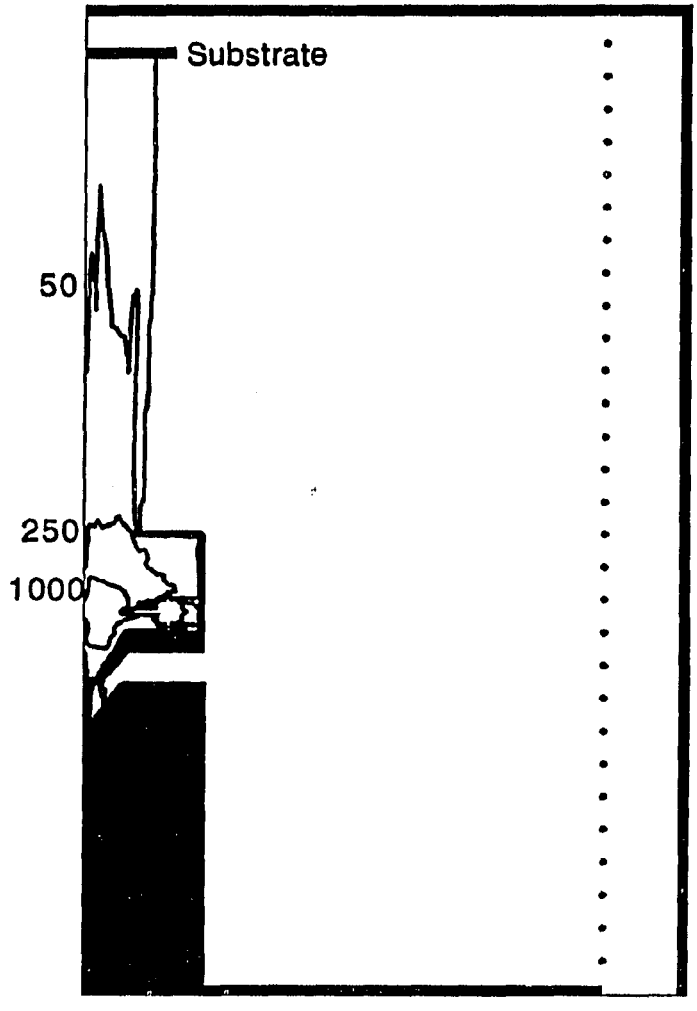

Figure 8 The ion charge density outside of the Eaton source

The ion charge density in Figure 8 shows that the ionized part of the beam is delivered fairly uniformly to the substrate without much divergence of the beam. The ions are moving quickly due to the acceleration so there is no significant space-charge effect outside of the source.

For film growth, it is important to have a uniform large ionized cluster beam so that any benefits get applied to the substrate evenly. It is also essential that none of the small

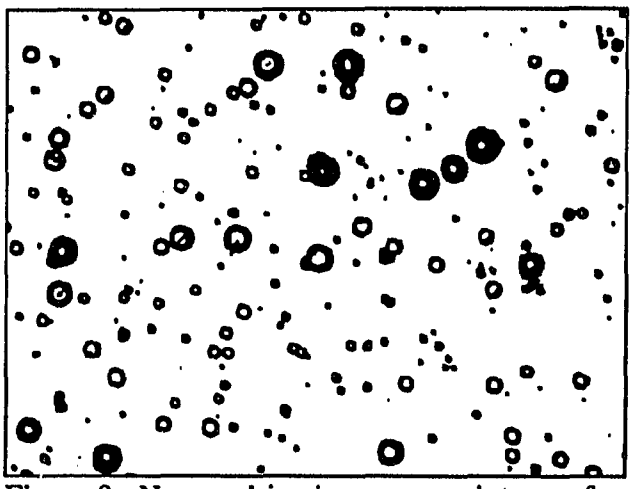

Figure 9 Namarski microscope picture of a silver ICB film grown at room temperature on silicon showing damage from the impact of energetic small ionized clusters when V_a=2000 volts is used. The largest features are 15 μm across.

ionized clusters reach the substrate since, with energies of thousands of electron volts per atom, they will have dramatic affects upon impact. The Eaton source is acceptable for delivery of any large ionized clusters to the substrate. They would not be affected much by the potential variations in the ionization can due to their large momentum. The ionized small clusters, however, are also delivered to the substrate resulting in heavy damage to any film grown with acceleration above 1000 volts (ICB deposition is typically done with V_a=1000-6000 volts). Experimental growth of silver on silicon at room temperature produces mirror smooth films when grown without ionization and acceleration but heavily damaged films that appear cloudy to visual inspection when even a moderate acceleration is used. Figure 9 shows the affects from the impact of energetic small ionized clusters. Higher substrate temperatures or heavy annealing may remove much of this damage, possibly even achieving beneficial affects from it, but it is clearly a significant factor for any film growth using the Eaton source. Therefore both computer simulation and experiment indicate that any benefit to film growth from the presence of large clusters is far outweighed by the effects of the highly energetic small ionized clusters in the Eaton ICB system.

One major technique used to detect the size distribution of ionized clusters is to analyze the energy of the ions that exit the source. If the clusters are all ionized at the same potential, their final energy will be just their initial kinetic energy plus the energy gained by the acceleration. Subtracting the energy gained by acceleration leaves the initial kinetic energy of the cluster which is proportional to the cluster's size (assuming each cluster has the same initial velocity). The presence of a potential hill in the ionization region due to space-charge buildup means that clusters will be ionized at different potentials well above the acceleration potential causing most to end up with extra energy. For this reason the Eaton source is not acceptable for use in energy analyzer experiments.

In summary, the Eaton source is greatly affected by the space-charge effects inside the ionization can at all levels of operation. This space-charge buildup is primarily a function of the ion current and is not very sensitive to the distribution of the small clusters, the presence of large ionized clusters, the source metal, the shape of the electron beam, or the starting potential in the ionization area. The space-charge buildup in the ionization region makes this source unacceptable for determining cluster size by energy analysis. It also results in less than 20% of all the ions being delivered to the substrate. While any large ionized clusters will reach the substrate, most of the ions that reach the substrate are energetic small clusters that have been observed experimentally to have dramatic affects. Therefore, even if it can be shown that large clusters are being produced, the Eaton source will be unacceptable for ICB film growth until it is modified to prevent small ionized clusters from getting to the substrate.

TIME-OF-FLIGHT MASS SPECTROMETER

The single most important question about the Eaton source is whether or not it produces large clusters in quantities significant enough to affect film growth. A time-of-flight mass spectrometer was developed to enable a search for even small quantities of large clusters and to accurately determine their size distribution. One of the original design criteria was to achieve a high resolution without altering the source so that a size distribution could be taken before a film was deposited.

The diagram in Figure 10 illustrates how the time-of-flight technique works. The ionization potential V_p is pulsed to 500 V for 3-30 μs every 3 ms producing a short burst of electrons that ionizes a narrow strip of clusters. The ionized clusters get extracted from the ionization can and accelerated toward the substrate by the acceleration potential. The smaller ionized clusters will accelerate more rapidly under the constant force leaving the larger ionized clusters lagging behind. A Faraday cup mounted on a shield and swung in front of the substrate detects this spatial distribution of the cluster sizes. The resulting signal is then

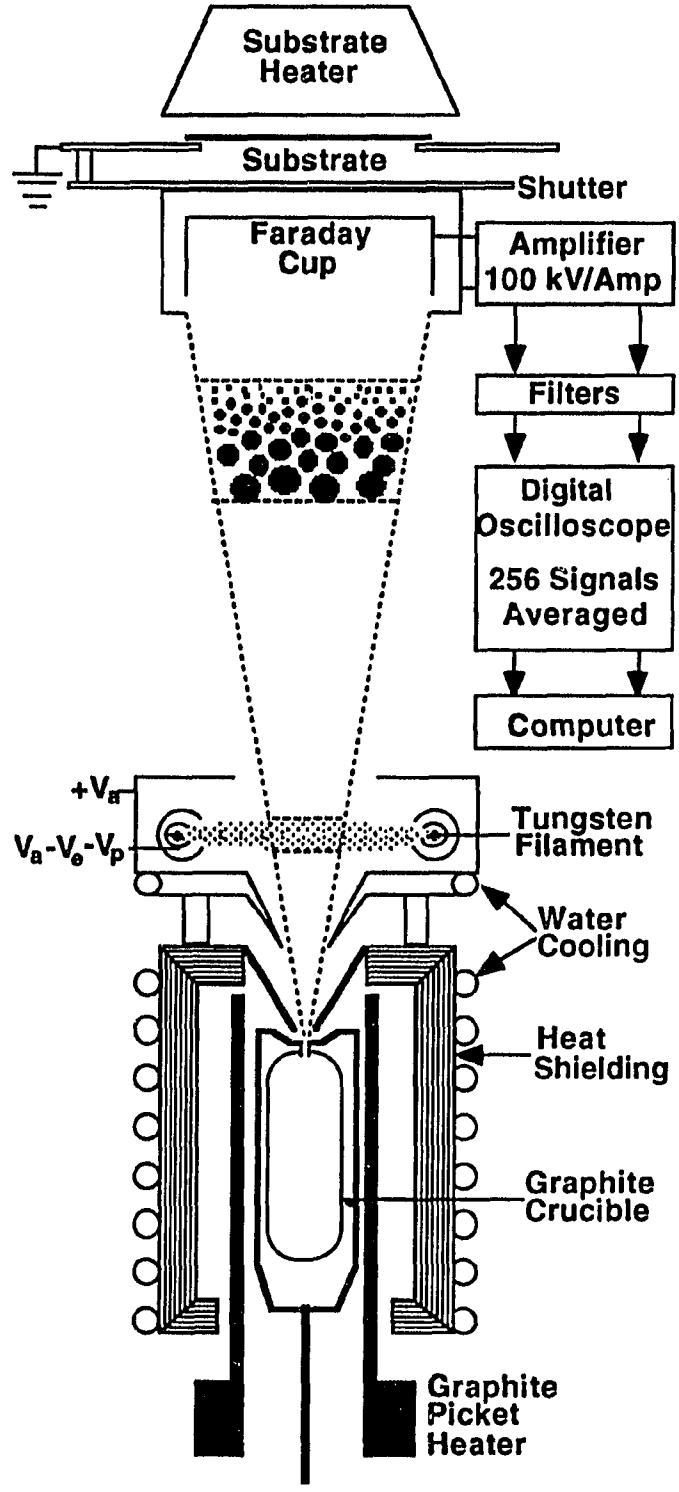

Figure 10 Diagram of the time-of-flight setup for the Eaton ICB source

amplified at 100 kV/A (dc to 100 MHz) and filtered before entering a digital oscilloscope where the signals from 256 pulses can be averaged to produce a smooth trace of the time-of-flight distribution. The pulse generator triggers the oscilloscope so the trace is an accurate measure of the time it took for the ionized clusters to reach the Faraday cup after being ionized. Short pulses of 3 μs are used to maximize time resolution to study the small clusters while longer pulses of 10 μs or 30 μs are used to maximize the signal strength to search for large clusters.

Discerning a cluster size from a time-of-flight spectrum turns out to be somewhat difficult. The potential between the ionization can and the Faraday cup provides a constant acceleration requiring only a simple calculation to determine the relationship between size and time-of-flight but the ionized clusters must first be extracted from the ionization area. The extraction force inside the ionization can is much lower than the acceleration force outside and it depends greatly on the complex relationship between the acceleration and ionization potentials as well as the geometry of the ionization can. Since the newly ionized clusters are moving slowly and the extraction force is weak, the extraction time is a substantial portion of the overall time-of-flight. For this reason it is necessary to do a computer simulation to accurately assign cluster sizes to a time-of-flight distribution. A close examination of the potential fields is also necessary to insure that no disparity exists in the time-of-flight due to where a cluster gets ionized.

Since the ionization occurs only for a short period of 3-30 μs and is not repeated for another 3 ms, there is not enough time for charge buildup to occur in the ionization region. This lack of space-charge effects greatly simplifies the computer simulation by allowing the electrons and ions to react only to the Laplace potential. The simulation is therefore similar to the first cycle in the space-charge calculation presented previously for the steady state. The electron density is determined using the Laplace fields and is dependent primarily on the pulsed ionization potential V_p. The ionization is again spatially proportional to the number of electrons and clusters present at each point in the ionization region. At this point, the effect of the ionization being pulsed on and off must be considered. Since it takes only 3 μs for a cluster to completely exit the ionization can, most ions will not be affected at all by the change in the potential in the ionization can when the pulse turns off. For the small number that are ionized late and in the back of the ionization region, the difference between the two potentials that the ions will see is not very large especially near the mouth of the ionization can. Therefore, the computer simulation can further be simplified by having the ions respond only to the "pulse on" potential without much loss in accuracy.

The Distribution of Small Ionized Clusters

This simulation is essential for assigning accurate cluster sizes to the experimental time-of-flight distribution. The distribution in Figure 11 of small ionized clusters in a typical experiment provides an ideal example of this. A computer simulation of this same experiment used a mixture of 80% monomers, 10% dimers, and 10% trimers to duplicate its shape as shown in Figure 12. Both the first minor peak (1a) and the main peak (1b) are due to the monomers. This double peak is an artifact of the spatial distribution of the electron beam. Figure 5 showed that there was a very strong central section where most of the ionization occurs with smaller bands above and below that also contributed. The atoms ionized in the strong central beam produce the main peak (1b) while those ionized in the upper area have a head start and produce a second peak (1a) before the primary peak. Those ionized below the main band lag and contribute to the back side of the main peak. This closeness in shape of the monomer distribution between experiment and computer simulation attests to the accuracy of the computer model. Both monomer peaks are within a microsecond of their predicted times-of-flight and their shapes are the same.

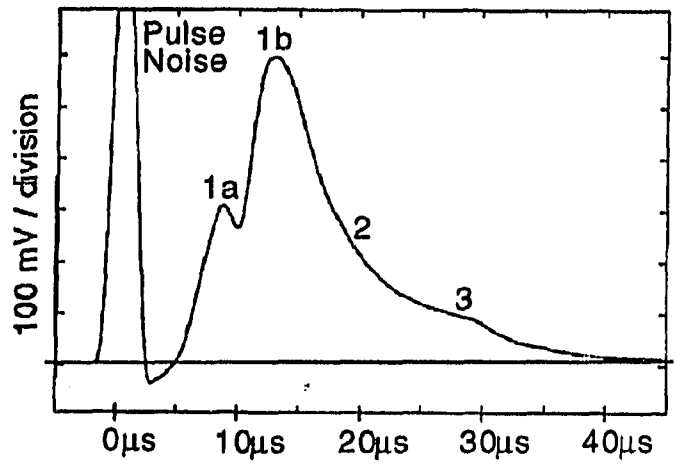

Figure 11 Experimental small ionized cluster distribution for silver showing trimers, dimers, and a double peak for monomers

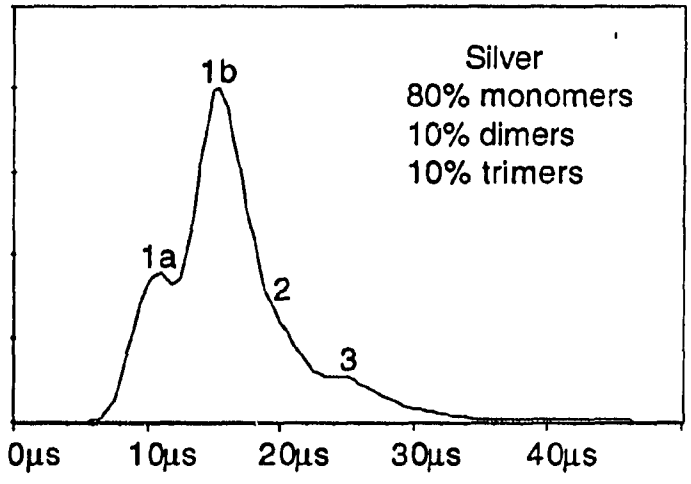

Figure 12 Computer simulated small ionized cluster distribution for silver showing trimers, dimers, and a double peak for monomers

The small number of dimers and trimers were added to the computer model to fill out the back side of the computer's distribution to more closely match experiment and to duplicate a small bump seen in some experiments and designated as a trimer peak. Experimental open

crucible tests showed a less filled out backside which would be expected from fewer dimers and trimers being produced than in a closely confined nozzle. These results for the small cluster distribution of silver match those of the Bell Laboratories photoionization experiment very closely.[28] Their setup incorporated a long drift space allowing the small cluster peaks to be completely separated while mine run together and are shaped due to the nonuniformity of the electron beam but the ratios of monomers to dimers and trimers are in reasonable agreement.

Experiments with germanium were duplicated using only monomers in a computer simulation. Germanium has more valence electrons which are instrumental in determining the stability of small clusters so it is probably less favorable for it to be in the form of these small clusters. All of the small cluster distributions from both the computer model and experiment behave identically and exactly as expected to changes in the acceleration and ionization voltages as well as for changes in all other parameters (see Appendix C).

Another area where the computer simulation is indispensable is in identifying any irregularities in the potential fields that could interfere with the experiment. An example of the importance of this is in the early experimental time-of-flight results. The first data taken showed a large number of ions that took 40-180 μs to reach the Faraday cup exactly as large clusters would be expected to. This distribution behaved as large clusters should to variations

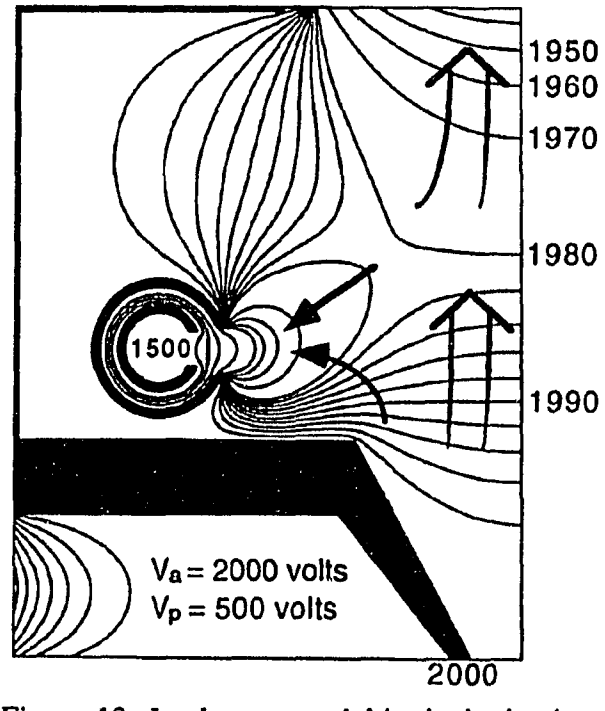

Figure 13 Laplace potential in the ionization can when the pulse is on

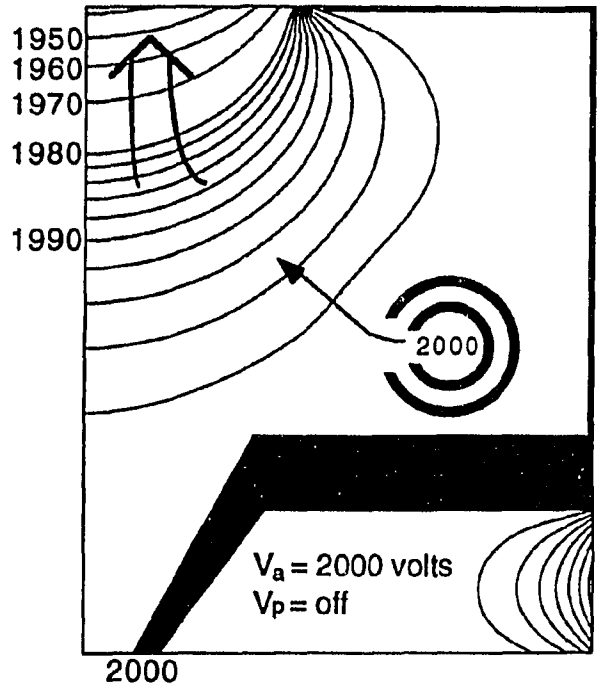

Figure 14 Laplace potential in the ionization can when the pulse is off

in V_a, V_p, I_e, and $T_{crucible}$ but it was determined experimentally that it was not due to large clusters since under certain circumstances the distribution persisted after the crucible had cooled down. The computer calculation of the potential fields was instrumental in sorting out the complex phenomenon responsible for this. When the pulse is on and electrons are being accelerated out of the filament area, enough of the ionization potential leaks into the ionization region to suck a small number of ions into the filament area as indicated by the small arrows in Figure 13. When the pulse is turned off, any ions in the filament area drift very slowly out into the ionization can and to the Faraday cup as illustrated in Figure 14. Simulations confirmed that this would delay ions by several hundred microseconds with the time delay being proportional to the acceleration voltage just like the travel time for all ionized clusters. Increasing the pulsed ionization voltage allows more ions to be sucked into and drift out of the filament area increasing the magnitude of the distribution which is the normal response for an increase in the ionization potential. Varying the electron current or crucible temperature alters the level of ionization which changes the magnitude of both the normal and delayed distributions equally. At very high filament temperatures, however, the delayed distribution persisted without the crucible emission because the filament's heat caused a small amount of silver on the inside of the filament tube to be expelled and ionized then drift outward when the pulse turned off. Once identified and understood, this problem was trivial to eradicate. A small negative bias applied to the filament keeps it in a 10 volt well when the pulse is off so that no ions can ever escape. While this problem was completely eliminated early in the project, it is presented here to illustrate the complex phenomena that can interfere with this type of experiment and to further emphasize the need for a complete understanding of the potential fields.

The Search for Large Clusters

With the computer simulation verifying that all ions, large and small, will be delivered to the Faraday cup without delay, the experimental search for large clusters is concentrated on maximizing the signal strength and minimizing the background noise (detailed in Appendix D). Longer pulse lengths of 10 μs and sometimes 30 μs are used to increase the signal while still providing sufficient time resolution and avoiding space-charge problems. A 40 kHz lowpass filter was designed to reduce the background noise to a minimum. An adjustable clipping circuit clips the pulse noise and small cluster distribution which would

otherwise disrupt the time-of-flight electronics. This combination provides a means to search for extremely small quantities of large clusters and great care was taken to assure that any distribution of large ionized clusters would not be distorted in any way. The filter and clipper were designed using SPICE software and tested using a simulated large cluster distribution suggested by the Kyoto University cluster size experiment on an Eaton source (see Figure 25 again). Furthermore, the whole detection system was extensively tested experimentally using a variety of methods to simulate distributions consistent in magnitude and shape to cluster distributions suggested by other experiments. An electron distribution of the same magnitude as a small ionized cluster distribution and having a long tail similar to what a large ionized cluster distribution would add was used to do a final, conclusive test that showed that the detection equipment would have no difficulty in accurately detecting any distribution of large ionized clusters of 100-2000 atoms or larger (the time-of-flight electronics are further detailed in Appendix D).

None of the high resolution searches showed any evidence of large clusters being produced by the Eaton source. Figure 15 shows an example of the results from a 10 μs pulse for a crucible pressure of 2.5 Torr, the conditions where the large cluster distribution should be maximized according to the Kyoto University experiments. The cluster sizes are marked at the times derived from the computer simulation of the time-of-flight experiment. The oscillations in the first 100 μs are a slight ringing in the 40 kHz filter caused by some remaining noise from the pulse. The region of interest at 100-240 μs shows no sign of any large clusters. The background noise level is around 10 μV while the corresponding small cluster distribution peaks at 550 mV. Experimental searches looking for any trace of large clusters were performed for crucible pressures up to 15 Torr and nozzle diameters of 1/2 mm, 1 mm, and an open crucible (5 m m nozzle diameter) which covers the entire regime where it is claimed that large clusters are produced.

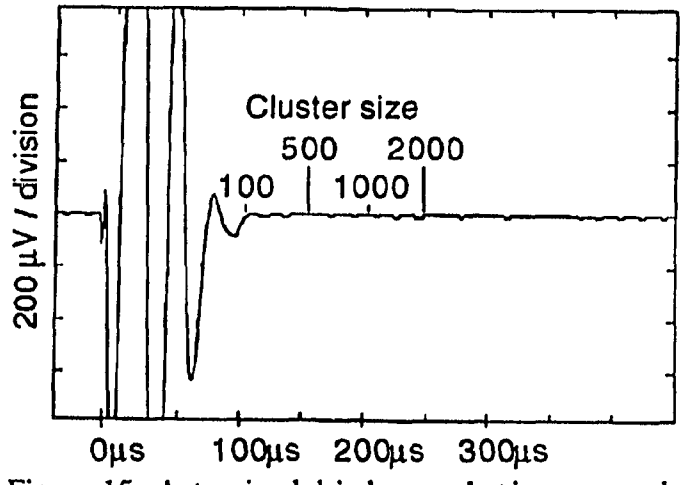

Figure 15 A typical high resolution search showing no large clusters

There are two comparisons used in Table 1 to illustrate the level of resolution achieved in this experiment. The first column is a comparison of the percentage of ionized clusters that were found to be large compared to four other

Table 1 The percentage of the ionized beam in large clusters by number and by mass.

Experiment	Percentage of ionized clusters that are large	Percentage of atoms in the ionized beam that are in large clusters
Iowa State University Time-of-Flight	<0.0006%	< 0.6%
Kyoto University Time-of-Flight[1,18]	~0.1%	~50%
Kyoto University Electrostatic Energy Analyzer[1,19]	~98%	~99.998%
Kyoto University Retarding Field Energy Analyzer[1,13,20-21]	~0.4%	~80%

major experiments (these experiments are discussed in greater detail in the following sections). The tilde indicates that it is my numerical approximation derived from the published data. The "less than" sign means that no large clusters were seen and the number given is an upper limit to the resolution. In my results, this upper limit was conservatively generated using a worst case approach to estimate the greatest number of large clusters that could go undetected in this experiment (see Appendix C for more details). The table shows that this time-of-flight experiment detected no large clusters down to several hundred times less than the levels found in the Kyoto University experiments. It also illustrates the great disparity between the Kyoto University electrostatic energy analyzer results that determined that almost all of the clusters were large and their other two experiments where almost all of the clusters were small.

The second column of the table shows the percentage of atoms in the ionized beam that are in large clusters. Since only 1% of the beam gets ionized, the less than 0.6% of the ionized beam that could be in large ionized clusters translates to less than 0.006% of the total vapor flux could be in the form of large ionized clusters and thus be available to gain energy through acceleration and affect film growth through its added kinetic energy. This maximum of 0.006% of the vapor flux is a conservative upper limit and in any case is much too small to affect film growth. The added energy that would be brought to the substrate by the acceleration of any large ionized clusters would be 30,000 times less than the energy brought by the shower of small ionized clusters and 300 times less than the thermal energy (~0.18 eV/atom) brought by the neutral atoms being deposited. Since the chance of ionization is roughly proportional to the spatial cross section of a cluster, almost all of the large clusters would get ionized if 1% of all the clusters were ionized so the number of large neutral clusters would be very small.

A Bell Laboratories laser ionized time-of-flight experiment done in conjunction with the Kyoto University group[28] also showed no evidence of large clusters down to nearly the same resolution (<0.02% of the total vapor flux could be in large clusters) and came to similar conclusions.

EXAMINATION OF THE EVIDENCE FOR LARGE CLUSTERS

The author's intention from the beginning was to go beyond just analyzing the Eaton source to explore the broader question of why there has been so much difficulty corroborating the existence of large clusters. Since the experiment on the Eaton source showed that no large clusters were being produced, the next logical step is to critically examine the experiments that form the basis for the claim that a Takagi-type source can produce large clusters. The Kyoto University group has detected large clusters in three major experiments using two different methods on two different sources. This foundation of ICB includes a time-of-flight mass spectrometer experiment and an electrostatic energy analyzer experiment, both using an electron bombardment heated crucible with highly specialized ionizers, and a retarding field energy analyzer experiment on an Eaton source. The fact that both time-of-flight and energy analyzer experiments showed large clusters of approximately the same size from two distinctly different detection methods has always been a strong argument in support of the existence of large clusters. There is also a body of indirect evidence of documented effects of ICB deposition that have been attributed to the presence of large ionized clusters.

Kyoto University Time-of-Flight Experiment

The time-of-flight experiment done by the Kyoto University group[1,18] used a specialized ionization and detection system as shown in the diagram of Figure 16 (Figure 18 shows greater detail). The neutral beam emitted from the electron bombardment heated crucible passes through a hole in the lower plate (kept at 290 volts) that separates the ionization region from the crucible area. It then passes into the ionization area which is bounded on the bottom and sides by plates kept at 500 volts and on top by an inset plate kept at 480 volts. These plates are designed to set up a 20 volt graded potential to quickly push ionized clusters upward out of the ionization region. These positively ionized clusters are then accelerated through a grounded plate mounted above the ionization area then enter a drift region before being detected by the ion collector.

Electrons are confined near the filament (biased at 310 volts) by the 290 volt potential of the ionizer walls and the gating plates. These two gating plates to the left of the filament are pulsed from 290 volts to 310 volts to allow a short 4 μs burst of electrons to pass between them. The electrons will accelerate into the ionization area where they will have 170-190 eV of

energy with which to ionize clusters. The electrons continue their trajectory across the ionization region to be collected on the far side by the electron collector biased at 590 volts.

The ionization electrons are pulsed so they will ionize only a small band of clusters that will undergo acceleration and drift to separate them spatially by size just like in the Eaton time-of-flight experiment. The shortness of the ionizing pulsed prevents any space-charge buildup and there is no danger of the potential fields in the ionization area being affected by the pulse since the plates that gate the electron beam are well separated from the ionization region.

Figure 17 shows the results of this experiment for tellurium clusters. This is a plot of the mass flux meaning that the number of clusters detected at a given time has been multiplied by the number of atoms attributed to that cluster in order to demonstrate that the number of atoms in large ionized clusters is significant compared to the number of atoms in small ionized clusters. The real time-of-flight signal representing the number of clusters of each size can be regained by simply dividing the mass flux of Figure 17 by the cluster size at each point. This distribution of cluster sizes would

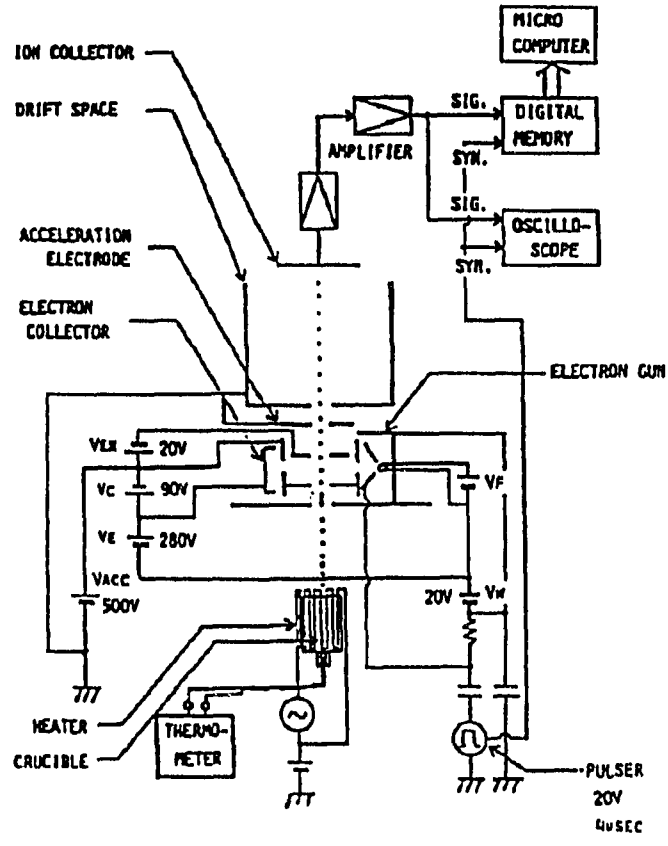

Figure 16 Diagram of the Kyoto University time-of-flight setup

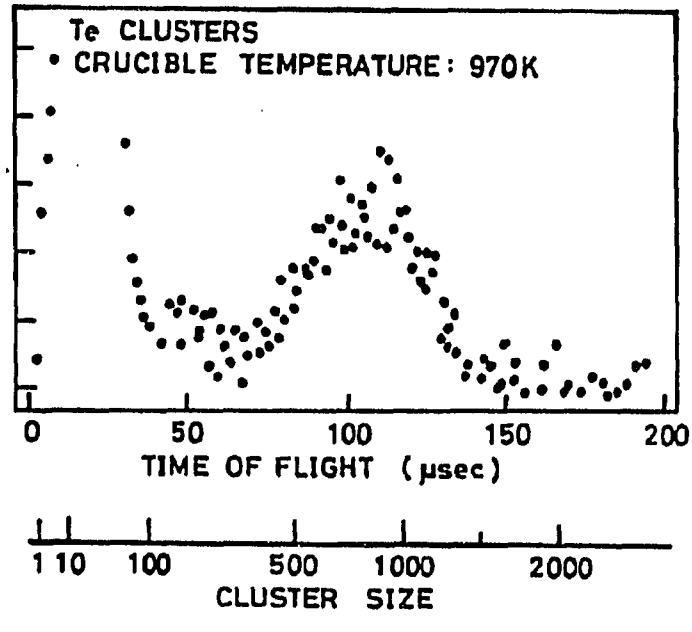

Figure 17 The Kyoto University time-of-flight distribution for tellurium clusters

demonstrate that most of the clusters are small and arrive in the first 40 μs while the large clusters would form a tail extending out to 140 μs. The small cluster distribution appears to be cropped to allow for better viewing of the large cluster distribution which makes quantitative comparisons difficult but qualitatively this experiment indicates that a measurable number of atoms are in large ionized clusters and that most of the ionized clusters are small.

As explained above, this experiment is designed with proper attention paid to avoiding problems of space-charge and pulse interference to the potential in the ionization region. However, this whole experiment hinges on the potential fields within the ionizer acting as expected. This is a very complex mix of six different voltages with ions being accelerated upward through three separate stages and electrons being accelerated and collected perpendicular to the ion beam. In order to investigate the potential fields in this experiment, the author made a computer model of the experimental setup as shown in part in Figure 18 and solved Laplace's equation using the same methods explained earlier for the Eaton source. The apparatus was modeled as mounted inside a large vacuum chamber with the crucible compartment being that of a Mitsubishi source, neither of which has any affect on the critical potential fields in the ionization region (the program listing is in Appendix E).

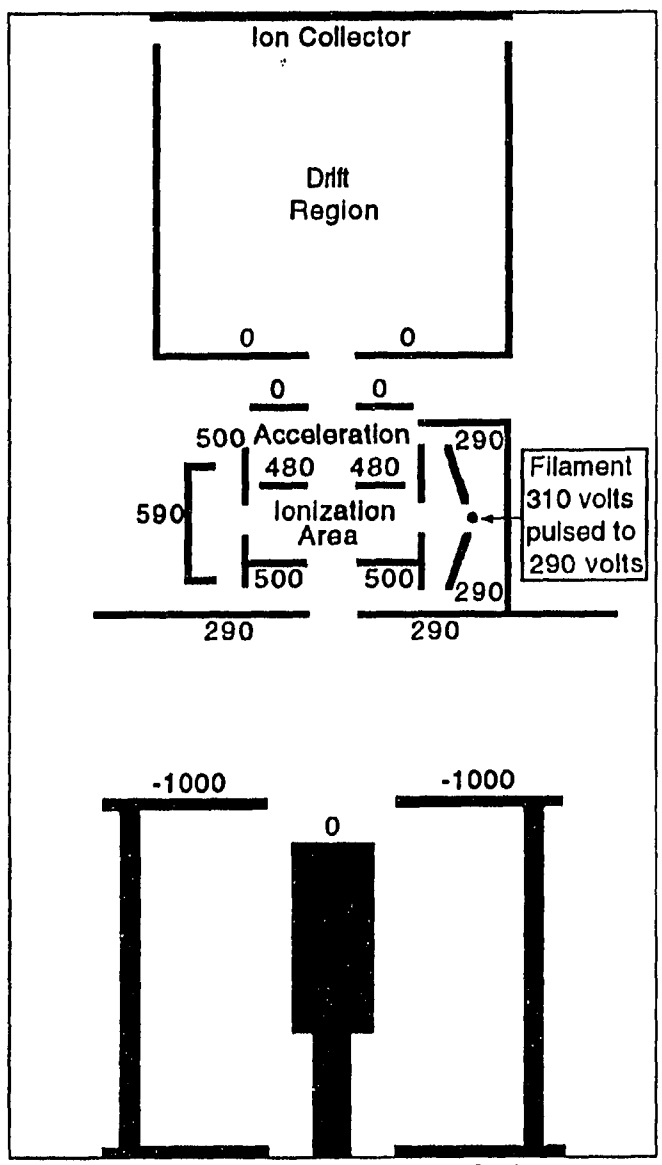

Figure 18 Computer model of the Kyoto University time-of-flight setup

After being emitted from the filament, the electrons are strongly accelerated up to 170-190 eV and pass into the ionization area. They drift across this region at a high velocity while a small force pulls the electrons toward the bottom of the ionization region. The

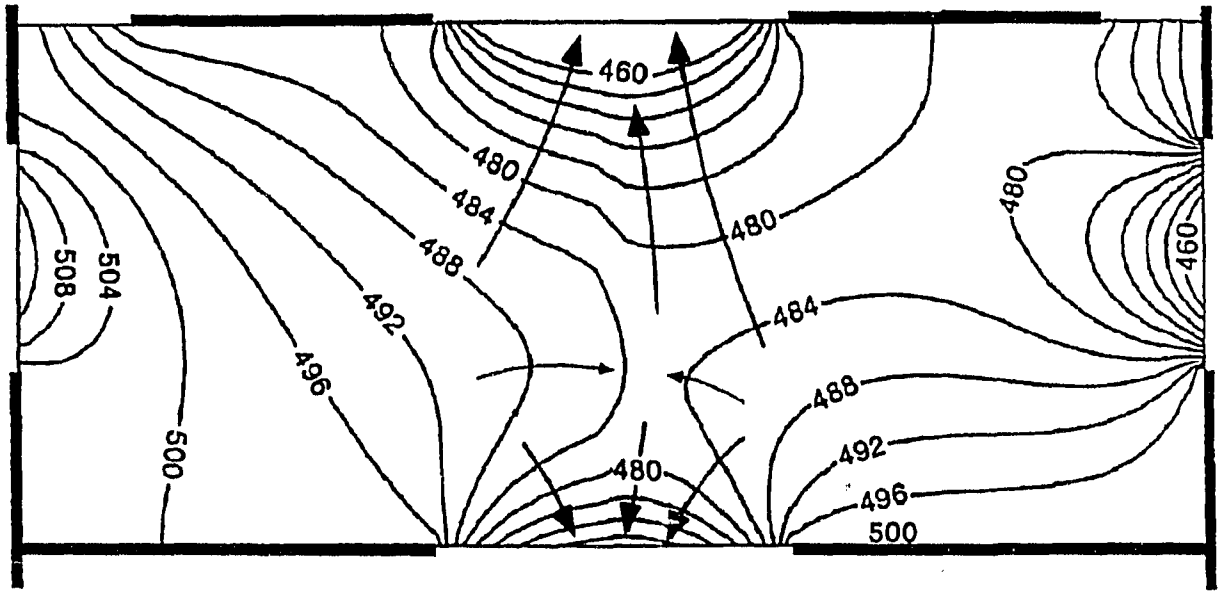

Figure 19 The potential fields in the ionization area of the Kyoto University time-of-flight experiment showing a potential ridge in the center of the ionization region

electrons will either hit the lower left plate or exit between the two plates and undergo another 90-100 volt acceleration into the electron collector. The fields are therefore appropriate as far as the electrons are concerned, delivering them through the path of the neutral beam with enough energy for ionization to occur.

As far as the ions are concerned, however, there are severe problems with the potential fields. Figure 19 shows the potential in the ionization area in great detail to illustrate these difficulties. The region where ionization occurs is the area where electrons cross the cluster beam as it passes vertically through the center of the ionizer. Clusters that are ionized in all areas are supposed to be swept upward by the 20 volt gradient across the ionization region but the potential in the lower part of the ionization region is pulled down by the close proximity of the 290 volt plate just under the ionization area. The clusters ionized in the upper part of the ionization region get swept upward as expected but the clusters ionized in the lower part encounter a "potential ridge" that can stall their progress or push them back toward the crucible. Figure 20 shows the

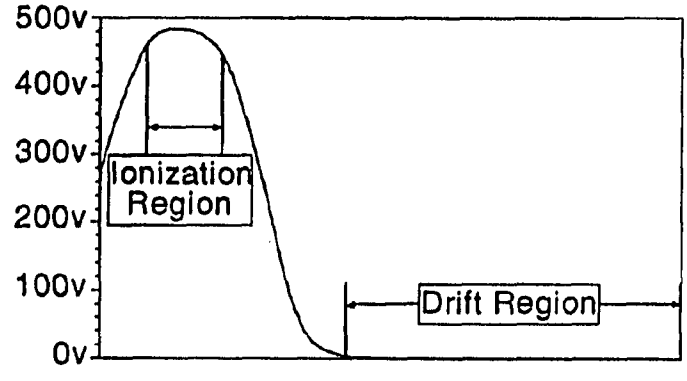

Figure 20 The potential along the center axis of the Kyoto University time-of-flight experiment

potential through the center axis showing a cross section of this ridge in the ionization region. The top of this potential ridge is lowest near the center of the ionization region producing a relatively flat saddlepoint offset slightly to the right of center. The arrows in Figure 19 illustrate the directions that ions will travel depending on where they get ionized. The initial energy before ionization is small (~0.2 eV for a single tellurium atom) compared to the strength of the potential fields so it is relatively unimportant to the ion's trajectory.

The presence of this potential ridge in the ionization region results in great differences in the time-of-flight of ions based on where they get ionized. A beam comprised only of single atoms would be expected to produce a time-of-flight distribution similar to that observed in the experiment. Atoms ionized near the front of the ionization region would be swept out of the ionization region, accelerated, and collected after the drift region with little deviation from what the experiment intended and would form the main peak in the time-of-flight distribution. Atoms ionized near the ridge will certainly be delayed in exiting the ionization region by the lack of any vertical gradient in the potential. Those atoms ionized on the top of the ridge are on a fairly flat potential so they will be delayed for extended periods while being slowly pulled into the higher graded regions. These delays would produce an extended tail to the time-of-flight distribution similar to the experimental distribution that has been interpreted as evidence for large clusters. A more sophisticated computer simulation would be needed to determine the magnitude and extent of the tail but this is judged to be unnecessary. The demonstration of the existence of this potential ridge in the ionization region is enough to invalidate this time-of-flight experiment.

It was reported that the magnitude of both parts of the distribution increased with greater vapor flux whether from a higher crucible temperature or a larger nozzle diameter. This is what is expected given the existence of the potential ridge. However, no mention was made of an open crucible test being done as a control to this experiment. An open crucible would produce the same tail as a nozzled crucible for a given vapor flux which would immediately indicate that the tail had nothing to do with large clusters.

Kyoto University Electrostatic Energy Analyzer

Electrostatic energy analyzers use two curved metal plates at different potentials to set up an electrostatic field that can be used to measure the kinetic energy of the incident ions. Ions enter through a slot in the front of the analyzer with only the ions of the desired energy

following the curved trajectory needed to exit through a second slot. A Faraday cup detects the intensity of this final ion beam as the potential difference between the two curved plates is varied to sweep through the energy range of interest. Even though the first slot blocks most of the incident beam, there is no doubt that the electrostatic energy analyzer can accurately measure the energy of even these small numbers of ions. The difficulty with energy analyzer experiments is in assigning cluster sizes to the energy distribution. This requires two assumptions, that all ions are at the same potential when they are ionized and that the initial velocity is the same (and known) independent of cluster size. The assumption that all ions start at the same potential allows the energy from an acceleration potential to be subtracted off as a constant, leaving only the initial kinetic energy of the ions. The second assumption means that the initial kinetic energy of an ion is only a function of the number of atoms in that ion, allowing the cluster size to be determined by dividing this initial kinetic energy by the energy of a single atom at the same velocity. The initial velocities will vary a little which will limit the resolution of the experiment somewhat but the variance is not nearly enough to interfere in distinguishing between small and large clusters. It is therefore only necessary that all ions be created at the same potential to derive cluster sizes from the energy distribution. The energy analyzer experiments discussed here assume a level starting potential but acknowledge that the experiments are susceptible to space-charge effects. The space-charge of the ions can raise the potential in the ionization region causing ions to start at a greater potential than expected producing higher energy ions which may get confused with the higher energy expected from large clusters.

The Kyoto University group electrostatic energy analyzer experiment[1,19] being discussed here is diagramed in Figure 21. All ions

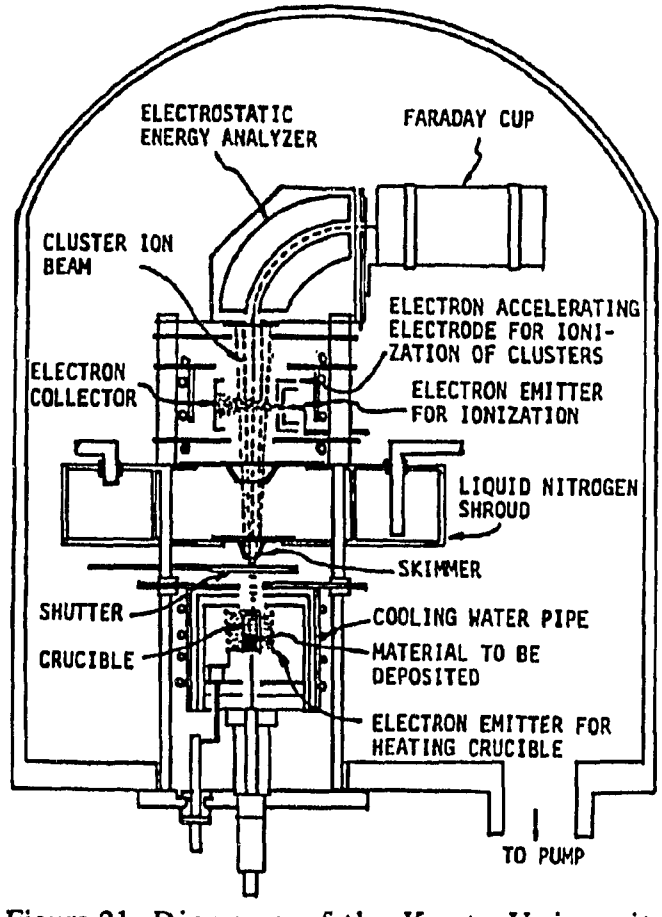

Figure 21 Diagram of the Kyoto University electrostatic energy analyzer experiment

underwent a 900 volt acceleration between the ionizer and the analyzer presumably to get more ions into the analyzer. A 20 mA electron current accelerated by a 300 volt ionization potential applied between two slotted plates is used to ionize the cluster beam[51]. The total ion current incident on the analyzer was not measured in the experiment. The potential fields in the ionizer are not affected by the crucible compartment since there is a liquid nitrogen shroud between them. Electron bombardment of the crucible is known to cause some ionization of clusters just above the nozzle. These crucible ions should all be created at or slightly below the 900 volt acceleration potential and therefore may contribute to a 0 eV peak (after the 900 eV from acceleration is subtracted off). Since the current from these crucible ions is reported to be small, it is unlikely that space-charge effects could raise the local potential enough for these ions to produce a higher energy peak.

The results from the Kyoto University experiment are reproduced in Figure 22. Strong peaks at 120 eV that are interpreted as evidence for large clusters are present for crucible pressures of 1-5 Torr and nozzle diameters below 3 mm. Most tests show a very small bump near 0 eV indicating small ions with a few having traces of ions between the two peaks or just below the high energy peak (see P_0~3 Torr). The high energy peak generally increases with increasing vapor flux whether due to a larger crucible temperature or a larger nozzle diameter.

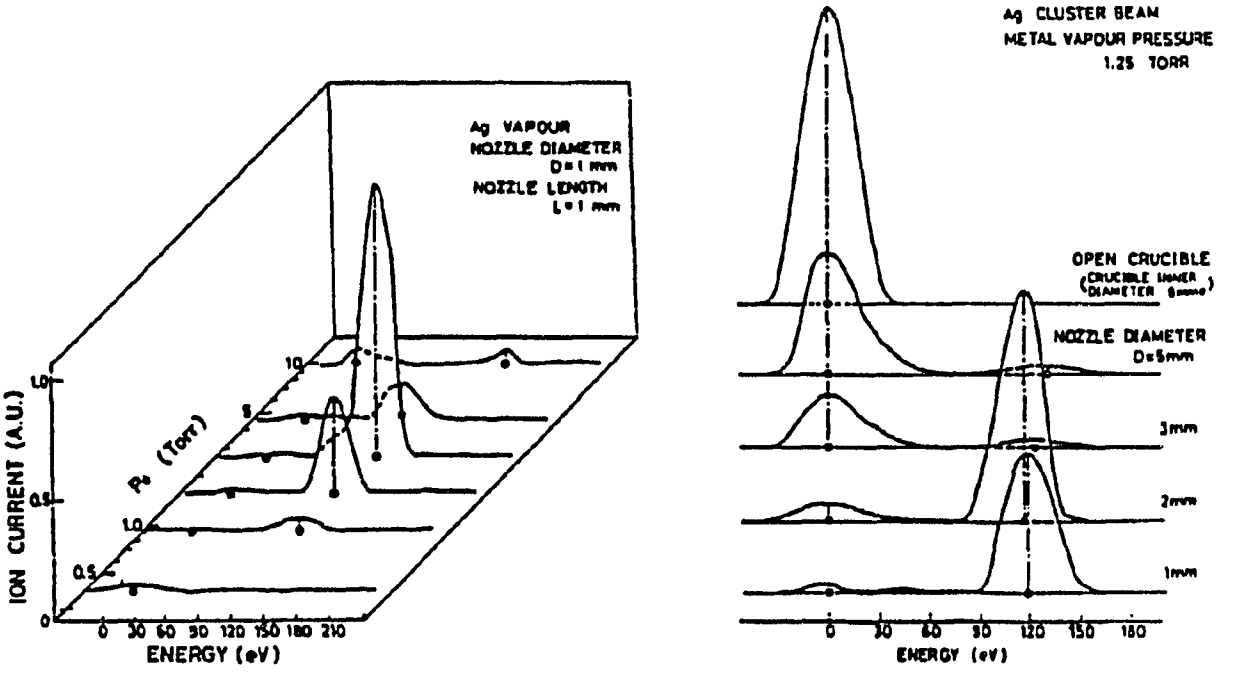

(a) (b)

Figure 22 The energy distribution from the Kyoto University electrostatic energy analyzer experiment as a function of (a) the crucible pressure and (b) the nozzle diameter

The data presented is the actual Faraday cup current which indicates the relative number of clusters as opposed to the Kyoto University time-of-flight plot that is a mass flux. The large ionized clusters greatly outnumber the small ionized clusters by up to two orders of magnitude. This is drastically different from both the Kyoto University time-of-flight and retarding field experiments where the number of large ionized clusters is reported to be at least a factor of 200 below the number of small ionized clusters (refer to Table 1).

The question that needs to be addressed is whether the high energy peaks are due to a space-charge buildup in the ionization region. The author didn't have access to enough details of this experiment to do an accurate space-charge simulation of it so the best that could be done was to simulate on the computer an electrostatic energy analyzer experiment using the well characterized Eaton source and then to compare and contrast the Eaton simulation with the Kyoto University experiment.

Even though the mechanics of the Eaton source and the Kyoto apparatus are quite different, the potential fields and charge dynamics in the ionization region in question are similar enough for strong conclusions to be drawn from this simulation to the Kyoto University experiment. The ionizers in the two setups are actually quite similar. Neither should suffer any interference from the crucible heating and both generate electron beams by accelerating electrons through two slotted metal plates by applying a potential difference between them. While the ion current is unknown in the Kyoto University experiment, the Eaton source operating at the same parameters produces an ion current of 4 μA that should be relatively close to the ion current in the Kyoto University experiment. The similarity between the two ionizers should make this a reasonably good approximation for a given vapor flux. An estimate of the total incident ion current calculated by integrating the energy analyzer current in Figure 22(a) taking into account the slot dimensions further corroborates this estimate. Therefore the magnitude and shape of the electron beam and the magnitude and shape of the ion beam in the simulation should be reasonably close to that produced by the Kyoto University apparatus. The starting potential in the ionizers should also be similar with the major difference being that the acceleration above the Eaton source occurs over a longer distance. The acceleration is low so its overall influence inside the ionizer will be small but the Kyoto University ionizer will be affected more than in the simulation.

The simulation was run at the parameters where the Kyoto University electrostatic energy analyzer experiment produced the largest high energy peak (see Figure 22(a) for P_o~3 Torr). The simulation, using only single atoms, produced the energy distribution of Figure 23 which shows a strong peak at 130 eV compared to the Kyoto University results

which showed the peak at 120 eV. The simulation shows a small shoulder below the main peak similar to the Kyoto University experiment but the small number of ions around 0 eV are not present in the simulation. These could be due to crucible ions or ions created by stray or scattered electrons in the ionizer, both of which the simulation does not consider. The concern that the affect of the acceleration potential on the acceleration potential in the ionizer was greater in the experiment than the simulation motivated a second simulation where the acceleration was increased more than five-fold from 900 volts to 5000 volts. This produced similar results with the position of the high energy peak shifted from 130 eV down to 100 eV. The space-charge buildup in the ionizer is just not very sensitive to changes in the starting potential. It is primarily a function of the level of ionization that occurs and could only be gotten rid of by setting up extremely large potential gradients across the ionization region or using extremely small ion currents.

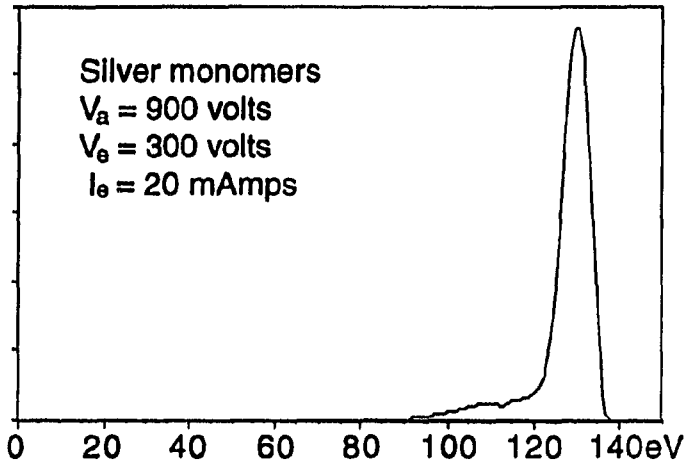

Figure 23 The energy distribution from a computer simulation of an electrostatic energy analyzer experiment on an Eaton source operating at the same parameters as the Kyoto University experiment

In summary, a simulation of an electrostatic energy analyzer experiment on the Eaton source used only single atoms to produce an energy distribution similar in magnitude and shape to that of the Kyoto University electrostatic energy analyzer experiment run under the same operating parameters. The similarities between the two systems leads to a conclusion that the high energy peak in the Kyoto University experiment is due to a space-charge buildup in the ionizer rather than large clusters.

Kyoto University Retarding Field Energy Analyzer

The third major cluster size measurement done by the Kyoto University group *et al.*[1,13,20-21] is another type of energy analyzer as pictured in Figure 24, this time using an Eaton source. The ionization can is held at the acceleration potential V_a while ions are extracted from the ionization region by a screen above the ionization can that is held 68 volts

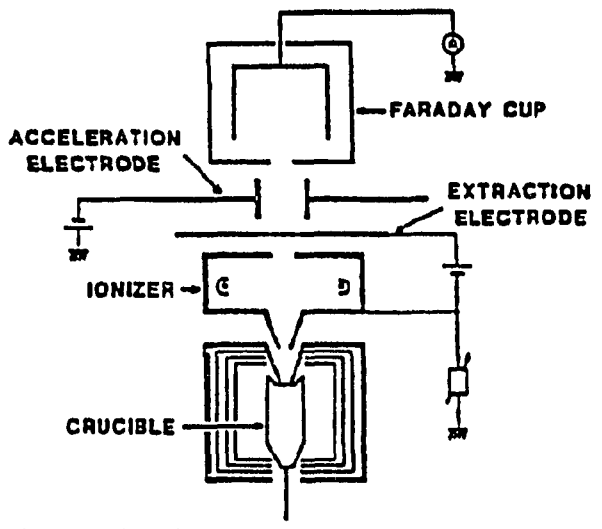

Figure 24 Diagram of the Kyoto University retarding field energy analyzer

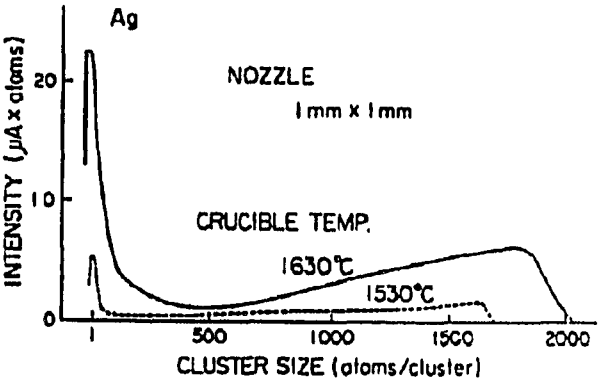

Figure 25 The mass flux from the Kyoto University retarding field energy analyzer experiment

below V_a. The acceleration electrode produces a potential barrier of 600 volts over which ions must pass to get to the Faraday cup that is inside a grounded case. The Faraday cup current is therefore a measure of the number of ionized clusters with initial energy greater than 600-V_a electron volts. The derivative of the Faraday cup current with respect to V_a produces a plot of the number of clusters at each energy level and the mass flux of Figure 25 is obtained by multiplying this current at each energy level by the cluster size it represents. The large cluster distribution corresponds to an energy range of 80-170 eV which is in agreement with the 120 eV peak of the Kyoto University electrostatic energy analyzer experiment but there are only a very small number of large ionized clusters compared to the vast majority indicated by the other energy analyzer.

This energy analyzer experiment has also been acknowledged to be susceptible to errors induced by space-charge buildup in the ionizer as discussed in the previous section. The problem with this data is that it was taken at unusually high crucible temperatures for silver. The crucible temperature of 1630° C corresponds to a crucible pressure of 25 Torr which is well above the 1-5 Torr range typical in ICB (see Figure 22[a]). The high crucible pressure produces an unusually high vapor flux which leads to a very large ion current of which 20 μA passes through the small hole in front of the Faraday cup. The total ion current is an order of magnitude greater than what the author considers experimentally and computationally as a high ion current for the Eaton source. The extreme level of space-charge buildup in the ionizer from this high ion current puts this experiment well above the level that my computer simulation technique can handle due to the significance of the local ion-ion forces as well as other

considerations. My computer simulation technique cannot handle these effects so it can't provide any insight into the shape of the distribution nor the change in the distribution with crucible temperature or with the different nozzle geometries that were also reported. What has already been demonstrated is that space-charge effects that produce monomers with energies as large as those observed in this experiment are known to occur even from ion currents one tenth as high as in this experiment. The lower distribution at 1530° C (10 Torr) also has too high of an ion current for a self-consistent simulation.

This experiment demands that all ions be created at the same potential and all computer simulations of the Eaton source insist that space-charge buildup in the ionizer will prohibit this even at much lower operating levels. The results of this retarding field energy analyzer should therefore be considered compromised by space-charge effects.

Other Evidence for Large Clusters

There is also a body of secondary evidence for the existence of large clusters in a Takagi-type source. This consists mainly of experimental observance of differences between ICB and MBE deposition in the initial growth stages and the final film qualities. These effects have been attributed to the presence of large clusters but could instead be due to any number of known differences between these two types of sources. The presence of high energy ions should greatly affect the substrate and subsequent film growth, possibly even beneficially. High energy ion bombardment may enhance the creation of nucleation sites in the initial stages of film growth and can cause localized annealing, either of which can greatly affect the final film quality[52]. The increase in the number of small clusters from a nozzled source may or may not be a significant affect. The difference in the vapor fluxes of these two types of sources can also make it difficult to accurately compare them. If the same crucible temperatures are used, the nozzled source will have a lower vapor flux so the growth rates will differ. If the deposition rates are matched by lowering the temperature of the open crucible, the atoms emitted from it will have a lower thermal velocity which could affect film growth. All of this indirect evidence in support of large clusters is not convincing on its own due to the existence of these other known effects that can influence conditions on the substrate.

There are several other groups who have tried to detect large clusters in a Takagi-type source. By far the most definitive of these is a recent study done at Bell Laboratories in conjunction with the Kyoto University group.[28] This is a time-of-flight study that used a

pulsed laser to photoionization silver clusters. A large potential was set up to accelerate the ionized silver clusters perpendicular to the original beam and into a field-free drift region before being collected by a Faraday plate. The high potential gradient in the ionization region and the short pulse lengths make this setup free of space-charge affects and the photoionization avoids many of the difficulties that can arise from electron impact ionization.

The results reported were very similar to the Eaton time-of-flight experiment described earlier. Most of the ions were found to be monomers with a small number being dimers and trimers. No reliable evidence was found that any large clusters were produced and the final conclusion was that less than 1 in every 5000 atoms in the vapor flux might be in a large cluster, a level that was considered incapable of affecting film growth in the manner originally envisioned by Takagi.

CONCLUSIONS

The ionized cluster beam sources and the systems used to detect any large clusters are greatly dependent on the potential fields especially inside the ionizers. The computer calculation of these fields is found to be crucial in establishing the validity of each experiment. The strong computer analysis coupled with the high resolution time-of-flight experiment on the Eaton source helps calibrate the results and the strong combination of computational and experimental techniques leads to a high confidence in the conclusions drawn from them. Severe problems with the three Kyoto University cluster size experiments have been identified where the potential fields in the ionization areas are critically distorted by either space-charge effects or design flaws, both of which are serious enough to invalidate the experiments. It is the strong tie between the computer simulations and the experimental details that allow strong conclusions to be drawn from these results.

1) Computer simulation of the Eaton ICB source shows that the dynamics of the ions are dominated by space-charge effects in the ionizer at all levels of operation.

2) The benefits to film growth from any large clusters would be greatly overshadowed by the affects of the high flux of energetic small ions that shower the film.

3) A high resolution time-of-flight mass spectrometer showed no sign of any large clusters being produced by the Eaton source. Less than 1 atom of every 17000 in the total vapor flux may be in a large ionized cluster which is more than two orders of magnitude below what the Kyoto University group has claimed.

4) Computer calculation of the potential fields in the Kyoto University time-of-flight experiment demonstrates the existence of a potential ridge in the ionization region that leads to severe time delays dependent on where a cluster gets ionized. This would produce a tail in time-of-flight distribution similar to what was found from experiment and interpreted as evidence for large clusters.

5) A simulation of an electrostatic energy analyzer experiment on the Eaton source operating at the same parameters as the Kyoto University electrostatic energy analyzer experiment used only single atoms to produced an energy distribution similar to it in magnitude and shape. The similarities of the important characteristics of the simulated Eaton source and the Kyoto University apparatus lead to a conclusion that the high energy peak in the Kyoto University experiment is due to a space-charge buildup in the ionization area rather than large clusters.

6) All computer simulations of the Eaton source insist that space-charge effects would greatly compromise the Kyoto University retarding field energy analyzer experiment even at much lower operating levels.

7) The three major experiments that form the basis of the claim that large clusters are produced in a Takagi-type source have been shown to be flawed. The two highest resolution experiments, the one presented here and the laser ionized time-of-flight experiment, have turned up absolutely no evidence for the existence of large clusters. The theory behind large cluster production and the body of indirect evidence attributed to the presence of large clusters are not convincing by themselves. It is therefore concluded that a Takagi-type source does not produce large clusters in quantities capable of affecting film growth.

The concept of using large clusters of loosely bound atoms to enhance film deposition is still alive. Several groups are developing the laser-ablation and seeded source techniques to generate beams of large clusters for film deposition.[29-30,53-54]

REFERENCES

1. T. Takagi, Ionized-Cluster Beam Deposition and Epitaxy, (Noyes Publications, New Jersey, 1988).

2. I. Yamada, Proc. Int'l Ion Engineering Congress - ISIAT 83 & IPAT 83, 1177 (1983).

3. P.R. Younger, Solid State Technology, 143 (November 1984).

4. I. Yamada, T. Takagi, P.R. Younger, and J. Blake, Advanced Applications of Ion Implantation - SPIE Vol. 530, 75 (1985).

5. I. Yamada, Proc. Spec. Seminar on ISIAT 90, 1 (1990).

6. Y. Yamamura, I. Yamada, and T. Takagi, Nuclear Instruments and Methods in Physics Research B37/38, 902 (1989).

7. Karl-Heinz Muller, J. Appl. Phys. **61** (7), 2516 (1 April 1987).

8. R.E. Hummel, A. Morrone, and E. Lambers, J. Vac. Sci. Technol. A8 (3), 1437 (May/Jun 1990).

9. Y. Yamamura, Proc. 14th Symp. on ISIAT 90, 27 (1990).

10. M.M.Kappes, R.W. Kunz, and E. Schumacher, Chemical Physics Letters **91** (6), 413 (1 October 1982).

11. O.F. Hagena, Surface Science **106**, 101 (1981).

12. I. Yamada, H. Usui, and T. Takagi, J. Phys. Chem. **91**, 2463 (1987).

13. H. Usui, A. Ueda, I.Yamada, and T. Takagi, Proc. 9th Symp. on ISIAT 85, 39 (1985).

14. W. Knauer and R.L. Poeschel, J. Vac. Sci. Technol. B6 (1), 456 (Jan/Feb 1988).

15. W. Knauer, J. Appl. Phys. **62** (3), 841 (1 August 1987).

16. O.F. Hagena, Z. Phys. D - Atoms, Molecules and Clusters **4**, 291 (1987).

17. S.-N. Mei, S.-N. Yang, J. Wong, C.-H. Choi, and T.-M Lu, Journal of Crystal Growth **87**, 357 (1988).

18. A. Ueda, H. Usui, I. Yamada, and T. Takagi, Proc. 9th Symp. on ISIAT 85, 45 (1985).

19. I. Yamada and T. Takagi, Thin Solid Films **80**, 105 (1981).

20. I. Yamada, H. Usui, and T. Takagi, J. Phys. Chem. **91**, 2463 (1987).

21. I. Yamada, H. Usui, and T. Takagi, Z. Phys. D - Atoms, Molecules and Clusters **3**, 137 (1986).

22. K. Kim, M.Y. Sung, K.C. Hsieh, E.W. Cowell, M.S. Feng, and K.Y. Cheng, J. Vac. Sci. Technol. A 7 (3), 792 (May/Jun 1989).

23. H. Usui, M Tanaka, I. Yamada, and T. Takagi, Nuclear Instruments and Methods in Physics Research B37/38, 886 (1989).

24. H. Usui, H. Hashimoto, I. Yamada, and T. Takagi, Proc. 11th Symp. on ISIAT 87, 133 (1987).

25. J.B. Theeten, R. Madar, A. Mircea-Roussel, A. Rocher, and G. Laurence, Journal of Crystal Growth **37**, 317 (1977).

26. T. Takagi, I. Yamada, and A. Sasaki, Thin Solid Films **39**, 207 (1976).

27. I. Yamada, G.H. Takaoka, H. Usui, and S.K. Koh, private communication (MRS 1990 preprint), (1991).

28. W.L. Brown, M.F. Jarrold, and R.L. McEachern, NIM Phys. Res. B, in press (1991).

29. J.G. Pruett, H. Windischmann, M.L. Nicholas, and P.S. Lampard, J. Appl. Phys. **64** (5), 2271 (1988).

30. A.E.T. Kuiper, G.E. Thomas, and W.J. Schouten, Journal of Crystal Growth **51**, 17 (1981).

301. F. Urban and M.J. Zahn, J. Vac. Sci. Technol. A 8 (3), 1453 (May/Jun 1990).

32. R. Weiel, T. Bornhaupt, A. Hofmann, M. Rub, and T. Tschudi, Proc. 14th Symp. on ISIAT 90, 33 (1990).

33. J. Gspann, private communication, (1988).

34. G.D. Stein, Proc. Int'l Ion Engineering Congress - ISIAT 83 & IPAT 83, 1165 (1983).

35. M. Sosnowski, S. Krommenhoek, Jyh Sheen, and R.H. Cornely, J. Vac. Sci. Technol. A 8 (3), 1458 (May/Jun 1990).

36. D.G. Armour, Mat. Res. Soc. Symp. Proc. Vol. **100**, 127 (1988).

37. T. Takagi, Thin Solid Films **92**, 17 (1982).

38. T. Takagi, I. Yamada, and A. Sasaki, Thin Solid Films **45**, 569 (1977).

39. T. Takagi, I. Yamada, and A. Sasaki, Proc. 7th Intern. Vac. Congr. & 3rd Intern. Conf. Solid Surfaces, 1915 (1977).

40. H. Usui, I. Yamada, and T. Takagi, Proc. Int'l Ion Engineering Congress - ISIAT 83 & IPAT 83, 1247 (1983).

41. M. Kyosaka, T. Saito, K. Matsubara, and T. Takagi, Proc. 6th Symp on ISIAT 82, 52 (1982).

42. Y. Minowa and K. Yamanishi, J. Vac. Sci. Technol. B 1 (4), 1148 (Oct - Dec 1983).

43. I. Yamada, K. Matsubara, M. Kodama, M. Ozawa, and T. Takagi, Journal of Crystal Growth **45**, 326 (1987).

44. L.L. Levenson, Proc. Spec. Seminar on ISIAT 90, 65 (1990).

45. L.L. Levenson, Proc. Int'l Workshop on ICBT, 131 (1986).

46. G.H. Takaoka *et al.*, Proc. Spec. Seminar on ISIAT 90, 127 (1990).

47. U. Dahmen and K.H. Westmacott, Proc. Spec. Seminar on ISIAT 90, 53 (1990).

48. I. Yamada, H. Inokawa, and T. Takagi, Thin Solid Films **124**, 179 (1985).

49. M. Sosnowski, J. Vac. Sci. Technol. A 8 (3), 1470 (May/Jun 1990).

50. I. Yamada, H. Usui, and S. Tanaka, J. Vac. Sci. Technol. A 8 (3), 1443 (May/Jun 1990).

51. I. Yamada, private communication, (January 1991).

52. P. Bai, G.-R. Yang, and T.-M. Lu, J. Vac. Sci. Technol. a 8 (3), 1465 (May/Jun 1990).

53. M.A. Duncan and D.H. Rouvray, Scientific American, 110 (December 1989).

54. L.A. Heimbrook, M. Rasanen, and V.E. Bondybey, J. Phys. Chem. **91**, 2468 (1987).

ACKNOWLEDGEMENTS

I would like to thank my committee: Howard Shanks, Bruce Harmon, Stan Burns, Kai-Ming Ho, and Alex Firestone. Special thanks go to Howard Shanks who supervised all of my work and Stan Burns who helped with much of the electronics. I am also grateful to Bruce Harmon who taught me about band structures and supervised the mercuric iodide band structure calculation. I would also like to recognize Doug Robinson and Kevin McCarron for their guidance in some of the everyday aspects of experimental research. This work was done entirely at the Microelectronics Research Center at Iowa State University.

APPENDIX A - COMPUTER CALCULATION OF THE LAPLACE POTENTIAL IN A MITSUBISHI ICB SOURCE

In addition to the calculations presented earlier, a Laplace calculation of the potential fields in a standard Mitsubishi source was done to investigate its steady state operation. Ions and electrons were introduced to determine how they would respond to these potential fields. These results were not presented in the main body because its focus is primarily on determining whether large clusters are being produced and most of the cluster measurement experiments use sources with highly specialized ionizers. This analysis is included here because it is very useful in beginning to understand how the ionized beam may affect film growth. While a full space-charge treatment would be necessary for complete characterization of the ion beam, the Laplace calculation points out severe problems with the potential fields in the ionizer that prevent the source from operating as designed. While strong conclusions must await this space-charge treatment, the problems identified in this paper suggest plausible explanations for some of the film growth properties that have been attributed to the presence of large clusters in the beam.

The paper that follows was presented at the Thirteenth Symposium on Ion Sources and Ion-Assisted Technology in Tokyo in June of 1990 and was published in the Proceedings of ISIAT 90. The programs used to do the calculations are presented immediately after the paper. The important details are described in the paper and follow the same basic procedures as the other calculations in this dissertation. The program EMITS calculates the potential fields for a given set of acceleration, ionization, and crucible voltages while EMTRAJ and IMTRAJ compute the electron and ion trajectories resulting from these potential fields.

COMPUTER CALCULATION OF THE POTENTIAL FIELDS IN A MITSUBISHI ICB SOURCE

D.E.Turner and H.R.Shanks

Microelectronics Research Center
Iowa State University
Ames, Iowa USA

Introduction

Ionized cluster beam deposition has been around for quite some time now but it is still plagued by an uncertainty as to whether large clusters are actually being produced and what role they may play in film growth. Many experiments have examined this question with only a few suggesting the presence of large clusters[1-4]. Much of the problem lies in the fact that the energy analyzers and the time-of-flight mass spectrometers that are commonly used are heavily dependent on the fields within the source. The characteristics of the ionized cluster beam are equally dependent on the potential fields in the ionization and acceleration regions. In order to better understand the ICB sources, several computer models have been generated to investigate the fields and how they vary with changes in the voltage parameters. The authors have recently completed a full space charge calculation for their Eaton ICB source but since many of the ICB sources in use today and in the past are more similar in design to the source made by Mitsubishi, an analysis of this type of source was deemed necessary as well. The results presented here are from the first step in that analysis; the solution of Laplace's equation for the full range of each of the voltage parameters. A more accurate and also more computationally intensive calculation that includes the effects of the space charge from all the electrons and ions is currently being undertaken and should clarify some of the ambiguities of this model.

Another question that has rarely been addressed is what happens to the small ionized clusters during film deposition. A vast majority of the clusters that get ionized are small clusters with fewer than ten atoms. These small ionized clusters get accelerated along with the larger ones resulting in a flux of energetic small clusters with kinetic energies of up to thousands of electron volts per atom. These should cause great damage as they impact the surface and penetrate deep into a film. Yet ICB films have always been reported to be smoother and more crystalline at higher acceleration voltages up to 6 kV[5-10]. So what happens to the small ionized clusters?

Computer Model

Any modeling of a system on a computer is limited by the speed of the computer and the amount of cpu time available. It would be nice to do a three dimensional model of an ICB source simulating all the electrons and ions in motion inside it, but this would take enormous amounts of computer time. Many approximations are therefore required but these must be examined carefully to insure that the physics is not being taken out of the model. Careful attention will be paid to justifying the approximations and expanding on how the source may vary from the computer model.

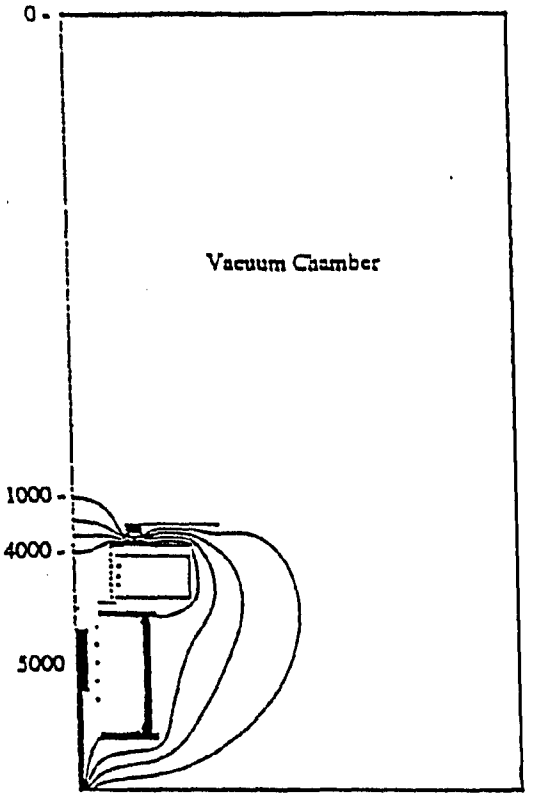

Figure 1 Mitsubishi source in a vacuum chamber. Va=5000v Vc=1000v

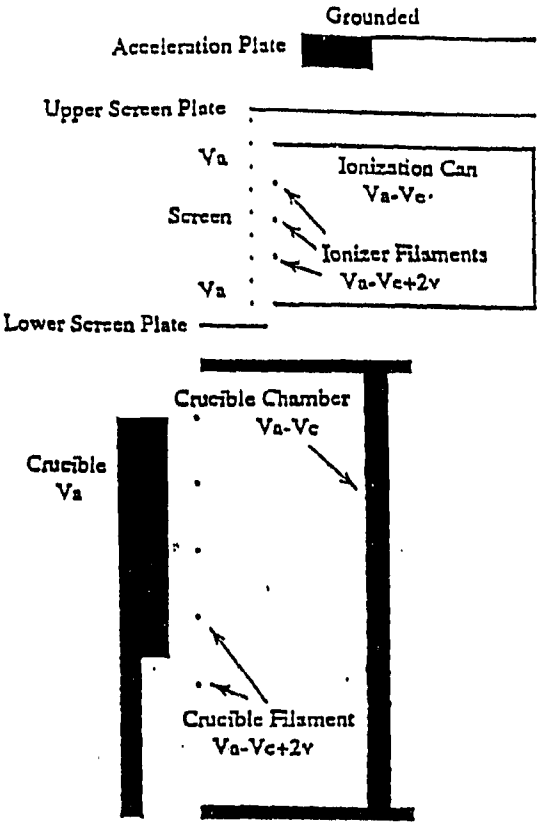

Figure 2 Computer model of the Mitsubishi ICB source.

The Mitsubishi ICB source is modeled inside a vacuum chamber as shown in figure 1 where the bottom of the source is inset a little into the base. The vacuum chamber has a 9 inch radius and is 16 inches tall. The fields inside the source will not vary significantly due to the type of vacuum chamber it is in. Since the vacuum chamber and most of the source have cylindrical symmetry, the computer model takes advantage of this fact to map the source onto a two dimensional, 1/16th inch mesh.

The heart of the Mitsubishi source is shown in figure 2 modeled on a finer 1/64th inch mesh for better accuracy. The crucible and its support rod are contained in the crucible chamber at the bottom of the figure. The crucible is kept at the ion acceleration potential Va while the crucible filament and the crucible chamber are kept at a potential Vc below this (at Va-Vc). Electrons emitted from the crucible filament are therefore accelerated by the potential difference Vc toward the crucible where their kinetic energy is used to heat the crucible. The crucible chamber is actually tied electrically to the negative side of the crucible filament so that electrons emitted from the filament will start at a slightly higher potential than that of the crucible chamber. While this potential varies linearly with the length of wire, this is difficult to model in two dimensions so a standard bias of +2 volts is put on the whole filament instead. Putting +2 volts on the filament provides a sufficient barrier to turn away the electrons from the chamber walls since the initial kinetic energy of the electrons is less than half an electron volt. The magnitude of this small bias is otherwise unimportant since the voltage between the crucible and the filament is around 1000 volts. All the physics is therefore kept in the calculation without sacrificing anything. The crucible filament actually zigzags up and down the length of the crucible instead of going in circles around it as in the computer model. A vertical two dimensional model can't handle vertical wires so they are approximated by horizontal ones with careful attention paid to keeping the same length of wire and the

same upper and lower bounds on the filament. This will of course give different local fields right around the filament but should fairly accurately model the fields everywhere else. The local fields that appear in the computer model around the horizontal wires simply represent a different orientation of the local fields around the vertical wires in the real source.

The electrons emitted from the three horizontal filament wires inside the ionization can are accelerated through the screen and toward the cluster beam by the potential difference Ve applied between the filaments and screen. The screen is made of vertical wires running between the upper and lower screen plates, all of which are at the ion acceleration potential Va. The screen wires are modeled as horizontal wires instead of vertical ones for the same reasons given previously for the crucible filament. This should still allow an accurate calculation of the fields except that the very local effects near the screen will again be vertical instead of horizontal. The ionizer filament is held at two volts above the potential of the ionization can (Va-Ve+2v) for the same reasons given previously for the crucible filament and crucible chamber. This is a multi-pass ionizer since the electrons get turned back by the slightly lower voltage of the ionization can and therefore may bounce back and forth between opposite sides of the ionization can until they hit the screen or screen plates. Although modeled as circular, the screen, lower screen plate, and the upper hole in the crucible chamber are actually rectangular with two ionizer filaments, each having three horizontal wires, facing each other on opposite sides of the ionization can. The computer model with its cylindrical symmetry approximates this by taking the radial distances as they are at the middle of the ionizer filament. The model should then be accurate for the fields near the center of the filaments on each side. Since the filament to screen distance stays constant in both the real source and the model, all that will really be different near the corners of the rectangular pieces is that the radial distance of the screen will be a little larger resulting in a stretching out of the ionization region. The ion acceleration plate above the ionization can is held at ground so that positively ionized clusters are accelerated through the acceleration plate and toward the substrate by the acceleration potential Va.

The potentials at each point on the two meshes are calculated simultaneously by solving Laplace's equation with an efficient mesh relaxation program run on a vector processing computer. At least 30,000 iterations were performed on each mesh point resulting in an accuracy better than 0.01 volts for each point on the large mesh and better than 0.001 volts for the finer mesh. The accuracy is defined by the maximum any mesh point would differ if an infinite number of iterations were done.

Probably the most significant shortcoming of the computer model presented here is that it does not consider space charge effects. The electron and ion densities are large enough that they almost certainly will affect the fields inside the source to some extent. The fields presented here can however be very useful in identifying the different effects the source may have on the electrons and ions. A full solution of Poisson's equation for the Mitsubishi source is currently being investigated. This should provide a more accurate view of the fields that can be used to evaluate these effects. The expected space charge effects are discussed qualitatively where needed.

Results

The electrostatic fields within the source result from three separate voltages; the ion acceleration voltage Va ranges from 0 kV to 10 kV, the crucible voltage Vc that accelerates electrons to heat the crucible ranges from 600 volts to about 1600 volts, and the ionization voltage Ve that accelerates the ionization electrons ranges from 200 volts to 400 volts typically. A standard set of voltages of Va=5000v, Vc=1000v, and Ve=300v was chosen from which to compare all others. These lie roughly in the middle of their respective ranges and

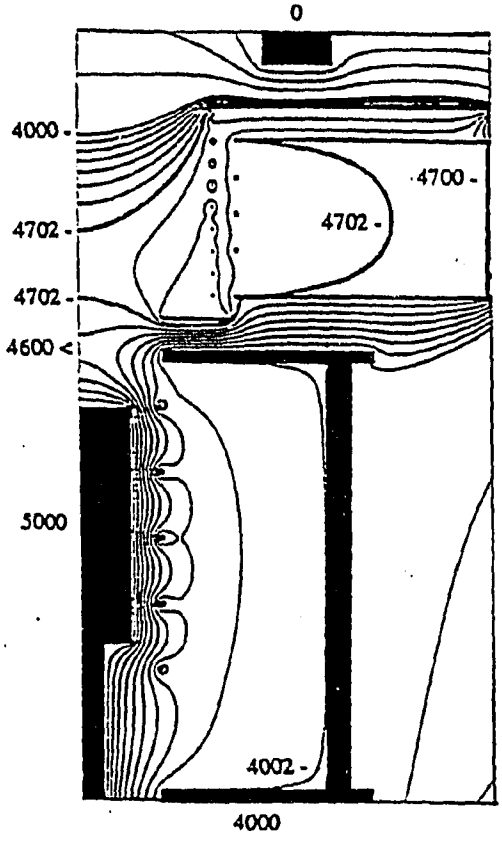

Figure 3 High acceleration potential. Va=5000v Ve=300v Vc=1000v

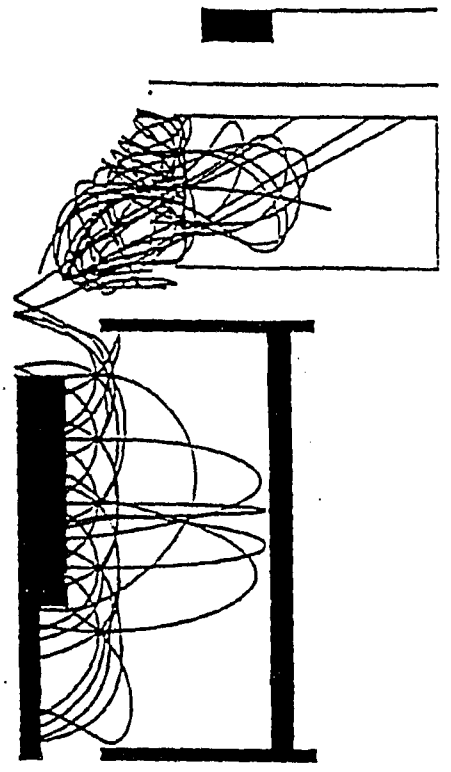

Figure 4 Electron trajectories under high acceleration. Va=5000v Ve=300v Vc=1000v

are chosen as typical values although 5000v would normally be considered as high acceleration.

The field inside the crucible chamber as shown in figure 3 looks much as expected and should deliver a good supply of 1000 eV electrons to the crucible. The ionization region is however plagued by two main problems. First, the top of the crucible chamber, at a potential of Va-Vc, pulls the potential down in the lower ionization region from between the crucible and the lower screen plate, both of which are at a potential of Va. On the top side, the acceleration plate likewise pulls the potential down in the upper ionization region. With the potential in the ionization region being pulled down through both the top and the bottom of the ionization can, the region where ionization electrons are allowed, marked by the thicker contour at 4702 volts, gets effectively pinched off. Electrons are still able to cross the axis in a small region but will have less than 42 eV of kinetic energy as they do. The most energetic electrons, and thus the most likely to ionize a cluster, are at the highest potential which is in the lower right side of the ionization region between the screen and the lower screen plate.

Figure 4 shows the trajectories of eight trial electrons emitted at 45 degree intervals from each of the filament wires in the source. This shows that most of the ionizer electrons pass through the screen and get deflected downward by the lower potential from the acceleration plate and are quickly absorbed by the lower screen plate. At this high acceleration, most electrons in the multi-pass source do not even make one pass through the cluster beam.

Also noticeable is the fact that some highly energetic electrons from the crucible filament cross the axis near the top of the crucible, possibly ionizing clusters there before they hit the ionization can. These electrons have energies of up to 1000 eV as they pass through the

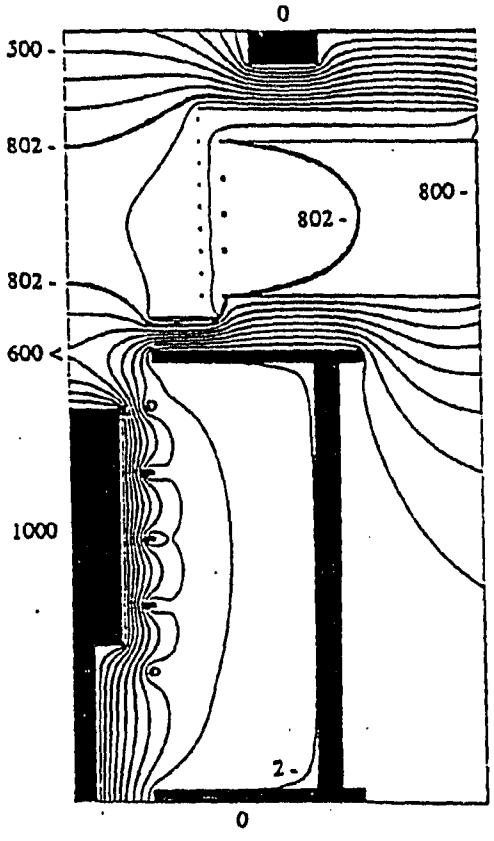

Figure 5 Low acceleration potential. Va=1000v Ve=200v Vc=1000v

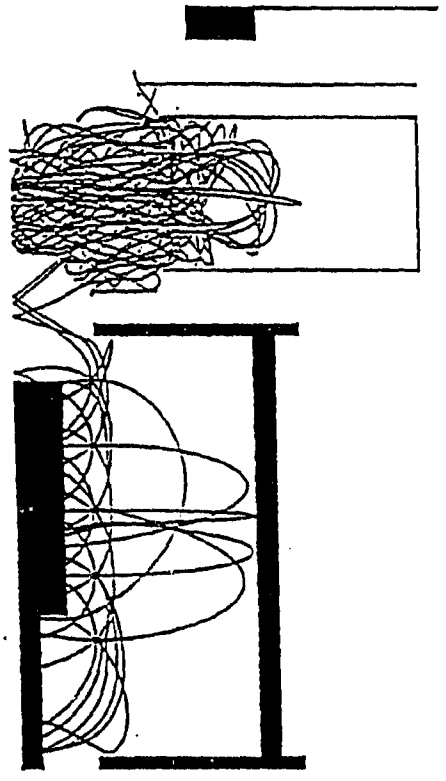

Figure 6 Electron trajectories under low acceleration. Va=1000v Ve=200v Vc=1000v

cluster beam near the mouth of the crucible, easily ionizing clusters at potentials up to hundreds of volts above that of the clusters ionized normally.

The ion trajectories were investigated by starting both singly ionized atoms of silver and large ionized clusters of 1000 silver atoms at intervals across the region where ionization is allowed to occur with an initial velocity of 570 m/s vectored directly away from the mouth of the crucible. Small ionized clusters from the lower part of the middle of the beam get sucked back toward the top of the crucible chamber while only those in the upper part of the middle of the beam, where the chance of ionization occurring is very low, will make it to the substrate. Those at the lower part of the outside of the beam, where the chance for ionization is the highest, will make it out of the ionization can but will swing wide of the substrate. The large ionized clusters from the center of the beam and especially toward the front of the beam will hit the substrate. But those from the lower right, where most of the ionization will occur, will either go through the ionization screen and hit the ionization can or they will swing wide of the substrate like the smaller clusters do. To summarize, most of the ionization will take place in the lower right corner and most of the large and small clusters ionized there will not hit the substrate.

The fields were calculated for the high and low voltages in each of the parameters Va, Vc, and Ve to determine how the fields are affected by each. Increasing the acceleration voltage to 7500 volts completely pinches off the ionization region so that no electrons can cross the axis. Increasing the crucible voltage Vc to 1600 volts has the same affect. Both of these result in a worsening of the effects of the standard model. The ionization of clusters is further restricted to the lower right corner with even less of a chance of anything ionized reaching the substrate. Lowering Va to 2500 volts or reducing Vc to 600 volts will do the opposite

by opening up the allowed region for ionization. Under these conditions electrons that cross the axis will have at most about 100 eV of kinetic energy so at least some ionization will take place in the middle of the beam and thus some of both the large and small ionized clusters can make it to the substrate. Increasing Ve by 100 volts will result in electrons with 100 eV more energy being able to cross the axis than before and conversely lowering Ve by 100 volts further restricts the ionization region to the lower right corner.

The most favorable settings for the source are at very low acceleration voltages. Figure 5 shows the fields for Va=1000v, Vc=1000v, and Ve=200v where the middle is fairly open with electrons of up to 75 eV passing through the axis. Having Va=Vc at this low voltage provides a balance between the two that allows electrons to make multiple passes. Even so, most everything that gets ionized in the lower half of the region will still be sucked back toward the crucible chamber and even more of the clusters ionized on the outside of the beam swing wide of the substrate. There will, however, be a uniform spread of small clusters from the upper part of the middle of the beam and the source produces a very uniform spread of large clusters with just a few on the outside of the beam not making it to the substrate.

There is also a single pass variation of the ionizer where the ionization can is held at the acceleration potential Va instead of just below the level of the filament at Va-Ve. The fields inside the ionization region do not differ significantly from those presented here. The only difference is that half the ionizer electrons will be accelerated away from the cluster beam and quickly absorbed by the ionization can instead of being redirected toward the beam. Thus, about the only change is that the efficiency of the delivery of electrons to the ionization region is cut in half.

Discussion

One of the goals of this study is to investigate the role that small ionized clusters (less than 10 atoms/cluster) play during film deposition, especially as a function of Va. If the ionization potential and the crucible potential are held constant at Ve=300v and Vc=1000v while the acceleration is increased from Va=1000v to 5000v, how would the resulting film growth be affected? At low Va, the computer model predicts that ionization will take place throughout the beam, with plenty of high energy electrons being available everywhere. Significant quantities of both large and small ionized clusters will reach the substrate. An ionized large cluster of 1000 atoms will have 1 eV/atom of added kinetic energy due to the acceleration which can contribute to the surface migration of the atoms after impact on the substrate. There will also, however, be a much larger number of small clusters of between one and ten atoms/cluster that will reach the substrate with between 100 eV/atom and 1000 eV/atom of additional kinetic energy. These highly energetic small clusters can easily upon impact break the interatomic bonds at the surface and continue deeper into the film causing additional damage.

At the higher acceleration voltage, the computer model predicts that most of the ionizarion will be restricted to the lower and outer part of the ionization region. Both large and small clusters that are ionized there have little chance of reaching the substrate so film growth is accomplished mostly by the neutral beam with few large ionized clusters to aid in surface migration and few small ionized clusters to damage the film.

One general characteristic of film growth by ICB is that the films grown at higher acceleration voltages up to 6 kV tend to be smoother and more crystalline than films grown with lower acceleration. The benefits of larger ionized clusters have always been assumed to be the reason for this while the harmful affects of the small ionized clusters have rarely been addressed. The scenario above suggests that higher acceleration may result in better films because fewer of the highly energetic small ionized clusters make it to the substrate resulting in the film being damaged less.

This is an interesting scenario but it should be remembered that at this point it is only a theory. Since this effect deals directly with the area that contains the highest concentration of electrons and ions, it will be affected the most by the change in the potential fields when space charge is considered. The space charge will probably alter the degree to which the ionization is restricted at high acceleration voltages but the tendency toward more restriction at higher Va should persist. The space charge may also affect the ion trajectories greatly which could mean that large or small clusters ionized in the outer portion of the beam might make it to the substrate at high acceleration. So while the results above suggest this scenario, the space charge calculation is really necessary to tell how likely it is. Clearly something must keep small ionized clusters from hitting the substrate at least at high acceleration. The question is whether large ionized clusters are also kept away.

This theory would be fairly easy to test experimentally. A Faraday Cup mounted in front of the substrate should detect a decreasing amount of ion current as the acceleration voltage is increased. Even better would be to have a Faraday Cup mounted on a shield that could be swung away from the center of the cluster beam to measure the radial distribution of the ion current as a function of Va. Either of these would give great insight into the characteristics of the source and tell how accurate the non-space-charge calculation is with regard to this effect.

The other goal of this investigation is to examine the model for effects that may disturb the measurement of cluster size by various methods. The primary method used for detecting large clusters is to analyze their energy after they leave the ionizer. This technique is based on the assumption that all material leaves the crucible with approximately the same velocity, whether it is in the form of large clusters or individual atoms. Basically, if anything is detected having higher energy than the main peak of ionized small clusters, it is assumed that the higher energy represents the excess momentum from a large cluster that got ionized. Conversely, if nothing is seen at higher energies it cannot be assumed that no large clusters are being producing since it may be that a cluster of 1000 atoms has an initial velocity of one thousandth that of a single atom.

Putting that aside, the other assumption that is made is that all clusters are ionized at the same potential so all gain the same amount of energy by undergoing the same acceleration. Although it is the initial kinetic energy that is of interest, some acceleration is needed to extract the ions from the ionization can due to the backwards pull on the ions from the crucible chamber potential. The energy analyzer could then distinguish a large cluster from a small cluster by its greater initial kinetic energy due to its large mass. But a single atom ionized at a potential 100 volts above that of the majority of the beam would be indistinguishable from a larger cluster ionized at the same potential as the majority of the beam.

The potential fields from the computer model suggest two ways in which this is possible in the Mitsubishi source. Both stem from the fact that the acceleration plate and the crucible chamber pull the potential in the ionization region down so that most of the ionization should take place at up to hundreds of volts below the expected potential Va. Thus most of the clusters may gain up to a couple hundred electron volts less energy due to the lower effective acceleration. A higher energy tail to the main peak then may occur either from some small clusters being ionized right near the screen where the potential is higher or, more likely, from highly energetic crucible filament electrons ionizing small clusters right near the crucible nozzle at potentials near Va. Ions from either of these places would see the full acceleration potential and would therefore end up with higher energies than the main ionized cluster beam. It has been known for some time that ion currents in the nanoamp range occur when the ionizer is turned completely off. Since the main beam current is typically in the microamp range, the factor of a thousand difference in magnitude between the two currents puts this effect at the same level that the large cluster current is expected to be at.

While it is expected that the fields in the ionization region will change somewhat when space charge is considered, it is unlikely that the fields will be both raised up and leveled out

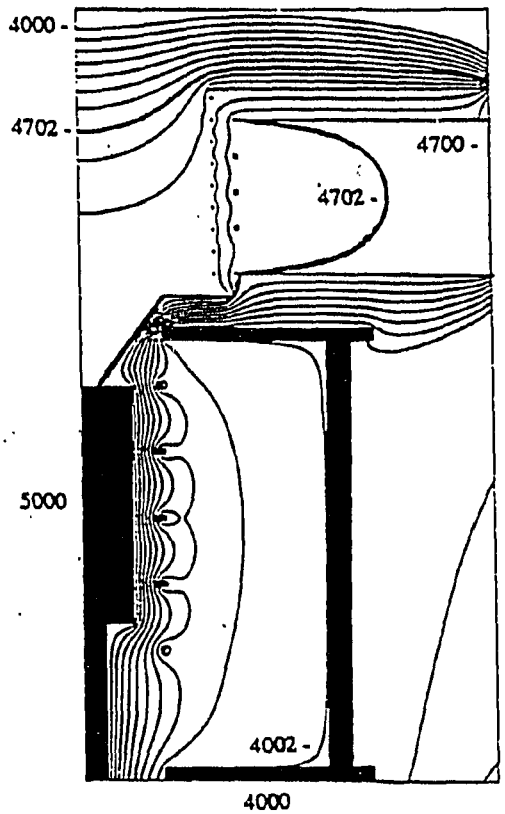

Figure 7 High acceleration after modifications. Va=5000v Ve=300v Vc=1000v

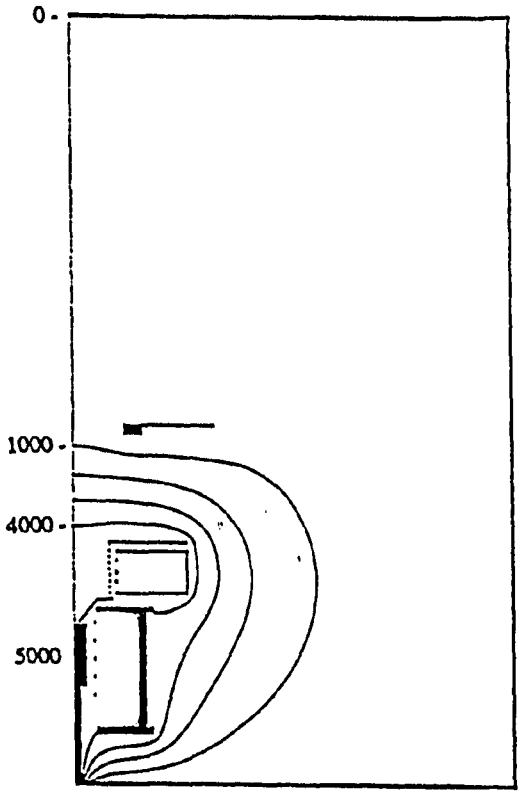

Figure 8 High acceleration after modifications. Va=5000v Ve=300v Vc=1000v

enough for the Mitsubishi source to be used as is in energy analyzer experiments. The bottom line is that the higher energy tail cannot be attributed to the presence of large clusters without first guaranteeing that all of the ionization is done at the same potential level and that there is no other source of higher energy particles.

Most of the problems suggested by this calculation arise from the crucible and acceleration potentials interfering with the ionization region. To remedy this, two modifications are considered to keep these fields out of the ionizer. First, the addition of a graphite cone is suggested to physically bridge the gap between the lower screen plate and the crucible as shown in figure 7 or alternatively the addition of a metal equivalent that hangs off the lower screen plate and ends in close proximity to the crucible nozzle. Either of these would improve the ionizer region greatly by totally isolating it from the crucible chamber. This would keep the crucible voltage from restricting the electrons in the ionizer and would also keep any ionized material from getting sucked backward toward the crucible chamber. It would also provide a physical barrier to separate the crucible filament electrons from the cluster beam. Secondly, too much acceleration is being packed into too little space right above the ionization can. If the acceleration plate is moved back two inches as in figure 8 or if it is eliminated totally, allowing the ions to be accelerated toward the grounded substrate, the leakage of the acceleration potential into the ionization can would be greatly reduced. This should result in a much larger ionization efficiency since the electrons would cross the center of the cluster beam at nearly their full energy and provide a much more level ionization region for energy analysis.

These modifications are not perfect though. Ion simulations show that they would produce a very uniform beam of small ionized clusters which is expected to be poor for film growth. The resulting large ionized cluster beam is then highly focused with most of the

large clusters landing within 3/16ths of an inch of the center of the substrate. This would be ideal for measurement of the cluster size or to study the effects of a high intensity large cluster beam on film growth but would be poor for growing a uniform film over the whole wafer. Again these characteristics of the ion trajectories may change significantly when space charge is introduced into the model.

Conclusions

The results of the computer calculation of the potential fields for the Mitsubishi ICB source point out several areas of concern. First is the question of the determination of cluster size by analyzing the energy of the ionized clusters produced by the source. The potential in the ionization region is lowered and sufficiently warped by the crucible and acceleration potentials that ionization can occur over a broad range of potentials. A high energy tail can also result from small clusters being ionized by highly energetic electrons from the crucible filament that pass near the crucible nozzle where the potential high. For these reasons, the Mitsubishi source as constructed is unsuitable for energy analyzer experiments.

The characteristics of the ionized cluster beam that are important for film deposition are also greatly influenced by the acceleration and crucible voltages interfering with the electrons in the ionization region. The multi-pass ionizer works as designed only at very low acceleration voltages. As the acceleration voltage is increased, the computer model shows that the ionization is restricted to the outer portion of the beam where the clusters ionized won't make it to the substrate. This may explain why films grown at higher acceleration voltages tend to be smoother and more crystalline instead of suffering more damage from the high energy flux of small ionized clusters. A full space charge treatment to be done in the near future will provide more insight into this. A simple experiment using a Faraday Cup placed in front of the substrate to measure the ion current as a function of the acceleration voltage would also be a quick way to determine the validity of this theory.

The addition of a conductor extending from the lower screen plate to the crucible cap would totally eliminate the problem of the crucible voltage interfering with the ionization region. Moving the acceleration plate back or totally removing it would then leave the ionization region free from interference and greatly increase the ionization uniformity and efficiency. While the resulting ion beam would be great for doing cluster measurements, it is not perfect. These modifications produce a very uniformly distributed beam of small ionized clusters that may damage the film and a tightly focused large cluster beam that hits only a small portion of the wafer. Modifying the source so that it produces a uniform large cluster beam and insures that few small ionized clusters hit the substrate will clearly take more effort and will probably require the consideration of the space charge.

References

1. I. Yamada and T. Takagi, Thin Film Solids 80, (1981) 105-115.

2. W. Knauer, J. Appl Phys 62 (3), (1 Aug 1987) 841.

3. H. Usui, A. Ueda, I. Yamada, and T. Takagi, ISIAT 85, (1985) 39.

4. H. Usui, A. Ueda, I. Yamada, and T. Takagi, ISIAT 85, (1985) 45.

5. T. Takagi, H.Takaoka, Y.Kuriyama, and K. Matsubara, Thin Solid Films 126, (1985) 149-154.

6. T. Takagi, I.Yamada, and A. Sasaki, Thin Solid Films 45, (1977) 569-576.

7. T. Takagi, I.Yamada, and A. Sasaki, Thin Solid Films 39, (1976) 207-217.

8. T. Takagi, I.Yamada, and A. Sasaki, Proc. 7th Intern. Vac. Congr., (1977) 1915.

9. H. Usui, I.Yamada, and T. Takagi, ISIAT 83, (1983) 1247.

10. M. Kyosaka, T. Saito, K. Matsubara, and T.Takagi, ISIAT 82, (1982) 52.

11. Y. Minowa, K. Yamanishi, and K. Tsukamoto, J. Vac. Sci. Technol. B 1 (4), (Oct-Dec 1983) 1148.

The Program EMITS

```
      PROGRAM EMITS
C
C
      REAL SOLD(0:148,0:280),SNEW(0:148,0:280),
     +     LOLD(0:144,0:256),LNEW(0:144,0:256),A,D,
     +     SMAXDIFF,LMAXDIFF
C
      INTEGER T,I,R,Z,ITER,VA,VE,VC,LR,LZ,SR,SZ
C
      CHARACTER*1 RD
C
C
      CALL LINK('UNIT5=(parms,TEXT),UNIT7=(sin,TEXT),
     +           UNIT8=(lin,TEXT),UNIT10=(maxdiff,TEXT),
     +           UNIT17=(sout,TEXT),UNIT18=(lout,TEXT)//')
C
      READ(5,1000)VA,VE,VC,RD,ITER
 1000 FORMAT(I5,I4,I5,A1,I7)
      IF (RD.NE.'Y') GOTO 25
      READ(8,*)
      DO 10 Z=0,256
      DO 10 R=0,144
   10 READ(8,*)LOLD(R,Z)
      READ(7,*)
      DO 20 Z=0,280
      DO 20 R=0,148
   20 READ(7,*)SOLD(R,Z)
C
C               SET PERMANENT BC'S
C
   25 DO 26 R=0,2
      LOLD(R,0)=VA
   26 LOLD(R,256)=0
      LOLD(3,0)=FLOAT(VA)/2.
      LOLD(3,256)=0
      DO 30 R=4,144
      LOLD(R,0)=0
   30 LOLD(R,256)=0
      DO 50 Z=1,255
   50 LOLD(144,Z)=0
C
C             ITERATION
C
      DO 500 I=1,ITER
```

```
      DO 100 R=1,147
      DO 100 Z=1,279
  100 SNEW(R,Z)=(SOLD(R,Z+1)+SOLD(R,Z-1)+SOLD(R+1,Z)
                 +SOLD(R-1,Z))/4
     +           +(SOLD(R+1,Z)-SOLD(R-1,Z))/(8*R)
       DO 110 Z=144,279
  110 SNEW(0,Z)=(SOLD(0,Z+1)+SOLD(0,Z-1)+2*SOLD(1,Z))/4
      SNEW(0,280)=(SOLD(0,279)+2*SOLD(1,280)+3*SOLD(0,280)/4+
     +              LOLD(0,89)/4)/4
      DO 120 R=1,65
      T=R/4
  120 SNEW(R,280)=(SOLD(R-1,280)+SOLD(R+1,280)+SOLD(R,279)+
     +              3*SOLD(R,280)/4+((R-4*T)*LOLD(T+1,89)+
     +              (4-R+4*T)*LOLD(T,89))/16)/4+
     +             (SOLD(R+1,280)-SOLD(R-1,280))/(8*R)
      DO 122 Z=1,279
      T=Z/4
      D=((Z-4*T)*LOLD(38,19+T)+(4-Z+4*T)*LOLD(38,18+T))/16+
     +   3*SOLD(148,Z)/4
  122 SNEW(148,Z)=(SOLD(147,Z)+SOLD(148,Z+1)+SOLD(148,Z-1)+D)/4+
     +              (D-SOLD(147,Z))/1184.
      SNEW(148,0)=(SOLD(147,0)+SOLD(148,1)+3*SOLD(148,0)/2+
     +              LOLD(38,18)/4+LOLD(37,17)/4)/4+
     +             (LOLD(38,18)/4+3*SOLD(148,0)/4
                   -SOLD(147,0))/1184.
      DO 124 R=105,147
      T=R/4
  124 SNEW(R,0)=(SOLD(R+1,0)+SOLD(R-1,0)+SOLD(R,1)+
     +            3*SOLD(R,0)/4+((R-4*T)*LOLD(T+1,17)+
     +            (4-R+4*T)*LOLD(T,17))/16)/4+
     +           (SOLD(R+1,0)-SOLD(R-1,0))/(8*R)
      DO 126 R=9,28
      T=R/4
  126 SNEW(R,0)=(SOLD(R+1,0)+SOLD(R-1,0)+SOLD(R,1)+
     +            3*SOLD(R,0)/4+((R-4*T)*LOLD(T+1,17)+
     +            (4-R+4*T)*LOLD(T,17))/16)/4+
     +           (SOLD(R+1,0)-SOLD(R-1,0))/(8*R)
C
      DO 130 Z=1,17
      DO 130 R=3,37
  130 LNEW(R,Z)=(LOLD(R,Z+1)+LOLD(R,Z-1)+LOLD(R+1,Z)
                 +LOLD(R-1,Z))/4
     +          +(LOLD(R+1,Z)-LOLD(R-1,Z))/(8*R)
      DO 140 R=1,37
      DO 140 Z=89,255
  140 LNEW(R,Z)=(LOLD(R,Z+1)+LOLD(R,Z-1)+LOLD(R+1,Z)
                 +LOLD(R-1,Z))/4
```

```
     +          +(LOLD(R+1,Z)-LOLD(R-1,Z))/(8*R)
      DO 145 R=38,143
      DO 145 Z=1,255
  145 LNEW(R,Z)=(LOLD(R,Z+1)+LOLD(R,Z-1)+LOLD(R+1,Z)
                 +LOLD(R-1,Z))/4
     +          +(LOLD(R+1,Z)-LOLD(R-1,Z))/(8*R)
      DO 160 Z=89,255
  160 LNEW(0,Z)=(2*LOLD(1,Z)+LOLD(0,Z+1)+LOLD(0,Z-1))/4
C
C            OVERWRITE OTHER BC'S ON NEW MESH
C
      DO 200 Z=1,17
      LNEW(0,Z)=VA
      LNEW(1,Z)=VA
  200 LNEW(2,Z)=VA
      DO 210 R=0,8
      DO 210 Z=0,143
  210 SNEW(R,Z)=VA
      DO 220 R=9,18
      DO 220 Z=57,143
  220 SNEW(R,Z)=VA
      DO 230 Z=48,144,24
      SNEW(29,Z)=VA-VC+2
      SNEW(29,Z-1)=VA-VC+2
      SNEW(28,Z-1)=VA-VC+2
  230 SNEW(28,Z)=VA-VC+2
      DO 240 Z=0,4
      DO 240 R=29,104
  240 SNEW(R,Z)=VA-VC
      DO 250 R=7,26
  250 LNEW(R,17)=VA-VC
      DO 260 R=88,96
      DO 260 Z=5,159
  260 SNEW(R,Z)=VA-VC
      DO 270 Z=160,164
      DO 270 R=30,104
  270 SNEW(R,Z)=VA-VC
      DO 280 Z=176,248,8
  280 SNEW(48,Z)=VA
      DO 281 R=30,53
  281 SNEW(R,176)=VA
      DO 282 R=48,148
  282 SNEW(R,252)=VA
      DO 284 Z=200,226,13
      SNEW(56,Z)=VA-VE+2
      SNEW(56,Z+1)=VA-VE+2
      SNEW(57,Z+1)=VA-VE+2
```

```
  284 SNEW(57,Z)=VA-VE+2
      DO 286 R=56,148
      SNEW(R,184)=VA-VE
  286 SNEW(R,240)=VA-VE
      DO 288 Z=185,239
  288 SNEW(148,Z)=VA-VE
      DO 290 Z=268,280
      DO 290 R=66,91
  290 SNEW(R,Z)=0
      DO 292 R=92,148
  292 SNEW(R,280)=0
      DO 294 R=38,46
  294 LNEW(R,88)=0
C
      DO 420 R=0,37
      DO 420 Z=18,88
  420 LNEW(R,Z)=SNEW(R*4,(Z-18)*4)
C
C             PRINT MAXDIFF EVERY 1000
      T=I/1000
      IF (I.NE.T*1000) GOTO 320
      LMAXDIFF=0
      DO 300 R=0,143
      DO 300 Z=1,255
      IF (ABS(LNEW(R,Z)-LOLD(R,Z)).LT.LMAXDIFF) GOTO 300
      LMAXDIFF=ABS(LNEW(R,Z)-LOLD(R,Z))
      LR=R
      LZ=Z
  300 CONTINUE
      SMAXDIFF=0
      DO 310 R=0,148
      DO 310 Z=0,280
      IF (ABS(SNEW(R,Z)-SOLD(R,Z)).LT.SMAXDIFF) GOTO 310
      SMAXDIFF=ABS(SNEW(R,Z)-SOLD(R,Z))
      SR=R
      SZ=Z
  310 CONTINUE
      WRITE(10,*)I,SR,SZ,SMAXDIFF,LR,LZ,LMAXDIFF
C
C             OLD<==NEW
  320 DO 400 R=0,143
      DO 400 Z=1,255
  400 LOLD(R,Z)=LNEW(R,Z)
      DO 410 R=0,148
      DO 410 Z=0,280
  410 SOLD(R,Z)=SNEW(R,Z)
C
```

```
  500 CONTINUE
C       END OF ITERATION LOOP
C
C            DUMP EVERYTHING OUT
      WRITE(18,*)' 145  257  0  0'
      DO 610 Z=0,256
      DO 610 R=0,144
  610 WRITE(18,*)LOLD(R,Z)
      WRITE(17,*)' 149  281  0  0'
      DO 620 Z=0,280
      DO 620 R=0,148
  620 WRITE(17,*)SOLD(R,Z)
      END
```

The Program EMTRAJ

```
      PROGRAM EMTRAJ
C
C
      REAL*8 V(0:148,0:280),VCF,VIF,
     +       AR,AZ,VR,VZ,Z,R,D,VA,VCC,VIC,T,K
C
      INTEGER RI,ZI,Z0,I,T1,RIN,ZIN,RB,ZB,KI
C
      DATA QME/-1.75641E+11/,H/.000396875/,PI/3.1415926/,
     +     RAD/0.64/
C
C
      READ(5,*)
      DO 10 ZI=0,280
      DO 10 RI=0,148
   10 READ(5,*)V(RI,ZI)
      VA=V(1,80)
      VCC=V(60,1)
      VCF=V(28,48)
      VIC=V(140,184)
      VIF=V(56,200)
      WRITE(6,*)' -1   20 !'
      CALL BC
      V0=300000
      DO 200 J=1,8
      DO 200 THETA=0,1.75*PI,PI/4
      WRITE(7,*)J,THETA*180/PI
      R=28.5
      IF (J.GT.5) R=56.5
      Z=47.5+24*(J-1)
      IF (J.GT.5) Z=200.5+13*(J-6)
      VR=V0*COS(THETA)
      VZ=V0*SIN(THETA)
      T=0
      WRITE(6,*)R,Z,' R !'
      DO 100 I=0,100000
      ZI=Z
      RI=R
      DT=3.968e-6/SQRT(VR**2+VZ**2)
      T=T+DT
      T1=I/50
      AR=QME*((ZI+1-Z)*(V(RI+1,ZI)-V(RI,ZI))+
     +        (Z-ZI)*(V(RI+1,ZI+1)-V(RI,ZI+1)))/H
      AZ=QME*((RI+1-R)*(V(RI,ZI)-V(RI,ZI+1))+
```

```
     +          (R-RI)*(V(RI+1,ZI)-V(RI+1,ZI+1)))/H
      R=R-(VR*DT+0.5*AR*DT**2)/H
      Z=Z+(VZ*DT+0.5*AZ*DT**2)/H
      VR=VR+AR*DT
      VZ=VZ+AZ*DT
      IF (R.LT.0.) VR=-VR
      IF (R.LT.0.) R=-R
      RIN=R
      ZIN=Z
      IF (((Z.LT.0.).OR.(Z.GT.280.)).OR.
     +    (R.GT.148.)) GOTO 190
      IF (RI.EQ.RIN) GOTO 80
      RB=RI
      IF (RIN.GT.RI) RB=RIN
      IF ((RB.NE.48).OR.((ZI.GT.252).OR.(ZI.LT.180)))
     +    GOTO 70
      KI=(Z+RAD-184)/8
      K=Z+RAD-184-KI*8
      IF (K.LE.2*RAD) GOTO 190
   70 IF (V(RB,ZI).NE.V(RB,ZI+1)) GOTO 80
      IF (((V(RB,ZI).EQ.VA).OR.(V(RB,ZI).EQ.VCC)).OR.
     +    (V(RB,ZI).EQ.VIC)) GOTO 190
      IF ((T.GT.1E-9).AND.((V(RB,ZI).EQ.VCF).OR.
     +    (V(RB,ZI).EQ.VIF)))  GOTO 190
   80 IF (ZIN.EQ.ZI) GOTO 90
      ZB=ZI
      IF (ZIN.GT.ZI) ZB=ZIN
      IF (V(RI,ZB).NE.V(RI+1,ZB)) GOTO 90
      IF (((V(RI,ZB).EQ.VA).OR.(V(RI,ZB).EQ.VCC)).OR.
     +    (V(RI,ZB).EQ.VIC)) GOTO 190
      IF ((T.GT.1E-9).AND.((V(RI,ZB).EQ.VCF).OR.
     +    (V(RI,ZB).EQ.VIF))) GOTO 190
   90 IF (I.EQ.T1*50) WRITE(6,1010)R,Z
 1000 FORMAT(0PF8.3,2X,1PE10.3,2X,0PF7.3,2X,1PE10.3,
             0PF8.3,' ns')
 1010 FORMAT(2F9.3,' !')
  100 CONTINUE
  190 WRITE(7,1000)R,VR,Z,VZ,T*1e9
  200 CONTINUE
      WRITE(6,*)' -1 !'
      END
C
      SUBROUTINE BC
C
C
      WRITE(6,*)' 0 0 B !'
      WRITE(6,*)' 8 0 !'
```

```
      WRITE(6,*)' 8 57 !'
      WRITE(6,*)' 18 57 !'
      WRITE(6,*)' 18 143 !'
      WRITE(6,*)' 0 143 !'
C
      WRITE(6,*)' 29 0 B !'
      WRITE(6,*)' 29 4 !'
      WRITE(6,*)' 88 4 !'
      WRITE(6,*)' 88 160 !'
      WRITE(6,*)' 30 160 !'
      WRITE(6,*)' 30 164 !'
      WRITE(6,*)' 96 164 !'
      WRITE(6,*)' 96 0 !'
      WRITE(6,*)' 29 0 !'
C
      WRITE(6,*)' 30 176 B !'
      WRITE(6,*)' 53 176 !'
C
      WRITE(6,*)' 56 184 B !'
      WRITE(6,*)' 148 184 !'
      WRITE(6,*)' 148 240 !'
      WRITE(6,*)' 56 240 !'
C
      WRITE(6,*)' 48 252 B !'
      WRITE(6,*)' 148 252 !'
      DO 1300 I=1,9
      WRITE(6,*)' 48 ',176+I*8,' B !'
 1300 WRITE(6,*)' 48 ',176.5+I*8,' ! '
C
      WRITE(6,*)' 91 280 B !'
      WRITE(6,*)' 91 268 !'
      WRITE(6,*)' 66 268 !'
      WRITE(6,*)' 66 280 !'
      WRITE(6,*)' 148 280 !'
      RETURN
      END
```

The Program IMTRAJ

```
      PROGRAM IMTRAJ
C
C
      REAL*8 V(0:144,0:256),
     +       AR,AZ,VR,VZ,Z,R,D,T
C
      INTEGER RI,ZI,R0,Z0,I,T1,N
C
      DATA QMA/892943./,H/.0015875/,PI/3.1415926/
C
C
      READ(4,*)N
      READ(5,*)
      DO 10 ZI=0,256
      DO 10 RI=0,144
   10 READ(5,*)V(RI,ZI)
      WRITE(6,*)' -1   20 !'
      CALL BC
      V0=570
      DO 200 Z0=66,76,2
      DO 200 R0=0,10,2
      R=R0
      Z=Z0
      VR=-V0*SIN(ATAN(R/(Z-54.)))
      VZ=V0*COS(ATAN(R/(Z-54.)))
      T=0
      WRITE(7,1000)N,R,VR,Z,VZ,T
      WRITE(6,*)R,Z,' R !'
      DO 100 I=0,10000
      ZI=Z
      RI=R
      DT=0.05*H/SQRT(VR**2+VZ**2)
      T=T+DT
      T1=I/10
      AR=QMA/N*((ZI+1-Z)*(V(RI+1,ZI)-V(RI,ZI))+
     +         (Z-ZI)*(V(RI+1,ZI+1)-V(RI,ZI+1)))/H
      AZ=QMA/N*((RI+1-R)*(V(RI,ZI)-V(RI,ZI+1))+
     +         (R-RI)*(V(RI+1,ZI)-V(RI+1,ZI+1)))/H
      R=R-(VR*DT+0.5*AR*DT**2)/H
      Z=Z+(VZ*DT+0.5*AZ*DT**2)/H
      VR=VR+AR*DT
      VZ=VZ+AZ*DT
      IF (R.LT.0.) VR=-VR
      IF (R.LT.0.) R=-R
```

```
      IF (((Z.LT.59).OR.(Z.GT.255)).OR.
     +    (R.GT.144)) GOTO 190
      IF ((Z.LE.88).AND.((R.GE.37).OR.((Z.GE.81).AND.
     +    (R.GE.16.5)))) GOTO 190
      IF (((Z.LE.81).AND.(Z.GE.78)).AND.
     +    (R.GE.12)) GOTO 190
      IF (I.EQ.T1*10) WRITE(6,1010)R,Z
 1000 FORMAT(I5,1X,0PF8.3,2X,1PE10.3,2X,0PF7.3,2X,
     +       1PE10.3,0PF8.3,' us')
 1010 FORMAT(2F9.3,' !')
  100 CONTINUE
  190 WRITE(7,1000)N,R,VR,Z,VZ,T*1e6
  200 CONTINUE
      WRITE(6,*)' -1 !'
      END
C
      SUBROUTINE BC
C
C
      WRITE(6,*)' 0 0 B !'
      WRITE(6,*)' 2 0 !'
      WRITE(6,*)' 2 32 !'
      WRITE(6,*)' 5 32 !'
      WRITE(6,*)' 5 54 !'
      WRITE(6,*)' 0 54 !'
C
      WRITE(6,*)' 0 0 B !'
      WRITE(6,*)' 144 0 !'
      WRITE(6,*)' 144 256 !'
      WRITE(6,*)' 0 256 !'
C
      WRITE(6,*)' 7 17 B !'
      WRITE(6,*)' 24 17 !'
      WRITE(6,*)' 24 59 !'
      WRITE(6,*)' 7.5 59 !'
      WRITE(6,*)' 7.5 58 !'
      WRITE(6,*)' 22 58 !'
      WRITE(6,*)' 22 19 !'
      WRITE(6,*)' 7 19 !'
      WRITE(6,*)' 7 17 !'
C
      WRITE(6,*)' 7.5 62 B !'
      WRITE(6,*)' 13 62 !'
C
      WRITE(6,*)' 14 64 B !'
      WRITE(6,*)' 37 64 !'
      WRITE(6,*)' 37 78 !'
```

```
      WRITE(6,*)' 14 78 !'
C
      WRITE(6,*)' 12 81 B !'
      WRITE(6,*)' 37 81 !'
      DO 10 ZI=64,80,2
      WRITE(6,*)' 12 ',ZI,' B !'
   10 WRITE(6,*)' 12 ',ZI,' !'
C
      WRITE(6,*)' 23 88 B !'
      WRITE(6,*)' 23 85 !'
      WRITE(6,*)' 16.5 85 !'
      WRITE(6,*)' 16.5 88 !'
      WRITE(6,*)' 46 88 !'
      RETURN
      END
```

APPENDIX B - COMPUTER PROGRAMS FOR THE EATON SIMULATIONS

Both the space-charge calculations and the time-of-flight simulations of the Eaton ICB source were done using the program EPERT15 that follows. The method used has already been described in general so this appendix will address the detailed operation and the testing of this program.

Laplace's equation states that the second derivative of the potential equals zero in the absence of charges. The first derivative, the electric field, is therefore a constant while the potential itself is linear. In a two dimensional mesh, the potential at a given point is just the average of its four neighboring mesh points. Mathematically, this point is reached by doing a second order Taylor's expansion of the potential for the four neighboring mesh points. Combining these expansions yields the equation below that can be used iteratively to determine the potential Ø(r,z) at each mesh point.

$$Ø(r,z) = \frac{Ø(r+h,z) + Ø(r-h,z) + Ø(r,z+h) + Ø(r,z-h)}{4}$$

This is the potential for a mesh where the separation between points is the distance h. All the calculations are done in a cylindrical coordinate system which adds another term proportional to the distance r from the center axis.

$$Ø(r,z) = \frac{Ø(r+h,z) + Ø(r-h,z) + Ø(r,z+h) + Ø(r,z-h)}{4} + \frac{Ø(r+h,z) - Ø(r-h,z)}{8\,r/h}$$

When the space-charge of the ions and electrons are considered, Poisson's equation is used where the second derivative of the potential is proportional to the charge density ρ(r,z). The potential at each mesh point is now the average of its four neighbors plus the cylindrical term and a constant proportional to the charge density at that mesh point.

$$Ø(r,z) = \frac{Ø(r+h,z) + Ø(r-h,z) + Ø(r,z+h) + Ø(r,z-h)}{4} + \frac{Ø(r+h,z) - Ø(r-h,z)}{8\,r/h} + \frac{h^2\,\rho(r,z)}{4\,\varepsilon}$$

Starting with the boundary conditions from the geometry of the source and the voltages applied to different parts of the source, the potential at all points between the boundaries can be determined by repeatedly applying this equation to the mesh until sufficient accuracy is achieved. After sweeping through the entire mesh 20,000-30,000 times, the potential converges to within a thousandth of a volt of the true potential. This is close enough to insure no chance of deviation of the electron and ion trajectories.

Each electron starts at the edge of the filament with a thermal velocity randomly generated from a gamma distribution around the average thermal velocity which is estimated from the temperature of the filament to be around 250,000 m/s (0.18 eV). This amount of detail is done to be as accurate as possible but the final results are not very sensitive to changes in these initial conditions. The distribution of starting positions for the ions is proportional to the beam density and the electron density in the ionization can. The neutral beam is assumed to be a uniformly expanding sphere centered on the crucible nozzle. The initial velocity V_0 is determined from the crucible temperature for a given source metal using the formula below.

$$V_o = \sqrt{\frac{8\,R\,T_{cruc}}{\pi\ m_a}}$$

R is the gas constant and m_a is the atomic mass of the source metal. For silver the thermal velocity is 570 m/s which is vectored directly away from the nozzle. No thermal distribution was used here but experiments at different initial velocities showed no significant differences. The potential fields everywhere are just too strong compared to the small initial energy of around 0.18 eV/atom for silver.

The iterative movement of the electrons and ions is demonstrated in the excerpt below.

```
 DO 840 I=1,IMX
  RI=R(I)
  ZI=Z(I)
  AR=QM2/N(I)*((ZI+1-Z(I))*(VO(RI+1,ZI)-VO(RI,ZI))+
+                  (Z(I)-ZI)*(VO(RI+1,ZI+1)-VO(RI,ZI+1)))
  AZ=QM2/N(I)*((RI+1-R(I))*(VO(RI,ZI)-VO(RI,ZI+1))+
+                  (R(I)-RI)*(VO(RI+1,ZI)-VO(RI+1,ZI+1)))
  DT(I)=0.1/SQRT(VR(I)**2+VZ(I)**2+0.05*(ABS(AR)+ABS(AZ)))
  TT(I)=TT(I)+DT(I)
  R(I)=R(I)-(VR(I)*DT(I)+0.5*AR*DT(I)**2)
  Z(I)=Z(I)+VZ(I)*DT(I)+0.5*AZ*DT(I)**2
  VR(I)=VR(I)+AR*DT(I)
  VZ(I)=VZ(I)+AZ*DT(I)
```

```
        RI=R(I)
        ZI=Z(I)
        F(I)=1-BC(RI,ZI)*BC(RI+1,ZI)*BC(RI+1,ZI+1)*BC(RI,ZI+1)
C          F(I)=0 iff four bc's are 1's
        T4=(RB-R(I))/RB
C          T4=0 : if (r le 0) T4=1
        T2=1-2*REFLECT*T4
C          Reflect particle if r lt 0 and reflect is on
        R(I)=R(I)*T2
        VR(I)=VR(I)*T2
        T1=(ZB-Z(I))/ZB
        T2=Z(I)/ZB
        T3=R(I)/RB
        F(I)=F(I)*(1-T1-T2)*(1-T3-T4*(1-REFLECT))
C          F=0 iff particle is out of bounds
  840   CONTINUE
```

The time step dt is determined for each particle from its velocity so that it moves approximately one tenth of the distance between mesh points in each time step. This assures a reasonable accuracy of the trajectories which are in response to a non-smooth potential. Runs set so each time step produced a movement of one hundredth of the distance between mesh points showed no difference. The acceleration AR and AZ in the $\hat{r}$ and $\hat{z}$ directions are calculated from the mesh potential V(R,Z). Each iteration, the change in position dx and the change in velocity dv is given by the equations below for each charged particle.

$$dx = x - x_o = v_x\, dt + \frac{1}{2}\, a_x\, dt^2$$

$$dv = v - v_o = a\, dt$$

The last lines in the program excerpt are to keep the particles within the boundaries. Particles get reflected as they cross the center axis at R=0 and get destroyed if they hit any part of the source. The source geometry is kept in the mesh BC(R,Z) in bitmapped fashion with a one meaning it is a boundary. The unusual lines at the end of the excerpt constitute a system of doing the necessary logic without using if/then statements that prevent vectorization of the code (which would cause the whole program to take about 50 times longer to execute). This method of applying the necessary logic as well as the bitmapped source boundaries are essential for the efficient operation of this code.

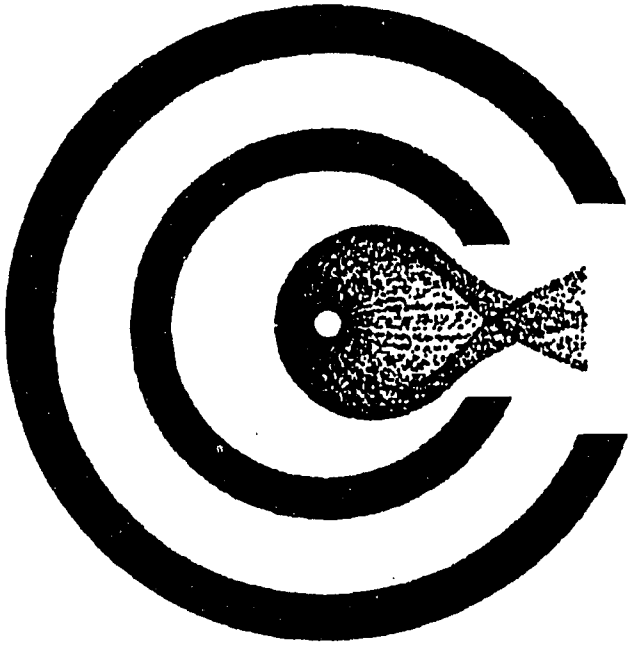

Figure 26 The electron density in the filament area from the program ESIM11

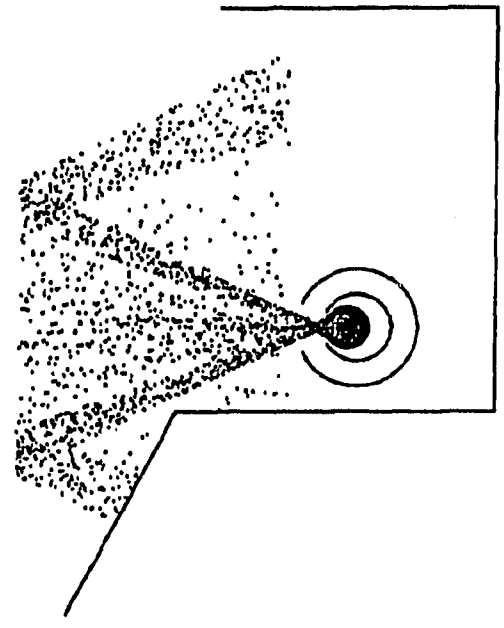

Figure 27 Electron beam in the ionizer from the program ESIM11

The program EPERT15 has checks built in to insure that no charge is lost at any point during a run and calculations were done by hand to double check everything possible. An example of this is that the magnitude of the potential can be verified by assuming a uniform charge distribution of a similar geometry to the computer generated charge distribution. Since this is a self-consistent method, a necessary test was that the final state that the program converges to be independent of the starting state. The final state in every test was found to be independent of whether the initial state was at a higher or lower operating point. In addition to these tests, extreme care was taken to trace every part of the program and recalculate every constant to assure accuracy of the program.

Furthermore, the results were matched where possible to those of the program ESIM11 that uses a more traditional approach to simulate the electron beam emitted by the filament. This program, listed at the end of this appendix, uses a particle-particle/particle-mesh technique in which Poisson's equation is solved at every time step as the electrons are moved. The long range force due to the boundary potentials and the distant electrons is solved on a mesh (particle-mesh) while the short range particle-particle forces are accounted for directly. This requires a careful separation of the long and short range forces which, along with the need to solve Poisson's equation at each iteration, makes for a very time consuming method. Figures 26 and 27 show the electrons in the filament area and the ionization can after the steady

state was reached. The electron beam is very similar to that predicted by EPERT15 which produced the same spread with the characteristics of higher concentrations near the edges of the beam for the same parameters. This 25 ns run took 11 hours of cpu time to simulate just a 1 mA electron beam, about one tenth of the standard electron current in the Eaton source. While this method requires too much computer time to be useful for investigating the normal operation of the source, it is helpful in corroborating the self-consistent method.

The Program EPERT15

```
      PROGRAM EPERT15

C         Epert is a program that uses a perturbative or
C     self-consistent technique to calculate the potential
C     fields and the charge distributions inside and outside
C     of the Eaton ionized cluster beam source.
C
C     Error in s & l is 10X error for f * w which is read in
C     Gamma (a=2) +/- 10% distribution of initial e- energies
C     Damping of VO=DF*VO+(1-DF)*VSAVE
C     Ionization is dependent on electron concentration

C     L=h=396.875 um   SLICE WIDTH (factors out of calc)
C     Vo=570 m/s  INITIAL VELOCITY OF IONS
C     Icreate is ion creation current (in uA) read in
C     Ie is electron current (in mA) read in

      REAL QL(0:144,0:240),QS(0:112,0:144),QSE(0:112,0:144),
     +     QF(0:128,0:128),QW(0:128,0:128),Q(100997)
      EQUIVALENCE (Q(1),QL(0,0)),(Q(34946),QS(0,0)),(Q(51331),
     +     QSE(0,0)),(Q(67716),QF(0,0)),(Q(84357),QW(0,0))

      REAL VLO(0:145,0:241),VSO(0:113,0:145),
     +     VFO(0:129,0:129),VWO(0:129,0:129),VO(85776)
      EQUIVALENCE (VO(1),VLO(0,0)),(VO(35333),VSO(0,0)),
     +     (VO(51977),VFO(0,0)),(VO(68877),VWO(0,0))

      REAL VLN(0:145,0:241),VSN(0:113,0:145),
     +     VFN(0:129,0:129),VWN(0:129,0:129),VN(85776)
      EQUIVALENCE (VN(1),VLN(0,0)),(VN(35333),VSN(0,0)),
     +     (VN(51977),VFN(0,0)),(VN(68877),VWN(0,0))

      REAL VSAVE(85776)

      INTEGER BCL(0:145,0:241),BCS(0:113,0:145),
     +     BCF(0:129,0:129),BCW(0:129,0:129),BC(85776)
      EQUIVALENCE (BC(1),BCL(0,0)),(BC(35333),BCS(0,0)),
     +     (BC(51977),BCF(0,0)),(BC(68877),BCW(0,0))

      REAL A,ED,MAXDIFF,E4HEO,QDT,QD(2500),ME,IW(0:48,143),
     +     V0,QMH2,RN,ERR,H,MA,AM,PHI,IWTOT,F,IWLO,
     +     R(2500),Z(2500),VR(2500),VZ(2500),MD(85776),
     +     TT(2500),TMN(40),TA(40),TMX(40),D,FV,QDSUM,
     +     TOF(0:1000),TH(0:1000),SM(0:1000),EF(0:1000),CF(20),
```

```
     +      TEXIT,DF,DFE,IEMULT,ECREATE,IFC,ICREATE,IE

      INTEGER T,I,RI,ZI,ITER,VA,VE,ZMX,ZMN,R4,Z4,CS(20),NCS,
     +        N(2500),CN,J,I2,NIONS,NMP,NI(60),RMX,IMX,CI,
     +        NTI,NTE,TNI,NIB,NIMP,NITS,RMN,MAXIND,ETER,
     +        NEXIT,NEE,NELF,CMX,MDLO,MDHI

      LOGICAL DAMP

      CHARACTER RDVIN*1,RDQIN*1,GARB*10,IEADJ*1,IFCADJ*1

      DATA V0/1.43622/,E/1.6E-19/,EO/8.85E-12/,H/0.000396875/,
     +     ME/9.1E-31/,PI/3.1415926/,
     +     E4HEO/1.13884E-5/,DAMP/.FALSE./

      COMMON QD,R,Z,VR,VZ,N,TT

      CALL LINK('UNIT5=(parms,TEXT),UNIT7=(lin,TEXT),
     + UNIT8=(sin,TEXT),UNIT9=(fin,TEXT),
     + UNIT10=(win,TEXT),UNIT17=(lout,TEXT),
     + UNIT18=(sout,TEXT),UNIT19=(fout,TEXT),
     + UNIT20=(wout,TEXT)//')
      CALL LINK('UNIT11=(kia,TEXT),
     + UNIT6=(pert6,TEXT),UNIT27=(ql,TEXT),
     + UNIT28=(qsi,TEXT),UNIT29=(qf,TEXT,ACCESS=RW),
     + UNIT30=(qw,TEXT,ACCESS=RW),UNIT38=(qse,TEXT,ACCESS=RW),
     + UNIT41=(tof,TEXT),UNIT42=(subth,TEXT),
     + UNIT43=(ef,TEXT)//')


C         READ IN PARAMETERS

      DO 5 I=1,85776
       BC(I)=0
       VO(I)=0
    5  VN(I)=0
      DO 6 I=1,100997
    6  Q(I)=0
 1000 FORMAT(A10,I8)
 1010 FORMAT(A10,F10.5)
 1020 FORMAT(A10,A1)
C       Va = Acceleration voltage
      READ(5,1000)GARB,VA
C       Ve = Ionization voltage
      READ(5,1000)GARB,VE
C       Err = Error limit for field calculations
      READ(5,1010)GARB,ERR
```

```
C       Df & Dfe = Damping coefficients
        READ(5,1010)GARB,DF
        READ(5,1010)GARB,DFE
        WRITE(6,*)' Va=',VA,'  Ve=',VE,'  Error=',ERR,'   DF=',DF,
       +          '  DFE=',DFE
C       Ecreate = Electron creation rate at filament (in mA)
        READ(5,1010)GARB,ECREATE
C       NTE = Number of Test Electrons
        READ(5,1000)GARB,NTE
C       Eter = Number of iterations for w & f meshes (electrons)
        READ(5,1000)GARB,ETER
        IF ((ETER.GT.0).AND.(ECREATE.LT.0.5)) STOP
C       IeAdj = Whether or not electron current is adjusted
                to Ie
        READ(5,1020)GARB,IEADJ
C       Ie = Electron current emitted from filament area (in mA)
        READ(5,1010)GARB,IE
        WRITE(6,*)' Ecreate=',ECREATE,'  NTE=',NTE,'  Eter=',ETER
        WRITE(6,*)' IeAdj=',IEADJ,'  Ie=',IE
C       Icreate = Ion creation rate in main slice (in uA)
        READ(5,1010)GARB,ICREATE
C       NTI = Number of Test Ions
        READ(5,1000)GARB,NTI
C       Iter = Number of iterations for the ions
        READ(5,1000)GARB,ITER
C       IfcAdj = Enable automatic adjusting of Icreate to
C                home in on the desired Ifc
        READ(5,1020)GARB,IFCADJ
C       Ifc = Faraday cup current
        READ(5,1010)GARB,IFC
        WRITE(6,*)' Icreate=',ICREATE,'  NTI=',NTI,'  ITER=',ITER
        WRITE(6,*)' IfcAdj=',IFCADJ,'  Ifc=',IFC
C       RdVIn = Whether or not to read in potential meshes or
C               start by calculating Laplace fields
        READ(5,1020)GARB,RDVIN
C       RdQIn = Whether or not to read in qw,qf,and qse
        READ(5,1020)GARB,RDQIN
C       AM = Atomic Mass (in grams)
        READ(5,1010)GARB,AM
        MA=AM/6.02E26
        NTE=2000*(NTE/2000)
        WRITE(6,*)' AM=',AM,'   RdVin=',RDVIN,'   RdQin=',RDQIN
        IF (RDQIN.EQ.'Y') THEN
         READ(38,*)
         DO 1 ZI=0,144
         DO 1 RI=0,112
          READ(38,*)QSE(RI,ZI)
```

```
     1    IF (QSE(RI,ZI).GT.0) QSE(RI,ZI)=0
          DO 3 ZI=0,144
     3    QSE(0,ZI)=QSE(0,ZI)/2
          READ(29,*)
          DO 7 ZI=0,128
          DO 7 RI=4,128
           READ(29,*)QF(RI,ZI)
     7    IF (QF(RI,ZI).GT.0) QF(RI,ZI)=0
          READ(30,*)
          DO 8 ZI=0,128
          DO 8 RI=0,128
           READ(30,*)QW(RI,ZI)
     8    IF (QW(RI,ZI).GT.0) QW(RI,ZI)=0
          ENDIF
C          NCS = Number of Cluster Sizes
         READ(5,1000)GARB,NCS
         WRITE(6,*)NCS,' Cluster sizes'
         IF (NCS.GT.0) THEN
          DO 2 I=1,NCS
C            CS = Cluster Size
C            CF = fraction of clusters that are this size
           READ(5,*)CS(I),CF(I)
     2    WRITE(6,*)' N=',CS(I),'  Fraction=',CF(I)
          ENDIF
         IF ((NCS.EQ.0).AND.(ITER.GT.0)) STOP
         IF (RDVIN.EQ.'Y') THEN
          READ(7,*)
          DO 10 ZI=0,240
          DO 10 RI=0,144
    10    READ(7,*)VLO(RI,ZI)
          READ(8,*)
          DO 20 ZI=0,144
          DO 20 RI=0,112
    20    READ(8,*)VSO(RI,ZI)
          READ(9,*)
          DO 30 ZI=0,128
          DO 30 RI=4,128
    30    READ(9,*)VFO(RI,ZI)
          READ(10,*)
          DO 40 ZI=0,128
          DO 40 RI=0,128
    40    READ(10,*)VWO(RI,ZI)
          DAMP=.TRUE.
          DO 50 I=1,85776
    50    VSAVE(I)=VO(I)
          ENDIF
```

```
C                SET BC MESH

C          LARGE MESH

       DO 120 RI=0,124
        BCL(RI,0)=1
  120   VLO(RI,0)=VA
       DO 130 RI=125,144
        BCL(RI,0)=1
  130   VLO(RI,0)=VA*(144.-RI)/20.
       DO 140 ZI=0,241
        BCL(145,ZI)=1
        BCL(144,ZI)=1
  140   VLO(144,ZI)=0
       DO 150 ZI=8,232,8
        VLO(124,ZI)=VA
  150   BCL(124,ZI)=1
       DO 160 RI=0,144
        VLO(RI,240)=0
        BCL(RI,240)=1
  160   BCL(RI,241)=1
       DO 170 RI=0,20
        VLO(RI,230)=0
        VLO(RI,229)=0
        BCL(RI,230)=1
  170   BCL(RI,229)=1
       DO 180 RI=0,28
       DO 180 ZI=1,64
        BCL(RI,ZI)=1
  180   VLO(RI,ZI)=VA
       DO 185 ZI=65,75
        RMN=(ZI-64)*7/11.+2
        DO 185 RI=RMN,28
         BCL(RI,ZI)=1
  185    VLO(RI,ZI)=VA
       DO 187 ZI=76,112
        DO 187 RI=0,28
  187    BCL(RI,ZI)=1

C          SMALL MESH

       DO 200 RI=0,12
  200   BCS(RI,0)=1
       DO 210 ZI=0,48
        RMN=ZI*26./48.+12
        RMX=ZI*3/4.+16
        IF (ZI.GE.32) RMX=113
```

```
      DO 210 RI=RMN,RMX
       VSO(RI,ZI)=VA
210    BCS(RI,ZI)=1
      DO 220 ZI=49,145
       VSO(112,ZI)=VA
       BCS(112,ZI)=1
220    BCS(113,ZI)=1
      DO 230 RI=48,111
       VSO(RI,144)=VA
       BCS(RI,144)=1
230    BCS(RI,145)=1
      DO 240 RI=65,96
      DO 240 ZI=52,84
       D=SQRT((RI-80.)**2+(ZI-68.)**2)
       IF (D.LE.16.) THEN
        IF (RDVIN.NE.'Y') VSO(RI,ZI)=VA
        BCS(RI,ZI)=1
        ENDIF
240    CONTINUE
      DO 245 RI=0,48
       BCS(RI,144)=1
245    BCS(RI,145)=1

C      FILAMENT AREA

      DO 250 ZI=0,128
      DO 250 RI=0,128
       D=SQRT((RI-64.)**2+(ZI-64.)**2)
       IF (D.LE.3.072) THEN
        VFO(RI,ZI)=VA-VE+1.5
        BCF(RI,ZI)=1
        ENDIF
       IF ((D.GE.32.AND.D.LE.40).AND.((RI.GT.64).OR.
     +       (ABS(ZI-64).GE.16))) THEN
        VFO(RI,ZI)=VA-VE
        BCF(RI,ZI)=1
        ENDIF
       IF ((D.GE.56).AND.((RI.GT.64).OR.(ABS(ZI-64).GE.24)))
        THEN
        VFO(RI,ZI)=VA
        BCF(RI,ZI)=1
        ENDIF
250    CONTINUE
      DO 255 ZI=40,88
       BCF(4,ZI)=1
255    BCF(3,ZI)=1
```

```
C       TUNGSTEN FILAMENT

        DO 260 RI=39,89
        DO 260 ZI=39,89
         D=SQRT((RI-64.)**2+(ZI-64.)**2)
         IF (D.LE.24.576) THEN
          VWO(RI,ZI)=VA-VE+1.5
          BCW(RI,ZI)=1
          ENDIF
   260  CONTINUE
        DO 270 RI=0,129
         BCW(RI,0)=1
         BCW(RI,128)=1
   270  BCW(RI,129)=1
        DO 280 ZI=1,127
         BCW(0,ZI)=1
         BCW(128,ZI)=1
   280  BCW(129,ZI)=1


C           START CYCLE

        CMX=ITER
        IF (ETER.GT.ITER) CMX=ETER
        IF ((RDQIN.EQ.'Y').AND.(ETER+1.GT.CMX)) CMX=ETER+1
        IF (RDVIN.NE.'Y') CMX=CMX+1
        DO 500 CN=1,CMX
        WRITE(6,*)'PERTURBATION NUMBER ',CN
C           Solve Laplace if no old potential read in
        IF (RDVIN.NE.'Y') GOTO 560
C           Turn off field solver when no change
        IF (ETER.EQ.0) ETER=-1
        IF (ITER.EQ.0) ITER=-1

C           SET UP Q MESH FOR PERTURBATION

C         ELECTRON DENSITY

        IF ((ETER.LE.0).OR.(RDQIN.EQ.'Y')) GOTO 801
C           ZERO OUT QSE, QF, AND QW ELECTRON CHARGE DENSITIES
        DO 705 I=51331,100997
   705   Q(I)=0
        NEE=0
        NELF=0
        QDT=-32552.*ECREATE
        DO 740 J=0,NTE/2000-1
         DO 700 I=1,2000
```

```
      QD(I)=QDT/NTE
      PHI=2*PI*(J*2000+I-RANF())/NTE
      R(I)=64+24.577*COS(PHI)
      Z(I)=64+24.577*SIN(PHI)
      P=RANF()
      E0=0.16
701   E0=E0+0.001
      PCALC=1-(1+(E0-0.16)/0.01055)*EXP(-(E0-0.16)/0.01055)
      IF (P.GT.PCALC) GOTO 701
      VE0=SQRT(2*E*E0/ME)*32E-9/H
      VR(I)=-VE0*COS(PHI)
      VZ(I)= VE0*SIN(PHI)
700   N(I)=1
     QMH2=-E/(ME*(H/32.)**2)*1E-18
     IMX=2000
     CALL ITERATE(IMX,VWO,BCW,QW,QMH2,128,128)
     IMX=0
     DO 710 I=1,2000
      D=SQRT((R(I)-64)**2+(Z(I)-64)**2)
      IF (D.GT.24.576) THEN
       IMX=IMX+1
       R(IMX)=R(I)/8+56
       Z(IMX)=Z(I)/8+56
       VR(IMX)=VR(I)/8
       VZ(IMX)=VZ(I)/8
       ENDIF
710    CONTINUE
     NELF=NELF+IMX
     I2=IMX
     IF (IMX.GT.0) CALL
       ITERATE(IMX,VFO,BCF,QF,QMH2/64,128,128)
     IMX=0
     DO 720 I=1,I2
      IF (R(I).LE.4.) THEN
       IMX=IMX+1
       R(IMX)=R(I)/4+64
       Z(IMX)=Z(I)/4+52
       VR(IMX)=VR(I)/4
       VZ(IMX)=VZ(I)/4
       ENDIF
720    CONTINUE
     NEE=NEE+IMX
     IF (IMX.GT.0) CALL
       ITERATE(IMX,VSO,BCS,QSE,QMH2/1024,112,144)
740  CONTINUE
    WRITE(6,*)NEE*100./NTE,'% of electrons leave filament
                            area'
```

```
C         If no electrons emitted, dump and stop
      IF (NEE.EQ.0) GOTO 607
C         Adjust qse to desired Ie if wanted
      IF (IEADJ.EQ.'Y') THEN
       IEMULT=NTE*IE/(NEE*ECREATE)
       WRITE(6,*)' IeMult = ',IEMULT
       ENDIF
C         Patch qw onto qf
      DO 750 RI=0,128
      DO 750 ZI=0,128
       R4=(RI+4)/8+56
       Z4=(ZI+4)/8+56
  750  QF(R4,Z4)=QF(R4,Z4)+QW(RI,ZI)
C         Normalize qw and qf edges
      DO 760 RI=0,128
       QW(RI,128)=QW(RI,128)*2
  760  QW(RI,0)=QW(RI,0)*2
      DO 770 ZI=0,128
       QW(0,ZI)=QW(0,ZI)*2
  770  QW(128,ZI)=QW(128,ZI)*2
      DO 780 ZI=41,87
  780  QF(4,ZI)=QF(4,ZI)*2
      ETER=ETER-1

C          GET ION DENSITY USING TEST PARTICLES

  801 REWIND 11
C         ZERO OUT QL AND QS ION CHARGE DENSITIES
      DO 802 I=1,51330
  802  Q(I)=0
      IF (ITER.LE.0) GOTO 975
      TEXIT=0.0
      NEXIT=0
      IWTOT=0
      FV=0
      DO 800 ZI=1,143
       RMX=ZI/4+12
       DO 800 RI=0,RMX
        IW(RI,ZI)=QSE(RI,ZI)/(RMX+0.5)
        FV=FV+RI*IW(RI,ZI)
  800   IWTOT=IWTOT+IW(RI,ZI)
      FV=IWTOT/(2*PI*FV)
C     WRITE(6,*)' F = ',F
      WRITE(6,*)' FV = ',FV,'    (~1.189e-2)'
      QDT=6.25E6*FV*ICREATE
      TNI=0
      NIB=0
```

```
      DO 810 ZI=1,143
       RMX=ZI/4+12
       DO 810 RI=0,RMX
        NIMP=((IW(RI,ZI)+IWLO)/IWTOT)*NTI+0.5
        IF (NIMP.EQ.0) THEN
         IWLO=IWLO+IW(RI,ZI)
         GOTO 809
         ENDIF
C          Ionize and initialize nimp ions at (Ri,Zi)
        DO 820 I=NIB+1,NIB+NIMP
         QD(I)=QDT*(IW(RI,ZI)+IWLO)/(IWTOT*NIMP)
         Z(I)=ZI+RANF()-0.5
         R(I)=ABS(RI+RANF()-0.5)
         RN=RANF()
         DO 825 J=1,NCS
          IF (RN.GE.0) N(I)=CS(J)
  825     RN=RN-CF(J)
         VR(I)=-V0*SIN(ATAN(RI/(ZI+48.)))
         VZ(I)= V0*COS(ATAN(RI/(ZI+48.)))
         TT(I)=0
  820    CONTINUE
        IWLO=0
        NIB=NIB+NIMP
        IF (NIB.LT.(2000-NTI/(50*LOG10(FLOAT(NTI/1000))))) GOTO
809
        IF (NIB.GT.2000) THEN
         WRITE(6,*)' NIB = ',NIB,'  ',NIB-2000,' Ions lost'
         NIB=2000
         ENDIF
  830   TNI=TNI+NIB
C          QMH2=constants for acceleration term
              (=5.67wun/(us**2*v))
        QMH2=E/(MA*H**2)*1E-12
        CALL ITERATE(NIB,VSO,BCS,QS,QMH2,112,144)
        I2=0
        DO 940 I=1,NIB
         IF ((R(I).LT.48).AND.(Z(I).GE.144)) THEN
          TEXIT=TEXIT+TT(I)
          NEXIT=NEXIT+1
          ENDIF
         IF ((R(I).LT.48).AND.((Z(I).GE.144).OR.(Z(I).LT.0)))
          THEN
          I2=I2+1
          N(I2)=N(I)
          R(I2)=R(I)/4
          Z(I2)=Z(I)/4+76
          VR(I2)=VR(I)/4
```

```
          VZ(I2)=VZ(I)/4
          QD(I2)=QD(I)
          TT(I2)=TT(I)
         ELSE
          WRITE(11,1110)N(I),R(I),Z(I),VR(I),VZ(I),QD(I),TT(I)
         ENDIF
  940    CONTINUE
        NIB=I2
        IF (NIB.GT.0) CALL
          ITERATE(NIB,VLO,BCL,QL,QMH2/16,144,240)
        DO 945 I=1,NIB
  945    WRITE(11,1110)N(I),R(I),Z(I),VR(I),VZ(I),QD(I),TT(I)
 1110   FORMAT(I5,6F8.3)
        NIB=0
C          Clean up last bits (Iw left over)
  809   IF ((RI.EQ.RMX).AND.(ZI.EQ.143)) THEN
         QD(NIB)=QD(NIB)+QDT*IWLO/IWTOT
         IF (NIB.GT.0) GOTO 830
         ENDIF
  810   CONTINUE
       ITER=ITER-1

C          STATISTICAL ANALYSIS OF IONS

      REWIND 11
      QDSUM=0
      DO 946 I=1,60
       TMN(I)=1000
       TA(I)=0
       TMX(I)=0
  946  NI(I)=0
      DO 948 I=1,TNI
       READ(11,1110)N(1),R(1),Z(1),VR(1),VZ(1),QD(1),TT(1)
       QDSUM=QDSUM+QD(1)
       DO 947 J=1,NCS
  947   IF (N(1).EQ.CS(J)) CI=J
C          NI(40+CI)=Number of ions of cluster size CS(CI)
       NI(40+CI)=NI(40+CI)+1
       D=SQRT((R(1)-80)**2+(Z(1)-68)**2)
       IF (D.LE.16) THEN
C          Sucked into filament
        NI(10)=NI(10)+1
        TA(10)=TA(10)+TT(1)
        IF (TT(1).LT.TMN(10)) TMN(10)=TT(1)
        IF (TT(1).GT.TMX(10)) TMX(10)=TT(1)
        ENDIF
       IF ((R(1).LT.10).AND.((Z(1).GT.63).AND.(Z(1).LT.77)))
```

```
C            Skimmered
     +     NI(11)=NI(11)+1
        IF ((Z(1).GE.229).AND.(R(1).LE.20)) THEN
C            Hit Faraday Cup
          NI(13)=NI(13)+1
C            Split on cluster size index
          NI(20+CI)=NI(20+CI)+1
          TA(20+CI)=TA(20+CI)+TT(1)
          IF (TT(1).LT.TMN(20+CI)) TMN(20+CI)=TT(1)
          IF (TT(1).GT.TMX(20+CI)) TMX(20+CI)=TT(1)
          ENDIF
C            Hit substrate
         IF ((Z(1).GE.229).AND.(R(1).LE.24)) NI(14)=NI(14)+1
C            Swung wide of substrate
         IF ((Z(1).GE.229).AND.(R(1).GT.24)) NI(15)=NI(15)+1
  948  CONTINUE
 1120 FORMAT(F8.3,'% ',A20)
 1130 FORMAT(F8.3,'% ',A20,F7.3,' us (',F7.3,'-',F7.3,')')
      WRITE(6,*)TNI,' test ions total'
      WRITE(6,*)' QDSUM = ',QDSUM,'    QDT = ',QDT
      DO 949 I=1,NCS
  949  WRITE(6,*)(NI(40+I)*10000/TNI)/100.,'% are size ',CS(I)
      WRITE(6,1120)100*(TNI-NI(11)-NI(14)-NI(15))/FLOAT(TNI),
     +             ' Hit ion can       '
       IF (NI(10).GT.0) WRITE(6,1130)NI(10)/FLOAT(TNI)*100,
     +     '  Sucked into fil    ',TA(10)/NI(10),TMN(10),TMX(10)
       WRITE(6,1120)100*(NI(11)+NI(14)+NI(15))/FLOAT(TNI),
     +             ' Exit ion can      '
       IF (NEXIT.GT.0) WRITE(6,*)'                 average
                                  exit time = ',
     +                            TEXIT/NEXIT,' us'
       WRITE(6,1120)NI(11)/FLOAT(TNI)*100,'  Skimmered          '
       WRITE(6,1120)NI(14)/FLOAT(TNI)*100,'  Hit substrate      '
       WRITE(6,1120)NI(15)/FLOAT(TNI)*100,'  Swung wide of sub '
       WRITE(6,1120)NI(13)/FLOAT(TNI)*100,'  Hit faraday cup    '
 1135 FORMAT(F8.3,'% are N = ',I4,'        ',F7.3,' us (',
     +       F7.3,'-',F8.3,')')
       IF (NI(13).NE.0) THEN
        DO 951 I=1,NCS
         IF (NI(20+I).GT.0)
     +    WRITE(6,1135)NI(20+I)/FLOAT(NI(13))*100,CS(I),
     +       TA(20+I)/NI(20+I),TMN(20+I),TMX(20+I)
  951   CONTINUE
        ENDIF
       WRITE(6,*)'  Ifc = ',NI(13)/FLOAT(TNI)*ICREATE,' uA'
C      Adjust Icreate for next round if enabled
       IF (IFCADJ.EQ.'Y') THEN
```

```
      A=TNI/FLOAT(NI(13))*IFC/ICREATE
      ICREATE=ICREATE*A
      WRITE(6,*)' Icreate adjusted from ',ICREATE/A,
               ' to ',ICREATE
C        Adjust Qs and Ql ion charge densities
      DO 811 I=1,51330
  811  Q(I)=Q(I)*A
      ENDIF
C     F=1
C     F=0.8*F+0.2*NI(13)/FLOAT(TNI)
C       Normalize ql and qs edges
      DO 950 ZI=65,239
  950  QL(0,ZI)=QL(0,ZI)*2
      DO 970 RI=0,47
       QS(RI,0)=QS(RI,0)*2
  970  QS(RI,144)=QS(RI,144)*2
C        Copy qse to qs
  975 DO 990 ZI=0,144
      DO 990 RI=1,112
  990  QS(RI,ZI)=QS(RI,ZI)+IEMULT*QSE(RI,ZI)
      DO 995 ZI=0,144
  995  QS(0,ZI)=2*QS(0,ZI)+2*IEMULT*QSE(0,ZI)

C            SOLVE POISSON'S EQUATION

  560 I=-1
      RDVIN='Y'
      MAXDIFF=1000
  300 I=I+1
C        Skip large and small meshes if no ions this iteration
      IF (ITER.LT.0) GOTO 359


C        LARGE MESH

      DO 310 ZI=1,239
      DO 310 RI=29,143
  310  VLN(RI,ZI)=(VLO(RI,ZI+1)+VLO(RI,ZI-1)+VLO(RI+1,ZI)
     +       +VLO(RI-1,ZI))/4+(VLO(RI+1,ZI)-VLO(RI-1,ZI))
     +       /(8*RI)+E4HEO*QL(RI,ZI)
       DO 315 ZI=113,239
       DO 315 RI=1,28
  315  VLN(RI,ZI)=(VLO(RI,ZI+1)+VLO(RI,ZI-1)+VLO(RI+1,ZI)
     +       +VLO(RI-1,ZI))/4+(VLO(RI+1,ZI)-VLO(RI-1,ZI))
     +       /(8*RI)+E4HEO*QL(RI,ZI)
       DO 317 ZI=65,75
       DO 317 RI=1,9
```

```
  317  VLN(RI,ZI)=(VLO(RI,ZI+1)+VLO(RI,ZI-1)+VLO(RI+1,ZI)
     +       +VLO(RI-1,ZI))/4+(VLO(RI+1,ZI)-VLO(RI-1,ZI))
     +       /(8*RI)+E4HEO*QL(RI,ZI)
       DO 320 ZI=113,239
  320  VLN(0,ZI)=(VLO(0,ZI+1)+VLO(0,ZI-1)+2*VLO(1,ZI))/4+
     +           E4HEO*QL(0,ZI)
       DO 322 ZI=65,75
  322  VLN(0,ZI)=(VLO(0,ZI+1)+VLO(0,ZI-1)+2*VLO(1,ZI))/4+
     +           E4HEO*QL(0,ZI)

C      SMALL MESH

       DO 330 ZI=1,143
       DO 330 RI=1,111
  330  VSN(RI,ZI)=(VSO(RI,ZI+1)+VSO(RI,ZI-1)+VSO(RI+1,ZI)
     +       +VSO(RI-1,ZI))/4+(VSO(RI+1,ZI)-VSO(RI-1,ZI))
     +       /(8*RI)+E4HEO*QS(RI,ZI)
       DO 340 ZI=1,143
  340  VSN(0,ZI)=(VSO(0,ZI+1)+VSO(0,ZI-1)+2*VSO(1,ZI))/4+
     +           E4HEO*QS(0,ZI)
       VSN(0,144)=(VSO(0,143)+2*VSO(1,144)+3*VSO(0,144)/4+
     +             VLO(0,113)/4)/4+E4HEO*QS(0,144)
       DO 350 RI=1,47
        T=RI/4
  350  VSN(RI,144)=(VSO(RI-1,144)+VSO(RI+1,144)+VSO(RI,143)+
     +              3*VSO(RI,144)/4+((RI-4*T)*VLO(T+1,113)+
     +              (4-RI+4*T)*VLO(T,113))/16)/4+
     +             (VSO(RI+1,144)-VSO(RI-1,144))/(8*RI)+
     +             E4HEO*QS(RI,144)
       VSN(0,0)=(VSO(0,1)+2*VSO(1,0)+3*VSO(0,0)/4+
     +            VLO(0,75)/4)/4+E4HEO*QS(0,0)
       DO 352 RI=1,111
        T=RI/4
  352  VSN(RI,0)=(VSO(RI-1,0)+VSO(RI+1,0)+VSO(RI,1)+
     +              3*VSO(RI,0)/4+((RI-4*T)*VLO(T+1,75)+
     +              (4-RI+4*T)*VLO(T,75))/16)/4+
     +             (VSO(RI+1,0)-VSO(RI-1,0))/(8*RI)+
     +             E4HEO*QS(RI,0)
       VSN(112,0)=(VSO(112,1)+VSO(111,0)+3*VSO(112,0)/2+
     +             VLO(28,75)/4+VLO(29,76)/4)/4+
     +            (VLO(29,76)/4+3*VSO(112,0)/4-VSO(111,0))/896+
     +            E4HEO*QS(112,0)
       DO 354 ZI=1,31
        T=ZI/4
        A=3*VSO(112,ZI)/4+((ZI-4*T)*VLO(29,77+T)+(4*T+4-ZI)*
     +                     VLO(29,76+T))/16
  354  VSN(112,ZI)=(VSO(112,ZI+1)+VSO(112,ZI-1)
```

```
                    +VSO(111,ZI)+A)/4+
     +           (A-VSO(111,ZI))/896

C        FILAMENT AREA

C         Skip filament area if no electrons this iteration
  359 IF (ETER.LT.0) GOTO 391

      DO 360 ZI=9,119
      DO 360 RI=5,119
  360  VFN(RI,ZI)=(VFO(RI,ZI+1)+VFO(RI,ZI-1)+VFO(RI+1,ZI)
     +       +VFO(RI-1,ZI))/4+E4HEO*QF(RI,ZI)
      DO 370 ZI=41,87
       T=ZI/4
       A=3*VFO(4,ZI)/4+((ZI-4*T)*VSO(64,53+T)+(4*T+4-ZI)*
     +                    VSO(64,52+T))/16
  370  VFN(4,ZI)=(VFO(4,ZI+1)+VFO(4,ZI-1)+VFO(5,ZI)+A)/4+
     +           E4HEO*QF(4,ZI)

C        TUNGSTEN FILAMENT

      DO 380 ZI=1,127
      DO 380 RI=1,127
  380  VWN(RI,ZI)=(VWO(RI,ZI+1)+VWO(RI,ZI-1)+VWO(RI+1,ZI)
     +       +VWO(RI-1,ZI))/4+E4HEO*QW(RI,ZI)
      DO 385 RI=1,127
       T=RI/8
       A=7*VWO(RI,0)/8+((RI-8*T)*VFO(57+T,55)+(8*T+8-RI)*
     +                    VFO(56+T,55))/64
       VWN(RI,0)=(VWO(RI+1,0)+VWO(RI-1,0)+VWO(RI,1)+A)/4+
     +           E4HEO*QW(RI,0)
       A=7*VWO(RI,128)/8+((RI-8*T)*VFO(57+T,73)+(8*T+8-RI)*
     +                    VFO(56+T,73))/64
  385  VWN(RI,128)=(VWO(RI+1,128)+VWO(RI-1,128)
                    +VWO(RI,127)+A)/4+
     +           E4HEO*QW(RI,128)
      DO 390 ZI=1,127
       T=ZI/8
       A=7*VWO(0,ZI)/8+((ZI-8*T)*VFO(55,57+T)+(8*T+8-ZI)*
     +                    VFO(55,56+T))/64
       VWN(0,ZI)=(VWO(0,ZI+1)+VWO(0,ZI-1)+VWO(1,ZI)+A)/4+
     +           E4HEO*QW(0,ZI)
       A=7*VWO(128,ZI)/8+((ZI-8*T)*VFO(73,57+T)+(8*T+8-ZI)*
     +                    VFO(73,56+T))/64
  390  VWN(128,ZI)=(VWO(128,ZI+1)+VWO(128,ZI-1)
                    +VWO(127,ZI)+A)/4+
     +           E4HEO*QW(128,ZI)
```

```
      VWN(0,0)=(VWO(0,1)+VWO(1,0)+7*VWO(0,0)/4+VFO(55,56)/8+
     +          VFO(56,55)/8)/4+E4HEO*QW(0,0)
      VWN(0,128)=(VWO(1,128)+VWO(0,127)+7*VWO(0,128)/4+
                  VFO(55,72)/8+
     +          VFO(56,73)/8)/4+E4HEO*QW(0,128)
      VWN(128,128)=(VWO(128,127)+VWO(127,128)+7*VWO(128,128)/4+
     +               VFO(72,73)/8+VFO(73,72)/8)/4
                   +E4HEO*QW(128,128)
      VWN(128,0)=(VWO(128,1)+VWO(127,0)+7*VWO(128,0)/4
                  +VFO(73,56)/8+
     +          VFO(72,55)/8)/4+E4HEO*QW(128,0)

C             CALCULATE MAXDIFF EVERY 100

  391 T=I/100
      IF (I.NE.T*100) GOTO 400
C       Patch vwn onto vfn
      DO 392 ZI=56,72
      DO 392 RI=56,72
  392  VFN(RI,ZI)=VWN((RI-56)*8,(ZI-56)*8)
      DO 395 J=1,85776
  395  MD(J)=ABS(VN(J)-VO(J))*(1-BC(J))
      IF (ETER.GE.0) THEN
        MAXDIFF=AMAXAF(MD,51977,85776,1,MAXIND)
       ELSE
        MAXDIFF=0
       ENDIF
      IF (ITER.GE.0) THEN
        A=AMAXAF(MD,1,51976,1,D)/10.
       ELSE
        A=0
       ENDIF
      IF (A.GT.MAXDIFF) THEN
       MAXDIFF=A
       MAXIND=D
       ENDIF
C     T=I/1000
C     IF (I.EQ.T*1000) WRITE(6,1400) I,MAXDIFF,MAXIND
 1400 FORMAT(I7,'    Maxdiff=',F10.5,' at index ',I7)

C             OLD<==NEW

C       Skip w & f copy if no changes made
  400 IF (ETER.LT.0) GOTO 447
      DO 405 J=51977,85776
  405  VO(J)=VO(J)*BC(J)+VN(J)*(1-BC(J))
      DO 410 ZI=1,127
```

```
      VWO(0,ZI)=VWN(0,ZI)
  410  VWO(128,ZI)=VWN(128,ZI)
      DO 420 RI=0,128
       VWO(RI,0)=VWN(RI,0)
  420  VWO(RI,128)=VWN(RI,128)
      DO 430 ZI=56,72
      DO 430 RI=56,72
  430  VFO(RI,ZI)=VWO((RI-56)*8,(ZI-56)*8)
      DO 445 ZI=41,87
  445  VFO(4,ZI)=VFN(4,ZI)
C        Skip s & l copy if no changes made
  447 IF (ITER.LT.0) GOTO 475
      DO 449 J=1,51976
  449  VO(J)=VO(J)*BC(J)+VN(J)*(1-BC(J))
      DO 450 ZI=52,84
      DO 450 RI=65,96
  450  VSO(RI,ZI)=VSO(RI,ZI)*(1-BCS(RI,ZI))+
     +             VFO((RI-64)*4,(ZI-52)*4)*BCS(RI,ZI)
      DO 460 RI=0,47
       VSO(RI,144)=VSN(RI,144)
  460  IF (RI.LT.12) VSO(RI,0)=VSN(RI,0)
      DO 470 ZI=76,112
      DO 470 RI=0,28
  470  VLO(RI,ZI)=VSO(RI*4,(ZI-76)*4)
  475 IF ((MAXDIFF.GT.ERR).AND.(I.LE.100000)) GOTO 300

C       Print final maxdiffs
      MAXDIFF=AMAXAF(MD,1,35332,1,MAXIND)
      WRITE(6,1400)I,MAXDIFF,MAXIND
      MAXDIFF=AMAXAF(MD,35333,51976,1,MAXIND)
      WRITE(6,1400)I,MAXDIFF,MAXIND
      MAXDIFF=AMAXAF(MD,51977,68876,1,MAXIND)
      WRITE(6,1400)I,MAXDIFF,MAXIND
      MAXDIFF=AMAXAF(MD,68877,85776,1,MAXIND)
      WRITE(6,1400)I,MAXDIFF,MAXIND
      WRITE(6,*)
      IF (DAMP) THEN
       DO 480 I=1,51976
  480   VO(I)=DF*VO(I)+(1-DF)*VSAVE(I)
       ENDIF
      IF (((RDQIN.NE.'Y').AND.(ETER.GE.0)).AND.DAMP) THEN
       DO 481 I=51977,85776
  481   VO(I)=DFE*VO(I)+(1-DFE)*VSAVE(I)
       ENDIF
      DAMP=.TRUE.
      RDQIN='D'
      DO 490 I=1,85776
```

```
  490  VSAVE(I)=VO(I)

  500 CONTINUE
C       END OF ITERATION LOOP

C            DUMP EVERYTHING OUT

      A=0
      DO 608 I=34946,51330
  608  IF (Q(I).GT.A) A=Q(I)
      WRITE(6,*)' Maximum ion density = ',A/H**3,' Ions/m3'
      IF (A.GT.0) WRITE(6,*)' Minimum ion seperation = ',
     +                       H/A**(1/3.)*1E6,' um'
      A=0
      DO 609 I=67716,84356
  609  IF (ABS(Q(I)).GT.A) A=ABS(Q(I))
      WRITE(6,*)' Maximum e- density = ',16*A/H**3,' e-/m3'
      IF (A.GT.0) WRITE(6,*)' Minimum e- seperation = ',
     +                       H/(16*A)**(1/3.)*1E6,' um'
C       Patch qs onto ql
  607 DO 601 ZI=0,144
      DO 601 RI=0,112
       R4=(RI+2)/4
       Z4=(ZI+2)/4+76
  601  QL(R4,Z4)=QL(R4,Z4)+QS(RI,ZI)
C        Patch bcs onto bcl
      DO 602 RI=0,28
      DO 602 ZI=76,112
  602  BCL(RI,ZI)=BCS(RI*4,(ZI-76)*4)
      DO 603 RI=0,11
  603  BCL(RI,112)=0
      DO 604 RI=0,2
  604  BCL(RI,0)=0
      DO 605 RI=5,28
  605  BCL(RI,0)=0
      DO 606 ZI=1,7
  606  BCL(28,ZI)=0
      WRITE(17,*)' 145  241  0  0'
      WRITE(27,*)' 145  241  0  0'
      DO 600 ZI=0,240
      DO 600 RI=0,144
       WRITE(27,*)QL(RI,ZI)*(1-BCL(RI,ZI))-BCL(RI,ZI)
  600  WRITE(17,*)VLO(RI,ZI)
      WRITE(18,*)' 113  145  0  0'
      WRITE(28,*)' 113  145  0  0'
      REWIND 38
      WRITE(38,*)' 113  145  0  0'
```

```
      DO 610 ZI=0,144
      DO 610 RI=0,112
       IF (RI.EQ.0) THEN
        WRITE(38,*)2*QSE(RI,ZI)*(1-BCS(RI,ZI))+BCS(RI,ZI)
        WRITE(28,*)(QS(RI,ZI)-2*IEMULT*QSE(RI,ZI))*
     +              (1-BCS(RI,ZI))-BCS(RI,ZI)
       ELSE
        WRITE(38,*)QSE(RI,ZI)*(1-BCS(RI,ZI))+BCS(RI,ZI)
        WRITE(28,*)(QS(RI,ZI)-IEMULT*QSE(RI,ZI))*
     +              (1-BCS(RI,ZI))-BCS(RI,ZI)
       ENDIF
  610  WRITE(18,*)VSO(RI,ZI)
      WRITE(19,*)' 125  129  0  0'
      REWIND 29
      WRITE(29,*)' 125  129  0  0'
      DO 620 ZI=0,128
      DO 620 RI=4,128
       WRITE(29,*)QF(RI,ZI)*(1-BCF(RI,ZI))+BCF(RI,ZI)
  620  WRITE(19,*)VFO(RI,ZI)
      WRITE(20,*)'  129   129  0  0'
      REWIND 30
      WRITE(30,*)'  129   129  0  0'
      DO 630 ZI=0,128
      DO 630 RI=0,128
       WRITE(30,*)QW(RI,ZI)*(1-BCW(RI,ZI))+BCW(RI,ZI)
  630  WRITE(20,*)VWO(RI,ZI)

C         Time-of-flight and energy distributions

      IF (NTI.LE.0) THEN
       REWIND 27
       REWIND 28
       STOP
       ENDIF
      DO 640 I=0,1000
      TOF(I)=0
      EF(I)=0
  640 TH(I)=0
      REWIND 11
      DO 650 I=1,TNI
       READ(11,1110)N(1),R(1),Z(1),VR(1),VZ(1),QD(1),TT(1)
       IF (((Z(1).GE.229).AND.(R(1).LE.20)).AND.(TT(1).LE.500))
        THEN
        T=TT(1)*2+0.5
        TOF(T)=TOF(T)+QD(1)
        T=(0.5*N(1)*MA/E*(VR(1)**2+VZ(1)**2)*1587.5**2-
     +      (VA-VE/2))*1000/(2*VE)+0.5
```

```
        IF (T.LT.1000) EF(T)=EF(T)+1
        ENDIF
       IF ((Z(1).GE.229).AND.(R(1).LE.24)) THEN
        T=R(1)*40+0.5
        TH(T)=TH(T)+QD(1)*N(1)
        ENDIF
  650   CONTINUE
      DO 652 I=1,999
  652  SM(I)=(TOF(I-1)+2*TOF(I)+TOF(I+1))/4
      DO 653 I=1,999
       TOF(I)=SM(I)
  653  SM(I)=(EF(I-1)+2*EF(I)+EF(I+1))/4
      DO 654 I=1,999
  654  EF(I)=SM(I)
      DO 655 I=9,991
       SM(I)=TH(I)/20
       DO 655 J=I-9,I+9
  655   SM(I)=SM(I)+TH(J)/20
      DO 656 I=0,991
       TH(I)=SM(I)
  656  IF (I.LT.9) TH(I)=SM(9)
      WRITE(41,*)'T Time-of-flight'
      WRITE(41,*)'  1001 1 '
      WRITE(42,*)'T Substrate thickness'
      WRITE(42,*)'  1001 1 '
      WRITE(43,*)'T Energy distribution'
      WRITE(43,*)'  1001 1 '
      DO 660 I=0,1000
C        Time-of-flight in uS
       WRITE(41,1042)FLOAT(I)/2,TOF(I)
C        Substrate thickness in inches
       WRITE(42,1042)FLOAT(I)/640.,TH(I)
C        Final energy in electron volts
  660  WRITE(43,1042)I*2*VE/1000.+VA-VE/2,EF(I)
 1042 FORMAT(F15.7,F15.3)
      END



      SUBROUTINE ITERATE(NIB,VO,BC,Q,QM2,RB,ZB)

      INTEGER RB,ZB,NIB,REFLECT

      REAL R(2500),Z(2500),VR(2500),VZ(2500),AR,AZ,DT(2500),
     +     VO(0:RB+1,0:ZB+1),Q(0:RB,0:ZB),QM2,QD(2500),
     +     SWAP,TT(2500)
```

```
      INTEGER N(2500),BC(0:RB+1,0:ZB+1),RI,ZI,I,T1,T2,T3,T4,
     +        MAX,MIN,MIND,ISWAP,IMX,I1,MAXIND,RI1,ZI1,F(2500)

      COMMON QD,R,Z,VR,VZ,N,TT

      REFLECT=0
      IF (ZB.GT.129) REFLECT=1
C         REFLECT=1 RESULTS IN REFLECTION AT R=0
      I1=0
      IMX=NIB
      DO 810 I=1,IMX
  810  F(I)=1
  830 I1=I1+1
      DO 840 I=1,IMX
       RI=R(I)
       ZI=Z(I)
       AR=QM2/N(I)*((ZI+1-Z(I))*(VO(RI+1,ZI)-VO(RI,ZI))+
     +                (Z(I)-ZI)*(VO(RI+1,ZI+1)-VO(RI,ZI+1)))
       AZ=QM2/N(I)*((RI+1-R(I))*(VO(RI,ZI)-VO(RI,ZI+1))+
     +                (R(I)-RI)*(VO(RI+1,ZI)-VO(RI+1,ZI+1)))
       DT(I)=0.1/SQRT(VR(I)**2+VZ(I)**2+0.05*(ABS(AR)+ABS(AZ)))
       TT(I)=TT(I)+DT(I)
       R(I)=R(I)-(VR(I)*DT(I)+0.5*AR*DT(I)**2)
       Z(I)=Z(I)+VZ(I)*DT(I)+0.5*AZ*DT(I)**2
       VR(I)=VR(I)+AR*DT(I)
       VZ(I)=VZ(I)+AZ*DT(I)
       RI=R(I)
       ZI=Z(I)
       F(I)=1-BC(RI,ZI)*BC(RI+1,ZI)*BC(RI+1,ZI+1)*BC(RI,ZI+1)
C         F(I)=0 iff four bc's are 1's
       T4=(RB-R(I))/RB
C         T4=0 : if (r le 0) T4=1
       T2=1-2*REFLECT*T4
C         Reflect particle if r lt 0 and reflect is on
       R(I)=R(I)*T2
       VR(I)=VR(I)*T2
       T1=(ZB-Z(I))/ZB
       T2=Z(I)/ZB
       T3=R(I)/RB
       F(I)=F(I)*(1-T1-T2)*(1-T3-T4*(1-REFLECT))
C         F=0 iff particle is out of bounds
  840  CONTINUE
      DO 850 I=1,IMX
       RI=R(I)+0.5
       ZI=Z(I)+0.5
  850  Q(RI,ZI)=Q(RI,ZI)+QD(I)*DT(I)*F(I)
  855 CALL MINMX(F,1,IMX,1,MIN,MAX,MIND,MAXIND)
```

```
C      WRITE(6,97)I1,IMX,R(IMX),Z(IMX),VR(IMX),VZ(IMX),
C     +           DT(IMX),F(IMX)
C   97 FORMAT(2I5,5F10.3,I5)
       IF (MIN.NE.0) GOTO 830
       SWAP=R(MIND)
       R(MIND)=R(IMX)
       R(IMX)=SWAP
       SWAP=Z(MIND)
       Z(MIND)=Z(IMX)
       Z(IMX)=SWAP
       SWAP=VR(MIND)
       VR(MIND)=VR(IMX)
       VR(IMX)=SWAP
       SWAP=VZ(MIND)
       VZ(MIND)=VZ(IMX)
       VZ(IMX)=SWAP
       SWAP=QD(MIND)
       QD(MIND)=QD(IMX)
       QD(IMX)=SWAP
       SWAP=TT(MIND)
       TT(MIND)=TT(IMX)
       TT(IMX)=SWAP
       ISWAP=N(MIND)
       N(MIND)=N(IMX)
       N(IMX)=ISWAP
       F(MIND)=F(IMX)
       IMX=IMX-1
       IF (IMX.NE.0) GOTO 855
C      WRITE(6,*)I1,' iterations'
  860  RETURN
       END
```

Data for EPERT15 for the Standard Simulation

```
Va       = 2000
Ve       = 300
Error    = 0.0001
Damp Fac= 0.25
DF elec  = 0.15
Ecreate  = 10.0
NTE      = 10000
Eter     = 10
Ie Adj   =Y
Ie(mA)   = 10.
Icreate  = 100.0
NTI      = 10000
Iter     = 10
Ifc Adj  =N
Ifc      = 10.0
RdVIn    =Y
RdQIn    =N
AM (Ag)  = 107.868
N Cl Sz  = 1
     1   0.80
     2   0.10
     3   0.10
```

The Program ESIM11

```
      PROGRAM ESIM11
C
C       FILAMENT PUT AT 1.5 VOLTS ABOVE THE VOLTAGE
C            OF THE SURROUNDING TUBE SINCE IT SHOULD
C            BE CONNECTED TO THE NEGATIVE SIDE OF FILAMENT
C
C       SIMULATES THE ELECTRON EMISSION FROM ICB FILAMENT
C            INCLUDING SPACE CHARGE EFFECTS
C
C            FQ FACTOR 64-*256 ERROR CORRECTED
C            PP ERROR CORRECTED (LABEL 645)
C            CHARGE DISTRIBUTION REDONE TO MORE CIRCULAR
C
C       L = 40um
C       NNE=33/TS WHICH SHOULD EXIT 33/TS
C       AIMING FOR 19685 ELECTRONS MAINTAINED
C
      REAL BC(0:128,0:128),VO(0:128,0:128),VN(0:128,0:128),
     +     R(120000),Z(120000),VR(120000),VZ(120000),
     +     AR(120000),AZ(120000),Q(0:128,0:128),
     +     FQ(0:64,0:64),FVN(0:64,0:64),FVO(0:64,0:64),
     +     FBC(0:64,0:64),VA,VE,PHI,R2(20000),Z2(20000),
     +     T,RN,A,L,H,K,MAXDIFF,ERROR,K2,K3,ARM,AZM,
     +     PPR,PPZ,PMR,PMZ,K4
C
      INTEGER I,RI,ZI,TS,NE,NNE,RM,ZM,I100,IN,NEIGR,GRSIZE,
     +     E(200000),EN,R4,Z4,NETNE,J,TI,NXTVEC,PVEC,EKILL,
     +     TS100,FKILL,FTKILL,TKILL,TTKILL,EXKILL,EXTKILL
C
      DATA DT/0.01/,PI/3.1415926/,H/.0000992/
C
      LOGICAL TSFLAG
C
C
      CALL LINK('UNIT5=(bcinp,TEXT),UNIT6=(esim6,TEXT),
     +          UNIT7=(eexit,TEXT),UNIT8=(q,TEXT),
     +          UNIT9=(vo,TEXT),UNIT10=(fvo,TEXT),
     +          UNIT11=(rz,TEXT)//')
      VA=1000.
      VE=500.
      V0=2.5197
      NNE=33
      L=0.403226
      ERROR=1.00E-4
```

```
      K=-1.8225E-4/L
      K2=2.58855E-4/L
      K3=17.8485
      GRSIZE=20
      NXTVEC=0
      FKILL=0
      FTKILL=0
      TKILL=0
      TTKILL=0
      EXKILL=0
      EXTKILL=0
      DO 5 I=1,200000
    5 E(I)=0
      DO 10 ZI=0,128
      DO 10 RI=0,128
      VO(RI,ZI)=0
      D=SQRT((RI-64.)**2+(ZI-64.)**2)
      IF (D.LE.3.072) VO(RI,ZI)=VA-VE+1.5
      IF (((D.GE.32.).AND.(D.LE.40.)).AND.
     +     ((RI.GT.64).OR.(ABS(ZI-64).GE.16))) VO(RI,ZI)=VA-VE
   10 IF (((D.GE.56).AND.((RI.GT.64).OR.(ABS(ZI-64).GE.24))).OR.
     +     (RI.LT.12)) VO(RI,ZI)=VA
      DO 15 RI=1,63
      DO 15 ZI=1,63
      FBC(RI,ZI)=1
      FVO(RI,ZI)=0
      D=SQRT((RI-32.)**2+(ZI-32.)**2)
      IF (D.LT.12.288) FBC(RI,ZI)=0
   15 IF (D.LT.12.288) FVO(RI,ZI)=VA-VE+1.5
      DO 20 I=40,88
   20 READ(5,*)VO(12,I)
      DO 30 RI=0,128
      DO 30 ZI=0,128
      VN(RI,ZI)=VO(RI,ZI)
      BC(RI,ZI)=1
   30 IF (VO(RI,ZI).NE.0) BC(RI,ZI)=0
C
      DO 900 TS=1,2500
      T=TS*DT
      TS100=TS/100
      TSFLAG=(TS.EQ.TS100*100)
      IF (TSFLAG) THEN
        WRITE(6,*)
        WRITE(6,*)T,' nS'
        PPR=0.
        PPZ=0.
        PMR=0.
```

```
        PMZ=0.
        ENDIF
C
C             INITIALIZE NEW ELECTRONS AT RANDOM POSITIONS
C
      DO 110 I=1,NNE
      RN=RANF(0.5)
      PHI=2*PI*RN
      NE=NE+1
      RN=RANF(0.5)
      VR(NE)=V0*COS(PHI)
      VZ(NE)=V0*SIN(PHI)
      R(NE)=64.+3.072*COS(PHI)+VR(NE)*RN*DT
  110 Z(NE)=64.+3.072*SIN(PHI)+VZ(NE)*RN*DT
C
C               ASSIGN CHARGE TO THE MESH Q(RI,ZI)
C                 IN NUMBERS OF ELECTRONS
C
      DO 205 ZI=30,98
      DO 205 RI=9,98
  205 Q(RI,ZI)=0
      DO 210 I=1,NE
      IF (R(I).EQ.0.) GOTO 210
      RI=R(I)
      ZI=Z(I)
      DO 220 RM=RI-2,RI+3
      DO 220 ZM=ZI-2,ZI+3
      D=SQRT((FLOAT(RM-RI)-0.5)**2+(FLOAT(ZM-ZI)-0.5)**2)
      K4=1.0
      IF (D.GT.2.8) K4=0.5
      IF (D.GT.3.0) K4=0.0
      Q(RM,ZM)=Q(RM,ZM)+K4/28.
  220 CONTINUE
  210 CONTINUE
C
C             CALCULATE POTENTIAL MESH BY
C                 MESH RELAXATION
C
      I=0
      MAXDIFF=1000.
  305 I=I+1
      DO 310 RI=13,119
      DO 310 ZI=9,119
  310 VN(RI,ZI)=(VO(RI+1,ZI)+VO(RI-1,ZI)+VO(RI,ZI+1)+
     +            VO(RI,ZI-1)+K*Q(RI,ZI))/4.
      I100=I/100
      IF (I.EQ.I100*100) THEN
```

```
        MAXDIFF=0
        DO 320 RI=13,119
        DO 320 ZI=9,119
  320   IF (ABS(VN(RI,ZI)-VO(RI,ZI))*BC(RI,ZI).GT.MAXDIFF)
     +        MAXDIFF=ABS(VN(RI,ZI)-VO(RI,ZI))
        ENDIF
      DO 330 RI=13,119
      DO 330 ZI=9,119
  330 VO(RI,ZI)=VO(RI,ZI)+(VN(RI,ZI)-VO(RI,ZI))*BC(RI,ZI)
      IF (MAXDIFF.GT.ERROR) GOTO 305
      IF (TSFLAG) WRITE(6,*)' MD=',MAXDIFF,' ITER=',I
C
C             CALCULATE THE POTENTIAL ON A FINER MESH
C                       NEAR THE FILAMENT
C
      DO 440 RI=0,64
      R4=RI/4
      FVO(RI,0)=((RI-4*R4)*VO(57+R4,56)+(4*R4+4-RI)*
     *           VO(56+R4,56))/4.
  440 FVO(RI,64)=((RI-4*R4)*VO(57+R4,72)+(4*R4+4-RI)*
     *           VO(56+R4,72))/4.
      DO 450 ZI=1,63
      Z4=ZI/4
      FVO(0,ZI)=((ZI-4*Z4)*VO(56,57+Z4)+(4*Z4+4-ZI)*
     *           VO(56,56+Z4))/4.
  450 FVO(64,ZI)=((ZI-4*Z4)*VO(72,57+Z4)+(4*Z4+4-ZI)*
     *           VO(72,56+Z4))/4.
      DO 460 RI=1,63
      R4=RI/4
      DO 460 ZI=1,63
      Z4=ZI/4
  460 FQ(RI,ZI)=(((ZI-4*Z4)*Q(56+R4,57+Z4)+(4*Z4+4-ZI)*
     *            Q(56+R4,56+Z4))*(4*R4+4-RI)+((ZI-4*Z4)*
     *            Q(57+R4,57+Z4)+(4*Z4+4-ZI)*
     *            Q(57+R4,56+Z4))*(RI-4*R4))/256.
      I=0
      MAXDIFF=1000.
  405 I=I+1
      DO 410 RI=1,63
      DO 410 ZI=1,63
  410 FVN(RI,ZI)=(FVO(RI+1,ZI)+FVO(RI-1,ZI)+FVO(RI,ZI+1)+
     +           FVO(RI,ZI-1)+K*FQ(RI,ZI))/4.
      I100=I/100
      IF (I.EQ.I100*100) THEN
        MAXDIFF=0
        DO 420 RI=1,63
        DO 420 ZI=1,63
```

```
  420    IF (ABS(FVN(RI,ZI)-FVO(RI,ZI))*FBC(RI,ZI).GT.MAXDIFF)
     +       MAXDIFF=ABS(FVN(RI,ZI)-FVO(RI,ZI))
         ENDIF
       DO 430 RI=1,63
       DO 430 ZI=1,63
  430  FVO(RI,ZI)=FVO(RI,ZI)+(FVN(RI,ZI)-FVO(RI,ZI))*FBC(RI,ZI)
       IF (MAXDIFF.GT.ERROR) GOTO 405
       IF (TSFLAG) WRITE(6,*)' FMD=',MAXDIFF,'  ITER=',I
C
C                PARTICLE-PARTICLE LOCAL FORCE CALCULATION
C
       DO 610 I=1,NXTVEC
  610  E(I)=0
       NXTVEC=12601
       DO 620 I=1,NE
       IF (R(I).EQ.0.) GOTO 620
       AR(I)=0
       AZ(I)=0
       RI=R(I)
       ZI=Z(I)
       PVEC=70*RI+ZI+5642
       IF (E(PVEC).EQ.0) THEN
         E(PVEC)=NXTVEC
         NXTVEC=NXTVEC+GRSIZE+1
         IF (NXTVEC.GE.200000) STOP
         ENDIF
       PVEC=E(PVEC)
       E(70*RM+ZM-658)=E(70*RM+ZM-658)+1
  625  IF (E(PVEC).GT.GRSIZE) THEN
         PVEC=E(PVEC)
         GOTO 625
         ENDIF
       IF (E(PVEC).EQ.GRSIZE) THEN
         E(PVEC)=NXTVEC
         PVEC=NXTVEC
         NXTVEC=NXTVEC+GRSIZE+1
         IF (NXTVEC.GE.200000) STOP
         ENDIF
       E(PVEC)=E(PVEC)+1
       E(PVEC+E(PVEC))=I
  620  CONTINUE
       IF (TSFLAG) WRITE(6,*)'NXTVEC=',NXTVEC
       DO 630 RI=12,95
       DO 630 ZI=32,95
       IF (E(70*RI+ZI+5642).EQ.0) GOTO 630
       IN=0
       DO 640 RM=RI-3,RI+3
```

```
      DO 640 ZM=ZI-3,ZI+3
      PVEC=70*RM+ZM+5642
      IF (E(PVEC).EQ.0) GOTO 640
  635 PVEC=E(PVEC)
      NEIGR=GRSIZE
      IF (E(PVEC).LT.GRSIZE) NEIGR=E(PVEC)
      DO 660 EN=1,NEIGR
      IN=IN+1
      R2(IN)=R(E(PVEC+EN))
      Z2(IN)=Z(E(PVEC+EN))
  660 CONTINUE
      IF (IN.GE.20000) WRITE(6,*)'IN=',IN
      IF (IN.GE.20000) STOP
      IF (E(PVEC).GT.GRSIZE) GOTO 635
  640 CONTINUE
      TI=0
      PVEC=RI*70+ZI+5642
      PVEC=E(PVEC)
  645 TI=TI+1
      IF (TI.GT.GRSIZE) THEN
        PVEC=E(PVEC)
        IF (PVEC.LE.GRSIZE) GOTO 630
        TI=1
        ENDIF
      I=E(PVEC+TI)
      IF (I.LE.0) GOTO 630
      DO 650 EN=1,IN
      D=SQRT((R(I)-R2(EN)+1.E-6)**2+(Z(I)-Z2(EN))**2)
      A=(1/D-D/9)
      A=-K2*(A+ABS(A))/2
      AR(I)=AR(I)+A*(R2(EN)-R(I))/D
      AZ(I)=AZ(I)+A*(Z2(EN)-Z(I))/D
  650 CONTINUE
      GOTO 645
  630 CONTINUE
      IF (TSFLAG) THEN
        DO 690 I=1,NE
        IF (R(I).EQ.0.) GOTO 690
        PPR=PPR+ABS(AR(I))
        PPZ=PPZ+ABS(AZ(I))
  690   CONTINUE
        WRITE(6,*)' PPR=',PPR,'  PPZ=',PPZ
        ENDIF
C
C             CALCULATE THE FORCE ON EACH ELECTRON
C              DUE TO THE LONG RANGE POTENTIAL MESH
C
```

```
      DO 510 I=1,NE
      IF (R(I).EQ.0) GOTO 510
      IF (((R(I).GE.56.).AND.(R(I).LT.72.)).AND.((Z(I).GE.56.)
        .AND.(Z(I).LT.72.))) THEN
        RI=(R(I)-56.)*4.
        ZI=(Z(I)-56.)*4.
        AR(I)=AR(I)+2*K3*(FVO(RI+1,ZI)+
     +          FVO(RI+1,ZI+1)-FVO(RI,ZI)-FVO(RI,ZI+1))
  520   AZ(I)=AZ(I)+2*K3*(FVO(RI,ZI+1)+
     +          FVO(RI+1,ZI+1)-FVO(RI,ZI)-FVO(RI+1,ZI))
        GOTO 510
        ENDIF
      RI=R(I)
      ZI=Z(I)
      AR(I)=AR(I)+K3*(VO(RI+1,ZI)+VO(RI+1,ZI+1)-VO(RI,ZI)-
     +              VO(RI,ZI+1))/2
      AZ(I)=AZ(I)+K3*(VO(RI,ZI+1)+VO(RI+1,ZI+1)-VO(RI,ZI)-
     +              VO(RI+1,ZI))/2
  510 CONTINUE
      IF (TSFLAG) THEN
        DO 590 I=1,NE
        IF (R(I).EQ.0.) GOTO 590
        PMR=PMR+ABS(AR(I))
        PMZ=PMZ+ABS(AZ(I))
  590   CONTINUE
        WRITE(6,*)' TOTR=',PMR,'  TOTZ=',PMZ
        ENDIF
C
C             UPDATE ELECTRON POSITIONS AND VELOCITIES
C               AND KILL OFF ELECTRONS AT BOUNDARIES
C
      DO 710 I=1,NE
      IF (R(I).EQ.0.) GOTO 710
      R(I)=R(I)+VR(I)*DT+AR(I)*DT**2/2
      Z(I)=Z(I)+VZ(I)*DT+AZ(I)*DT**2/2
      VR(I)=VR(I)+AR(I)*DT
      VZ(I)=VZ(I)+AZ(I)*DT
      D=SQRT((Z(I)-64.)**2+(R(I)-64.)**2)
      IF (D.LE.3.072) THEN
        FKILL=FKILL+1
        R(I)=0.
        ENDIF
      IF (((D.GE.32.).AND.(D.LE.40.)).AND.((R(I).GT.64.).OR.
     +     (ABS(Z(I)-64.).GE.16.))) THEN
        TKILL=TKILL+1
        R(I)=0.
        ENDIF
```

```
      IF ((D.GT.40.).AND.((Z(I).GE.88.).OR.(Z(I).LE.40.))) THEN
        TKILL=TKILL+1
        R(I)=0.
        ENDIF
      IF (((R(I).LE.12.).AND.(R(I).GT.0.))
     +     .AND.(ABS(Z(I)-64.).LT.24.)) THEN
        WRITE(7,1700)I,R(I),Z(I),VR(I),VZ(I),T
        EXKILL=EXKILL+1
        R(I)=0.
        ENDIF
 1700 FORMAT(I6,4F6.1,F6.2)
  710 CONTINUE
      IF (TSFLAG) THEN
        FTKILL=FTKILL+FKILL
        TTKILL=TTKILL+TKILL
        EXTKILL=EXTKILL+EXKILL
        WRITE(6,*)FKILL,' more e- killed at fil  Total=',FTKILL
        WRITE(6,*)TKILL,' more e- killed at the tube
                        Total=',TTKILL
        WRITE(6,*)EXKILL,' more e- leave thru slit
                         Total=',EXTKILL
        FKILL=0
        TKILL=0
        EXKILL=0
        EKILL=FTKILL+TTKILL+EXTKILL
        NETNE=NNE*TS-EKILL
        WRITE(6,*)EKILL,' e- killed so far leaving ',NETNE
        ENDIF
  900 CONTINUE
      WRITE(7,1700)-1,0.,0.,0.,0.,T
      WRITE(8,*)' 129 129 0 0'
      WRITE(9,*)' 129 129 0 0'
      DO 810 ZI=0,128
      DO 810 RI=0,128
      WRITE(8,*)Q(RI,ZI)
  810 WRITE(9,*)VO(RI,ZI)
      WRITE(10,*)' 65 65 0 0'
      DO 820 ZI=0,64
      DO 820 RI=0,64
  820 WRITE(10,*)FVO(RI,ZI)
      DO 830 I=1,NE
  830 IF (R(I).NE.0.) WRITE(11,1830)R(I),Z(I),VR(I),VZ(I)
 1830 FORMAT(4F9.3)
      WRITE(11,1830)-1.,0.,0.,0.
      END
```

APPENDIX C - TIME-OF-FLIGHT DETAILS

This appendix provides more detailed evidence to back the accuracy of the experimental time-of-flight results for the Eaton source. The experimental small ionized cluster distribution for germanium in Figure 28 is matched using only monomers in the computer simulated distribution of Figure 29. Germanium differs from silver in that it has more valence electrons and is less massive. These distributions are similar to those of silver because the basic shape is due to the nonuniformity of the ionization. They differ from silver in that the first minor peak is less pronounced and the main peak drops off more sharply due to the absence of dimers and trimers.

Some other basic tests of the time-of-flight experiment involve investigating how the small ionized cluster distribution varies with changes of the basic parameters. Changes in the electron current or the pulsed ionization voltage change the overall level of ionization producing a proportional change in the magnitude of the time-of-flight distribution as shown in Figures 30 and 31 on the next page. The time-of-flight is directly proportional to the acceleration potential as shown in Figure 32 which shows the distribution moving left and increasing for higher acceleration voltages. The magnitude is also proportional to the amount of vapor being emitted from the crucible and the distribution does not change when the background pressure changes. The time-of-flight mass spectrometer is sensitive enough to detect some background gases when the pressure gets in the 10^{-5} Torr range but this doesn't normally interfere since the pressure is usually below 10^{-7} Torr.

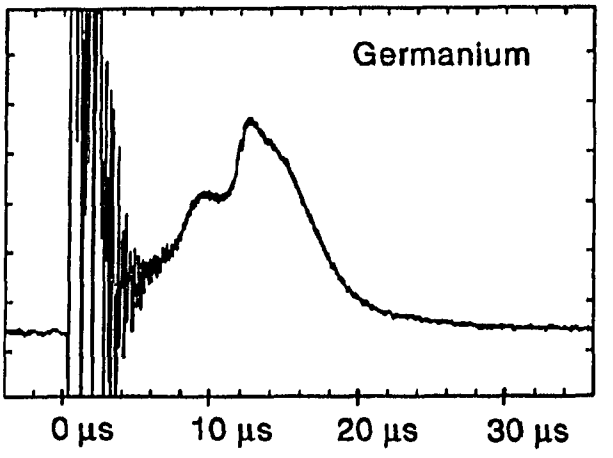

Figure 28 Experimental time-of-flight distribution for germanium

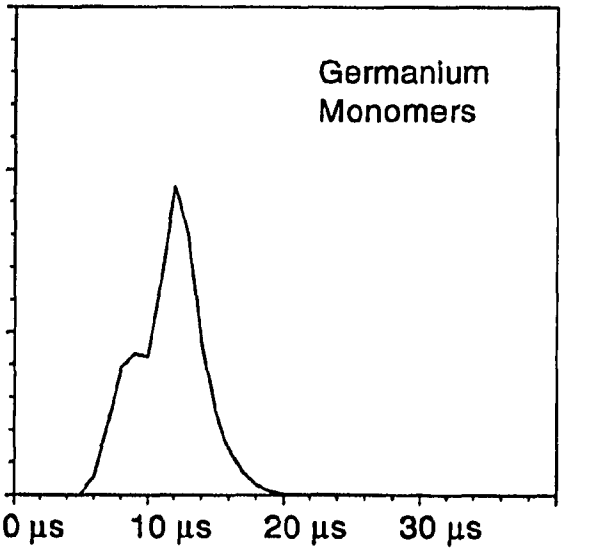

Figure 29 Computer simulated time-of-flight distribution for germanium

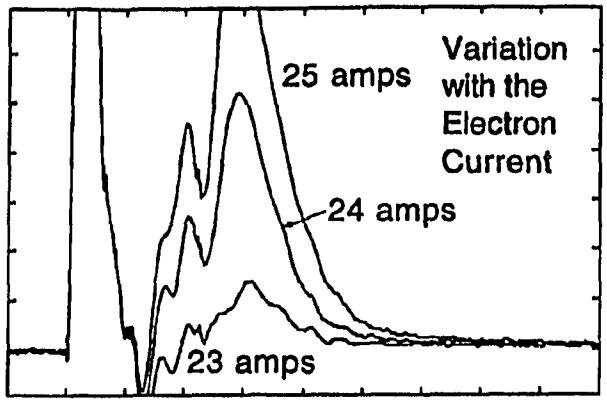

Figure 30 The variation of the small ionized cluster distribution with the electron beam current

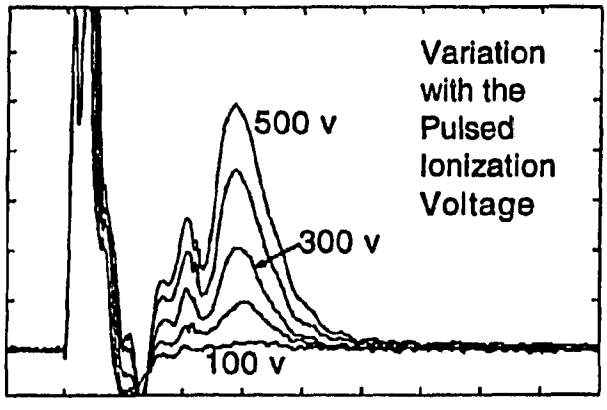

Figure 31 The variation of the small ionized cluster distribution with the pulsed ionization voltage

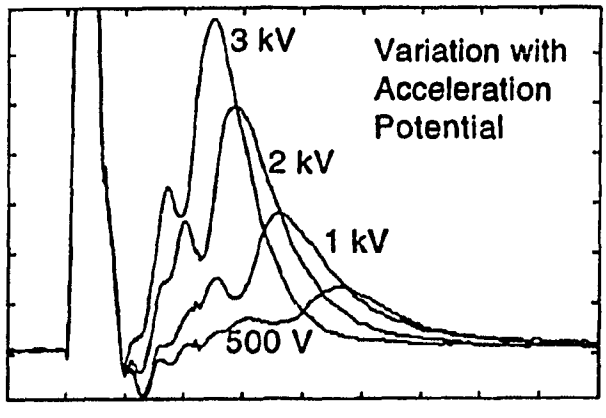

Figure 32 The variation of the small ionized cluster distribution with the acceleration potential

Since the experiment showed no sign of any large clusters, it is important to determine an upper limit to the accuracy of the detection system. A worst case scenario was used to determine the maximum number of large clusters that could hide in the noise level during a search for large clusters. A time-of-flight distribution with a magnitude of half the background noise level was assumed for the entire time range where clusters of 100-2000 atoms in size would appear. The mass flux from this distribution was calculated by hand by splitting the time range into several discrete divisions and multiplying this signal strength by the corresponding cluster size. This mass was compared to the mass of the small ionized clusters which was integrated by computer using the most conservative estimates for cluster size (all were assumed to be monomers). This worst case scenario puts a very conservative upper limit to the number of atoms that could be in large ionized clusters and not be detected by this time-of-flight mass spectrometer. The comparisons from other experiments of the number of clusters and the mass flux ratio between large and small clusters as shown in Table 1 in the main discussion were carefully calculated by hand from the data provided by the respective authors. These are approximations derived from their published results and are marked as such.

APPENDIX D - TIME-OF-FLIGHT ELECTRONICS

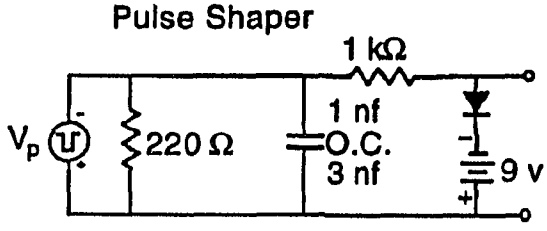

Figure 33 Schematic of the pulse shaping circuit

The accuracy of the results in the time-of-flight experiment are dependent on the electronics involved in detecting and processing the time-of-flight signal. Great care was taken to ensure that the signal was not distorted in any way and that even the smallest concentration of large clusters could be detected.

The pulse generator produces a square pulse usually of -500 volts for a duration of 3 μs, 10 μs, or 30 μs to accelerate a burst of electrons across the cluster beam ionizing a narrow band of clusters. The rapid rise and fall times of the pulse produce a great deal of electronic noise that is picked up radiatively by the Faraday cup a foot above the ionization can. This noise can obscure some of the features of the small ionized cluster distribution so it was necessary to minimize it as much as possible. This was accomplished by rounding the pulse slightly so that the rise and fall times were not as severe. Figure 33 shows the pulse shaping circuit that uses a three way switch to choose the level of capacitance desired for rounding. The degree of rounding does not affect the ionization noticeably which is checked often by using the open circuit position that leaves the pulse unrounded. It is essential for the pulse generator to see a 200 Ω load for proper delivery of a square pulse so a 220 Ω resistor is placed parallel to the pulse generator to guarantee the proper loading. The other three components are added to produce a continuous -9 volt bias when the pulse is off. This keeps the filament in a 9 volt well at all times so that no positive ions that get sucked into the filament area can ever escape. When the pulse is off, the diode is on so the -9 volts at the negative terminal of the battery produces an output voltage of -8.5 volts with the 1 kΩ resistor providing the voltage drop in the other direction. When the pulse is on, the diode is off and the 1 kΩ resistor is inconsequential since the outputs of this circuit are just connected to separate pieces of metal (an open circuit). Therefore the final pulse is from -8.5 volts to $-V_p$ with the pulse being square or slightly rounded.

The ions are detected by a Faraday cup placed on a shield in front of the substrate. The 2.5 inch diameter allows the Faraday cup to detect most of the ions that would normally hit the substrate. The small current signal from the Faraday cup is amplified by a 100 kV/A GaAs FET current amplifier. It is designed for high gain with low noise across the wide bandwidth

of dc to 100 MHz. The noisy environment and a less than perfect ground necessitated slight modifications of the amplifier. Ferrite beads were placed between the amplifier case and circuit board and the whole amplifier was mounted inside another box to shield it from electromagnetic radiation that is abundant in the room and braided cable was used to ground the two cases.

Trying too improve the resolution of the time-of-flight mass spectrometer, especially for the search for large clusters, was primarily a fight to maximize the signal strength and minimize the background noise. The abundance of electromagnetic radiation in the room from sources such as an rf sputtering system, a magnetically levitated turbo pump, the computer monitor, and all the ac lines meant that all the connecting cables had to be heavily shielded and all the components needed to be inside of metal boxes and carefully placed where they would be naturally shielded from the most severe sources of radiation. Several components of the experiment itself produced further problems from radiation outside of the vacuum chamber. The pulse generator produced an extremely small tail of under 100 μV that appeared right in the area where the large cluster search was taking place and the crucible heater produced 60 Hz spikes of very low intensity that also interfered. Both of these were eliminated by placing the amplifier and filters out of sight from the sources. Inside the vacuum chamber, the Faraday cup acts like an antenna to pick up small signals from the Eaton acceleration, ionization, and filament supplies so these all had to be replaced with cleaner supplies. The crystal monitor that measures the deposition rate and the substrate temperature controller both added noise to the system through the imperfect ground and through the air. These were both simply disconnected and turned off during time-of-flight runs. Two 12 volt batteries were used to supply $\pm$12 volts to the amplifier and the clipper circuit to prevent any noise from coming through the ac line and the power leads in both of these were heavily protecting using ferrite beads. The few things that did not cause problems were the turbo pumps, sublimation pump, and the ion gauge.

With all of the sources of noise eliminated or minimized, the remaining background noise was further reduced using home built filters. The 3.5 MHz lowpass filter in Figure 34 is a three pole Butterworth filter designed to reduce the background noise without distorting any part of the time-of-flight signal. Tests on a frequency analyzer showed that it cut nearly everything above 6 MHz while it passed nearly everything below

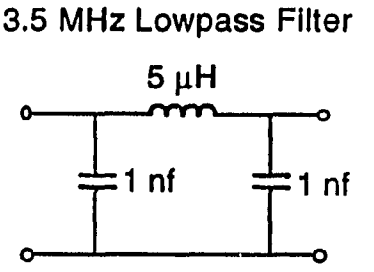

Figure 34 Lowpass filter with a 3.5 MHz cutoff

3 MHz. This was used when looking at the small cluster distribution. It is not really necessary in most situations to use this filter because of the large signal strength of the small ionized cluster distribution but it conveniently reduces noise producing a smoother trace.

The digital oscilloscope itself has a built in filter that was set at a 20 MHz cutoff at all times. In addition, the scope allowed 256 individual signals to be averaged continuously to further minimize the affects of the background noise. A built in smoothing function was also used to reduce the noise even further. Great care was taken at the low voltage settings used in the search for large clusters that the noise level never got cropped before averaging. This could cause any signal that was buried in the noise to be reduced rather than cleaned up so the noise level entering the scope was noted to put a lower limit to the voltage setting that could be used without danger of distorting the signal due to cropping.

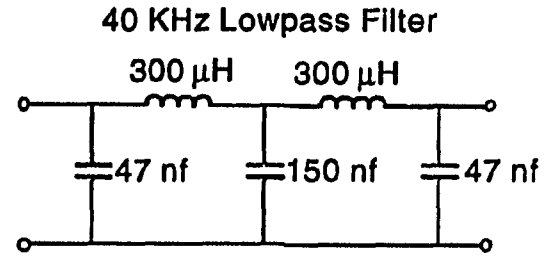

Figure 35 Five-pole Butterworth filter with a 40 kHz cutoff

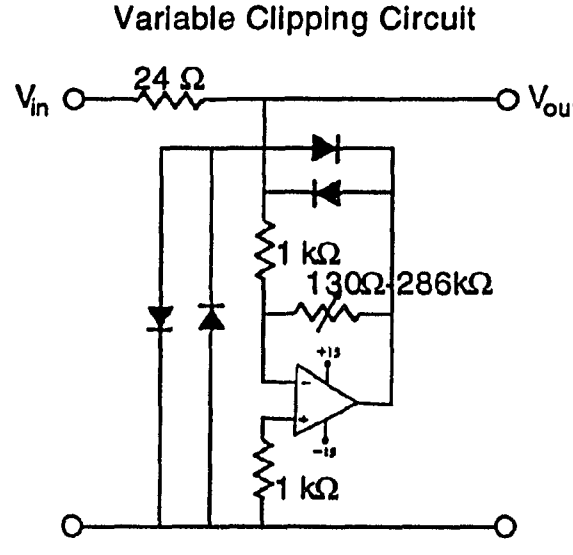

Figure 36 Variable clipping circuit adjustable between ±(2-400mV)

The search for large clusters required even further filtering of the signal to achieve the desired level of accuracy. While the small cluster distribution is typically within a 20 µs range, the large cluster signal will be spread over several hundred microseconds so a filter with a lower cutoff frequency of 40 kHz was designed to filter out a maximum amount of the background noise without chancing distortion of any large cluster distribution. The five-pole Butterworth design of Figure 35 produced a sharper cutoff to further lessen any affect on the lower frequencies. The large signals at high frequencies in the pulse noise and the small cluster distribution caused a low level ringing in the area of interest so the clipper circuit of Figure 36 was developed to clip all signals above and below ±(2-400 mV) level chosen before the signal entered the filter. By reducing these large signals, the ringing was minimized so that it only affected the first 100 µs after the pulse leaving the area of interest between 100-250 µs nice and flat with noise levels as low as 10 µV. The clipper's efficiency is demonstrated on a large

scale in Figure 37 where a ±2 mV clip cuts most of the 600 mV small cluster peak and some of the pulse noise. The clipper is basically an adjustable superdiode where the inverting op-amp circuit provides adjustable amplification through the variable resistor with the two diodes above it providing a half-volt clamp between the amplifier's input and output that clips both positive and negative parts of the signal to levels adjustable between ±(2-400 mV). The two vertical diodes provide a tradition diode clip for large signals and the 24 Ω resistor was found to be necessary to provide a means to drop the voltage between the amplifier and clipper due to the low output resistance of the amplifier.

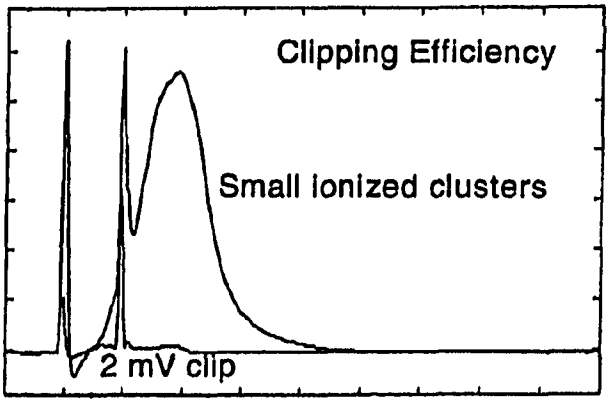

Figure 37 The small ionized cluster distribution from a 10 μs pulse unclipped and with 2mV clipping

The clipper and 40 kHz filter were simulated using SPICE software. A distribution having a long tail of large ionized clusters modeled after the Kyoto University retarding field energy analyzer results (see Figure 25) was used as a test distribution to investigate the affects of the clipper and filter. Figure 38 shows the test signal before and after it goes through a ±2 mV clip and the 40 kHz filter. The tail is intact and relatively undistorted in the 100-250 μs range of interest.

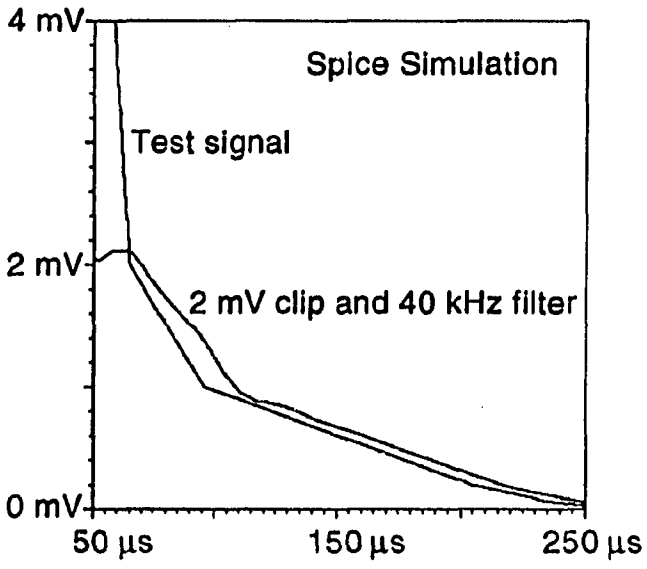

Figure 38 Spice simulation of the affects of the clipper and 40 kHz filter on a simulated tail of large clusters

Computer simulation of the components is very important but cannot take the place of experimental verification of the capabilities of the detection system. The best test of the entire system was done by reversing the polarity of the acceleration potential which allows a pulse of electrons to reach the Faraday cup. Figure 39 shows the electron signal used to test the entire system. It is the same magnitude as the ion distributions encountered and has a long tail like

large clusters would produce so it is an ideal case for studying the detection system. The 40 kHz filter distorts the large signal of Figure 39 slightly due to the high frequencies involved and a 400 mV clip further reduces the magnitude because the 24 Ω resistor acts as a voltage divider with the 50 Ω input of the scope. This distortion of the large signal is expected and it is the tail under a low clip that is being tested here. Figure 40 shows the tail section at the lowest 200 μV/division setting of the scope. The three smooth lines are through the 40 kHz filter with high, low, and no clipping which show no distortion compared to the noisier signal that is unfiltered and unclipped. The clipping occurs at -2 mV which is below the screen in this figure but it is clear that the entire detection system does not distort the tail in any way and is very effective in cleaning the signal up. This and other testing demonstrates the capabilities of the time-of-flight experiment to detect even small amounts of large clusters in whatever distribution they are in.

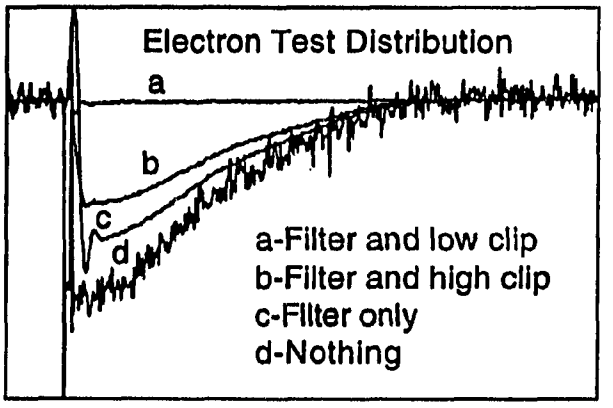

Figure 39 The electron time-of-flight distribution used to test the detection electronics

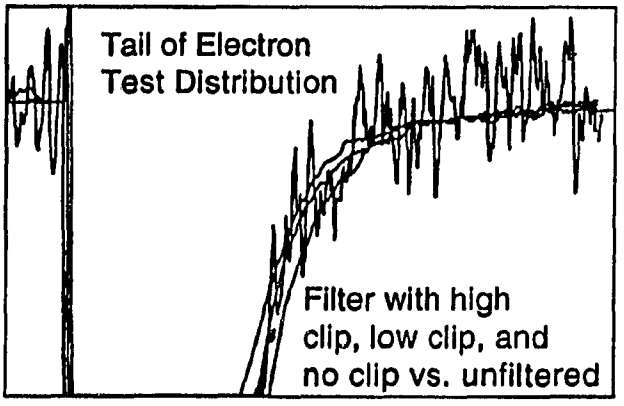

Figure 40 The tail to the electron distribution used to test the accuracy of the clipper and 40 kHz filter

APPENDIX E - PROGRAM FOR TESTING THE KYOTO UNIVERSITY TIME-OF-FLIGHT EXPERIMENT

The program EMTOF that follows uses the same methods for solving Laplace's equation as discussed previously, only the boundary conditions have changed. These boundary conditions were taken from the diagram of the experimental apparatus that was published with the results by the Kyoto University group. It should be a reasonably accurate representation of the geometry of the source and the important conclusions reached from this calculation are not very sensitive to minor differences that may exist.

While the demonstration that a potential ridge exists in the ionization region is enough to invalidate the Kyoto University time-of-flight experiment, it would have been nice to do a full simulation resulting in a time-of-flight distribution presumably similar to that of the experiment. This was abandoned when it became too difficult to be worth the effort. Ions balanced on the top of a ridge are difficult to simulate using a potential on a mesh and a finite time step. The potential mesh can be smoothed out by doing a one dimensional simulation using a polynomial approximation to the mesh potential along the axis but the finite time step makes it very difficult to accurately balance an ion on the top of the ridge.

The Program EMTOF

```
      PROGRAM EMTOF
C
C     Laplace calculation of both sides
C     of the Kyoto TOF setup
C
      REAL SOLD(-148:148,0:528),SNEW(-148:148,0:528),
     +     LOLD(-144:144,0:256),LNEW(-144:144,0:256),A,D,
     +     SMAXDIFF,LMAXDIFF,D2
C
      INTEGER T,I,R,Z,ITER,VA,VE,VC,VAIC,VEC,VEXT,LR,LZ,SR,SZ
C
      CHARACTER*1 RD
C
C
      CALL LINK('UNIT5=(parms,TEXT),UNIT7=(sin,TEXT),
     +           UNIT8=(lin,TEXT),UNIT10=(maxdiff,TEXT),
     +           UNIT17=(sout,TEXT),UNIT18=(lout,TEXT)//')
C
      VA=0
      VE=280
      VC=1000
      VAIC=500
      VEC=90
      VEXT=20
      RD='N'
      ITER=50000
      IF (RD.NE.'Y') GOTO 25
      READ(8,*)
      DO 10 Z=0,256
      DO 10 R=-144,144
   10  READ(8,*)LOLD(R,Z)
      READ(7,*)
      DO 20 Z=0,528
      DO 20 R=-148,148
   20  READ(7,*)SOLD(R,Z)
C
C               SET PERMANENT BC'S
C
   25 DO 26 R=-2,2
       LOLD(R,0)=VA
   26  LOLD(R,256)=0
      LOLD(3,0)=FLOAT(VA)/2.
      LOLD(3,256)=0
```

```
      DO 30 R=4,144
       LOLD(R,0)=0
   30  LOLD(R,256)=0
      LOLD(-3,0)=FLOAT(VA)/2.
      LOLD(-3,256)=0
      DO 31 R=-144,-4
       LOLD(R,0)=0
   31  LOLD(R,256)=0
      DO 50 Z=1,255
       LOLD(-144,Z)=0
   50  LOLD(144,Z)=0
C
C             ITERATION
C
      DO 500 I=1,ITER
      DO 100 R=-147,147
       IF (R.EQ.0) GOTO 100
       DO 101 Z=1,527
  101   SNEW(R,Z)=(SOLD(R,Z+1)+SOLD(R,Z-1)+SOLD(R+1,Z)
                  +SOLD(R-1,Z))/4
     +            +(SOLD(R+1,Z)-SOLD(R-1,Z))/(8*R)
  100   CONTINUE
      DO 110 Z=144,527
  110  SNEW(0,Z)=(SOLD(0,Z+1)+SOLD(0,Z-1)+SOLD(1,Z)
                 +SOLD(-1,Z))/4
      DO 120 R=49,147
       T=R/4
  120  SNEW(R,528)=(SOLD(R-1,528)+SOLD(R+1,528)+SOLD(R,527)+
     +               3*SOLD(R,528)/4+((R-4*T)*LOLD(T+1,151)+
     +               (4-R+4*T)*LOLD(T,151))/16)/4+
     +              (SOLD(R+1,528)-SOLD(R-1,528))/(8*R)
      DO 121 R=-147,-49
       T=-(ABS(R)/4)
  121  SNEW(R,528)=(SOLD(R-1,528)+SOLD(R+1,528)+SOLD(R,527)+
     +               3*SOLD(R,528)/4+(ABS(R-4*T)*LOLD(T-1,151)+
     +               (4-ABS(R-4*T))*LOLD(T,151))/16)/4+
     +              (SOLD(R+1,528)-SOLD(R-1,528))/(8*R)
       SNEW(148,528)=(SOLD(147,528)+SOLD(148,527)
                      +3*SOLD(148,528)/2+
     +                 LOLD(38,150)/4+LOLD(37,151)/4)/4+
     +        (3*SOLD(148,528)/4+LOLD(38,150)/4
              -SOLD(147,528))/1184
       SNEW(-148,528)=(SOLD(-147,528)+SOLD(-148,527)
                       +3*SOLD(-148,528)/2+
     +                 LOLD(-38,150)/4+LOLD(-37,151)/4)/4+
     +        (3*SOLD(-148,528)/4+LOLD(-38,150)/4
              -SOLD(-147,528))/1184
```

```
      DO 122 Z=1,527
       T=Z/4
       D=((Z-4*T)*LOLD(38,19+T)+(4-Z+4*T)*LOLD(38,18+T))/16+
     +    3*SOLD(148,Z)/4
       SNEW(148,Z)=(SOLD(147,Z)+SOLD(148,Z+1)
                   +SOLD(148,Z-1)+D)/4+
     +              (D-SOLD(147,Z))/1184.
       D2=((Z-4*T)*LOLD(-38,19+T)+(4-Z+4*T)*LOLD(-38,18+T))/16+
     +    3*SOLD(-148,Z)/4
  122  SNEW(-148,Z)=(SOLD(-147,Z)+SOLD(-148,Z+1)
                    +SOLD(-148,Z-1)+D2)/4+
     +              (D2-SOLD(-147,Z))/1184.
       SNEW(148,0)=(SOLD(147,0)+SOLD(148,1)+3*SOLD(148,0)/2+
     +              LOLD(38,18)/4+LOLD(37,17)/4)/4+
     +             (LOLD(38,18)/4+3*SOLD(148,0)/4
                  -SOLD(147,0))/1184.
       SNEW(-148,0)=(SOLD(-147,0)+SOLD(-148,1)+3*SOLD(-148,0)/2+
     +              LOLD(-38,18)/4+LOLD(-37,17)/4)/4+
     +             (LOLD(-38,18)/4+3*SOLD(-148,0)/4
                   -SOLD(-147,0))/1184.
       DO 124 R=105,147
        T=R/4
  124  SNEW(R,0)=(SOLD(R+1,0)+SOLD(R-1,0)+SOLD(R,1)+
     +             3*SOLD(R,0)/4+((R-4*T)*LOLD(T+1,17)+
     +             (4-R+4*T)*LOLD(T,17))/16)/4+
     +            (SOLD(R+1,0)-SOLD(R-1,0))/(8*R)
       DO 125 R=-147,-105
        T=-(ABS(R)/4)
  125  SNEW(R,0)=(SOLD(R+1,0)+SOLD(R-1,0)+SOLD(R,1)+
     +             3*SOLD(R,0)/4+(ABS(R-4*T)*LOLD(T-1,17)+
     +             (4-ABS(R-4*T))*LOLD(T,17))/16)/4+
     +            (SOLD(R+1,0)-SOLD(R-1,0))/(8*R)
       DO 126 R=9,28
        T=R/4
  126  SNEW(R,0)=(SOLD(R+1,0)+SOLD(R-1,0)+SOLD(R,1)+
     +             3*SOLD(R,0)/4+((R-4*T)*LOLD(T+1,17)+
     +             (4-R+4*T)*LOLD(T,17))/16)/4+
     +            (SOLD(R+1,0)-SOLD(R-1,0))/(8*R)
       DO 127 R=-28,-9
        T=-(ABS(R)/4)
  127  SNEW(R,0)=(SOLD(R+1,0)+SOLD(R-1,0)+SOLD(R,1)+
     +             3*SOLD(R,0)/4+(ABS(R-4*T)*LOLD(T-1,17)+
     +             (4-ABS(R-4*T))*LOLD(T,17))/16)/4+
     +            (SOLD(R+1,0)-SOLD(R-1,0))/(8*R)
C
       DO 130 R=-37,37
        IF (ABS(R).LT.3) GOTO 130
```

```
      DO 131 Z=1,17
  131   LNEW(R,Z)=(LOLD(R,Z+1)+LOLD(R,Z-1)+LOLD(R+1,Z)
                  +LOLD(R-1,Z))/4
     +             +(LOLD(R+1,Z)-LOLD(R-1,Z))/(8*R)
  130   CONTINUE
      DO 140 R=-37,37
       IF (R.EQ.0) GOTO 140
       DO 141 Z=151,255
  141   LNEW(R,Z)=(LOLD(R,Z+1)+LOLD(R,Z-1)+LOLD(R+1,Z)
                 +LOLD(R-1,Z))/4
     +             +(LOLD(R+1,Z)-LOLD(R-1,Z))/(8*R)
  140   CONTINUE
      DO 145 R=-143,143
       IF (ABS(R).LT.38) GOTO 145
       DO 146 Z=1,255
  146   LNEW(R,Z)=(LOLD(R,Z+1)+LOLD(R,Z-1)+LOLD(R+1,Z)
                  +LOLD(R-1,Z))/4
     +             +(LOLD(R+1,Z)-LOLD(R-1,Z))/(8*R)
  145   CONTINUE
      DO 160 Z=151,255
  160 LNEW(0,Z)=(LOLD(1,Z)+LOLD(-1,Z)+LOLD(0,Z+1)+LOLD(0,Z-1))/4
C
C             OVERWRITE OTHER BC'S ON NEW MESH
C
C           RIGHT SIDE
      DO 200 Z=1,17
      LNEW(0,Z)=VA
      LNEW(1,Z)=VA
  200 LNEW(2,Z)=VA
      DO 210 R=0,8
      DO 210 Z=0,143
  210 SNEW(R,Z)=VA
      DO 220 R=9,18
      DO 220 Z=57,143
  220 SNEW(R,Z)=VA
      DO 230 Z=48,144,24
      SNEW(29,Z)=VA-VC+2
      SNEW(29,Z-1)=VA-VC+2
      SNEW(28,Z-1)=VA-VC+2
  230 SNEW(28,Z)=VA-VC+2
      DO 240 Z=0,4
      DO 240 R=29,104
  240 SNEW(R,Z)=VA-VC
      DO 250 R=7,26
  250 LNEW(R,17)=VA-VC
      DO 260 R=88,96
      DO 260 Z=5,159
```

```
  260 SNEW(R,Z)=VA-VC
      DO 270 Z=160,164
      DO 270 R=30,104
  270 SNEW(R,Z)=VA-VC
      DO 272 R=12,128
  272  SNEW(R,248)=VAIC+VEC-VE-20
      DO 274 Z=249,335
  274  SNEW(80,Z)=VAIC+VEC-VE-20
      DO 276 R=40,80
  276  SNEW(R,336)=VAIC+VEC-VE-20
      DO 278 R=12,39
  278  SNEW(R,272)=VAIC
      DO 280 Z=260,284
  280  SNEW(40,Z)=VAIC
      DO 282 Z=300,324
  282  SNEW(40,Z)=VAIC
      DO 284 R=12,32
  284  SNEW(R,308)=VAIC-VEXT
      DO 286 Z=264,284
       R=52+(Z-264)*8/20
  286  SNEW(R,Z)=VAIC+VEC-VE
      DO 288 Z=300,320
       R=52+(320-Z)*8/20
  288  SNEW(R,Z)=VAIC+VEC-VE
      SNEW(68,292)=VAIC+VEC-VE
      DO 290 R=12,36
  290  SNEW(R,344)=0
      DO 292 R=12,80
  292  SNEW(R,368)=0
      DO 294 Z=369,512
  294  SNEW(80,Z)=0
      DO 296 R=0,48
  296  SNEW(R,528)=0
C
      DO 420 R=0,37
      DO 420 Z=18,150
  420 LNEW(R,Z)=SNEW(R*4,(Z-18)*4)
C
C        LEFT SIDE
      DO 700 Z=1,17
      LNEW(0,Z)=VA
      LNEW(-1,Z)=VA
  700 LNEW(-2,Z)=VA
      DO 710 R=-8,0
      DO 710 Z=0,143
  710 SNEW(R,Z)=VA
      DO 720 R=-18,-9
```

```
      DO 720 Z=57,143
  720 SNEW(R,Z)=VA
      DO 730 Z=48,144,24
      SNEW(-29,Z)=VA-VC+2
      SNEW(-29,Z-1)=VA-VC+2
      SNEW(-28,Z-1)=VA-VC+2
  730 SNEW(-28,Z)=VA-VC+2
      DO 740 Z=0,4
      DO 740 R=-104,-29
  740 SNEW(R,Z)=VA-VC
      DO 750 R=-26,-7
  750 LNEW(R,17)=VA-VC
      DO 760 R=-96,-88
      DO 760 Z=5,159
  760 SNEW(R,Z)=VA-VC
      DO 770 Z=160,164
      DO 770 R=-104,-30
  770 SNEW(R,Z)=VA-VC
      DO 772 R=-108,-12
  772  SNEW(R,248)=VAIC+VEC-VE-20
      DO 778 R=-39,-12
  778  SNEW(R,272)=VAIC
      DO 780 Z=260,284
  780  SNEW(-40,Z)=VAIC
      DO 782 Z=300,324
  782  SNEW(-40,Z)=VAIC
      DO 784 R=-32,-12
  784  SNEW(R,308)=VAIC-VEXT
      DO 786 R=-66,-54
  786  SNEW(R,264)=VAIC+VEC
      DO 788 Z=265,316
  788  SNEW(-66,Z)=VAIC+VEC
      DO 789 R=-66,-54
  789  SNEW(R,317)=VAIC+VEC
      DO 790 R=-36,-12
  790  SNEW(R,344)=0
      DO 792 R=-80,-12
  792  SNEW(R,368)=0
      DO 794 Z=369,512
  794  SNEW(-80,Z)=0
      DO 796 R=-48,0
  796  SNEW(R,528)=0
C
      DO 820 R=-37,0
      DO 820 Z=18,150
  820 LNEW(R,Z)=SNEW(R*4,(Z-18)*4)
C
```

```
C             PRINT MAXDIFF EVERY 1000
      T=I/1000
      IF (I.NE.T*1000) GOTO 320
      LMAXDIFF=0
      DO 300 R=-143,143
      DO 300 Z=1,255
      IF (ABS(LNEW(R,Z)-LOLD(R,Z)).LT.LMAXDIFF) GOTO 300
      LMAXDIFF=ABS(LNEW(R,Z)-LOLD(R,Z))
      LR=R
      LZ=Z
  300 CONTINUE
      SMAXDIFF=0
      DO 310 R=-148,148
      DO 310 Z=0,528
      IF (ABS(SNEW(R,Z)-SOLD(R,Z)).LT.SMAXDIFF) GOTO 310
      SMAXDIFF=ABS(SNEW(R,Z)-SOLD(R,Z))
      SR=R
      SZ=Z
  310 CONTINUE
      WRITE(10,*)I,SR,SZ,SMAXDIFF,LR,LZ,LMAXDIFF
C
C             OLD<==NEW
  320 DO 400 R=-143,143
      DO 400 Z=1,255
  400 LOLD(R,Z)=LNEW(R,Z)
      DO 410 R=-148,148
      DO 410 Z=0,528
  410 SOLD(R,Z)=SNEW(R,Z)
C
  500 CONTINUE
C       END OF ITERATION LOOP
C
C            DUMP EVERYTHING OUT
      WRITE(18,*)' 289  257  0  0'
      DO 610 Z=0,256
      DO 610 R=-144,144
  610 WRITE(18,*)LOLD(R,Z)
      WRITE(17,*)' 297  529  0  0'
      DO 620 Z=0,528
      DO 620 R=-148,148
  620 WRITE(17,*)SOLD(R,Z)
      END
```